Towards Bottom-up Reconstitution of Minimal Modules of Eukaryotic Pattern Formation

Sonal

München 2018

Towards Bottom-up Reconstitution of Minimal Modules of Eukaryotic Pattern Formation

Dissertation
an der Fakultät für Physik
der Ludwig-Maximilians-Universität
München

vorgelegt von

Sonal
aus Neu Delhi, Indien

München, den 06. Februar 2018

Erstgutachter: Prof. Dr. Petra Schwille

Zweitgutachter: Prof. Dr. Claudia Veigel

Tag der mündlichen Prüfung: 20. März 2018

For the mouse and the lion inside...

ZUSAMMENFASSUNG

Räumliche Muster sind allgegenwärtig in der Biologie, in der sie auf einer breiten Größenskala beobachtet werden können: von der bemerkenswerten Symmetrie in Meeresplankton bis zur geordneten Flugformation von Zugvögeln. Die mathematische Präzision, mit der diese Ordnung aus von Natur aus chaotischen biologischen Systemen hervorgeht, inspirierte diverse theoretische Abhandlungen der biologischen Musterbildung. Die zunehmende Weiterentwicklung von experimentellen sowie computergestützten Methoden hat es Wissenschaftlern ermöglicht, durch immer tieferer Einblicke in die subzellulären Strukturen die fein abgestimmten molekularen Mechanismen zu identifizieren, aus denen diese neuauftretende Ordnung der Zelle hervorgeht.

Ein „Bottom-up“ Rekonstitutionsansatz bietet sich an, um diese multidisziplinären Konzepte zu vertiefen, indem ein biologisches System von seinen einzelnen Komponenten ausgehend sukzessive aufgebaut wird; ein Ansatz, der von Richard Feynman so treffend mit den Worten beschrieben wurde: „Was ich nicht erschaffen kann, das kann ich auch nicht verstehen“. Um das grundsätzliche Konstruktionsprinzip des zugrundeliegenden molekularen Moduls herauszuarbeiten, werden nur die Komponenten ausgewählt, die für den Kern der biologischen Funktion absolut notwendig sind. Diese vereinfachten Module sind zudem einfacher mit biophysikalischen Methoden zu charakterisieren. Dieser Ansatz eignet sich besonders für das Studium der spontanen Selbstorganisation in der Biologie: sowohl, weil diese direkt aus biologischen Systemen selbst hervorgeht, als auch, weil eine reichhaltige theoretische Grundlage existiert, die eine rationale Vereinfachung der zu untersuchenden Systeme ermöglicht.

Diese Arbeit beschreibt die Bemühungen, zwei molekulare Module eukaryotischen Ursprungs zu rekonstituieren, die bezüglich ihrer emergenten Musterbildung bereits gut untersucht sind. In beiden Fällen beruht die Selbstorganisation auf einem komplexen Zusammenspiel verschiedener Protein-Interaktionen, und der diesen durch biologische Membranen verliehenen diffusiven Eigenschaften.

Für die Untersuchung des ersten Models haben wir einen minimalen biomimetische Zellkortex konstruiert, in dem membrangebundene Katalyse von dendritischer Aktinpolymerisation mit Myosin-II Aktivität koexistiert. Während vorangegangene Studien mit in vitro rekonstituierten Zellkorteces schon viel dazu beigetragen haben, die Rolle der Myosinkontraktilität in der Reorganisation von Aktinfilmenten aufzuklären, wurde der Einfluss eines

ausgleichenden Wachstumsprozesses (des Aktins) auf das Resultat dieser Vorgänge noch nicht im mikroskopischen Detail untersucht. Wir konnten in dieser Arbeit zeigen, dass Myosinaktivität zum Abbau und zur Umverteilung von Aktin in diesem vereinfachten Kortex führt, was zu einem neuen dynamischen Gleichgewichtszustand führt, bei dem die Aktinfilamente kontinuierlich auf- und abgebaut werden. Wir identifizierten auch eine myosin(motor)-unabhängige Quelle räumlicher Heterogenität während dieser dendritischen Netzwerkassemblierung. Weiterhin zeigten wir, dass die Verzweigung und Bündelung von Filamenten die Selbstorganisation von Aktinmustern während der Assemblierung auf Lipidmembranen bestimmen kann.

Für die Untersuchung des zweiten Moduls haben wir ein minimales Modul konzipiert, dass die Symmetriebrechung während der Etablierung der Zellpolarität in Hefen nachempfindet. Dieses Modul basierte auf einem Reaktions-Diffusions-Netzwerk, in dessen Mittelpunkt die reversible Membranbindung der RhoGTPase Cdc42 steht. Während wir in der Lage waren, einige der beteiligten Reaktionen auf artifiziellen Membranen nachzustellen, wurde die Aufklärung der Musterbildung durch den Hang der involvierten Proteine zur Aggregation erschwert. Eine weitergehende biochemische Charakterisierung der interagierenden Proteinspezies könnte dazu verwendet werden, das Design des Minimalmodules zu optimieren. Nichtsdestotrotz konnten wir einen Arbeitsablauf etablieren, der durch Nutzung diverser Methoden in der Zukunft als guter Ausgangspunkt dafür dienen kann, synthetische Proteinnetzwerke auf Modell-Membranen zu rekonstituieren.

ABSTRACT

Spatial patterns are omnipresent in the biological world, occurring across a range of scales– from the striking symmetries of oceanic plankton to the coordination of bird flight. The mathematical precision with which this order emerges from inherently noisy biology has inspired diverse theoretical frameworks for biological pattern formation. Increased sophistication of both experimental and computational techniques has enabled researchers to delve deeper into subcellular scales to identify the intricate molecular pathways that determine emergent order in a cell.

A bottom-up reconstitution approach offers to consolidate these multidisciplinary concepts by building the described biological system from its components; succinctly conveyed by Feynman as- "What I cannot create, I do not understand". To extract the basic design principles of the underlying molecular module, only the components minimally required for the core biological function are selected. These simplified modules are also more amenable to biophysical characterization. Spontaneous self-organization in biology, by virtue of its self-containment as well as a rich theoretical foundation for simplification, is a particularly enticing problem for applying this approach. This thesis describes the efforts to reconstitute two molecular modules of eukaryotic origin, well-studied in the context of emergent pattern formation. In both cases, self-organization relies on an intricate interplay between protein interactions and the diffusive properties imposed by membrane scaffolding.

Firstly, we constructed a minimal biomimetic cortex, where catalytic dendritic actin polymerization localized to the membrane coexisted with myosin-II activity. While previous studies on *in vitro* cortices have provided immense insight into the role of myosin contractility in actin reorganization, the impact of a counterbalancing growth process on the outcome has not been studied in microscopic detail. We demonstrated that myosin activity leads to disassembly and redistribution of actin in this simplified cortex and results in an emergent dynamic steady state with the actin filaments undergoing continuous turnover. During the process, we also identified a motor-independent source of spatial heterogeneity in dendritic network assembly. We further showed that branching and bundling of filaments can determine the self-organization of actin patterns during assembly on lipid membranes.

Secondly, we designed a minimal module that could recreate symmetry breaking during polarity establishment in yeast cells. This module was based on a reaction-diffusion frame-

work, centered on the reversible membrane binding of the RhoGTPase Cdc42. While we succeeded in implementing some of the participating reactions on artificial membranes, the elucidation of pattern formation was confounded by the inherent propensity of the involved proteins to aggregate. Further biochemical characterization of the interacting species may potentially be used to optimize the design of the minimal module. Nevertheless, we consolidated a workflow with diverse methodologies that can serve as a platform for future reconstitutions of synthetic protein networks on model membranes.

Contents

List of Figures

List of Abbreviations

aa	amino acid
Arp2/3	Actin-related proteins 2/3
BSA	Bovine Serum Albumin
CRIB	Cdc42- and Rac-interactive binding
CV	Coefficient of Variance
DGS-NTA	1,2-Dioleoyl-sn-glycero-3-phosphoethanolamine
DOPC	1,2-Dioleoyl-sn-glycero-3-phosphocholine
DOPE	1,2-Dioleoyl-sn-glycero-3-phosphoethanolamine
DOPS	1,2-dioleoyl-sn-glycero-3-phospho-L-serine
eGFP	enhanced Green Fluorescent Protein
GAP	GTPase-activating protein
GDI	Guanosine nucleotide dissociation inhibitor
GEF	Guanine nucleotide Exchange Factor
GGPP	Geranylgeranyl pyrophosphate
GGTase-I	Geranylgeranyl transferase-I
GUV	Giant Unilamellar Vesicle
NMM-II	non-muscle Myosin-II
NPF	Nucleation Promoting Factor
PIP2	Phosphatidylinositol 4,5-bisphosphate

SEC	Size Exclusion Chromatography
sfGFP	superfolder Green Fluorescent Protein
SLB	Supported Lipid Bilayer
TIRF	Total Internal Reflection Fluorescence
VCA	verpolin homology, cofilin, and acidic domain

I

INTRODUCTION

Pattern formation in biology has been a subject of fascination to scientists of various branches for many decades. The rich diversity of design observable in the biological world naturally inspires intrigue into the processes that reproducibly create these patterns and order. Consequently, the earliest theoretical frameworks for describing pattern formation in biology sought to address phenomena in developmental biology. Transplantation experiments had suggested that morphogenesis, or the development of form in a growing organism, was guided by coordinate systems that could be defined by concentration of molecules. The initiation of this spatial differentiation, i.e. the assignment of different functional fates to parts of a relatively homogeneous cell mass, was considered a fundamental problem of symmetry breaking [Cross and Hohenberg, 1993].

In 1952, Alan Turing wrote a seminal paper titled "The Chemical Basis of Morphogenesis", which set a foundation for mathematical formalizations of biological pattern formation [Turing, 1952]. The paper inspired an entire generation of reaction-diffusion models– a theoretical paradigm wherein the emergence of large scale patterns can be explained by a specialized set of local interactions between molecules and difference in their diffusion properties. While simulated Turing-type patterns bore striking visual resemblance to animal coat patterns, the underlying diffusion-based principles were more likely to be consequential in subcellular lengthscales. Gierer and Meinhardt (1972) used one such model to explain regeneration in hydra [Gierer and Meinhardt, 1972]. Turing-type instabilities were also used to describe segmentation in *Drosophila* embryos. While models of this lineage are still predominant conceptual paradigms, later models diversified by incorporating additional physical attributes of the biological systems, with emphasis on mechanical, electrical or hydrodynamic sources of symmetry breaking.

Technical advances in both experimental as well as computational methodology subsequently resulted in elucidation of subcellular processes in much greater detail. Motifs of pattern formation models could be identified in the complex molecular interaction networks that were being uncovered. Many of these involved modulation of the cytokeleton, that provides the eukaryotic cell its dynamic shape and hence its functionality. Common molecules and regulatory motifs have been identified in diverse systems, feeding back into the increased curiosity of theoreticians.

The essence of a bottom-up reconstitution approach is to consolidate the multidisciplinary concepts developed over the years and use them to build the described biological system from its components; succinctly conveyed by Feynman as- "What I cannot create, I do not understand". However, to recreate a biological system in its full complexity is not just impractical, but also counterproductive for seeking insight into the basic design principles underlying the molecular phenomena. We, therefore, aim to reconstitute these modules with the minimal molecular components required for the core function of interest. Spontaneous self-organization in biology is particularly enticing for a synthetic biology approach. Theoreticians have delved deeply into this phenomenon, revealing a lot of conceptual scope for simplified module designs. Additionally, the self-contained nature of self-organization modules makes them suitable for *in vitro* isolation.

An example of successful implementation of bottom-up approaches for self-organization is found in the development of advanced biomimetic membrane systems. Differences in diffusion rates are considered crucial for reaction-diffusion models to work. Within a cell, such differences were likely to be produced by molecular scaffolding that could slow down diffusion on certain molecules. A prime candidate for such scaffolding is the plasma membrane of the cell. A membrane-bound protein shows considerably lower rates of diffusion than one in solution. Artificial membrane systems thus present an opportunity to study pattern forming molecular modules *in vitro* in detail. Such reduced systems enable us to isolate the essential molecular interactions from their complex cellular environments and study them in more controlled settings. The molecular players could be modified or substituted with minimally functional units to be able to identify the core design principles that are needed in modules of pattern formation. Furthermore, these *in vitro* systems are more amenable to advanced biophysical analyses, which allow us to measure various parameters that are required for effective theoretical modeling.

In this thesis, we discuss the use of synthetic biology approaches to gain an insight into two different molecular modules of pattern formation from eukaryotic cells. The first module pertains to the actin cytoskeleton that provides the cells both dynamic structure and function, and is consequential to eukaryotic polarization. The second module delves into the symmetry breaking process that initiates polarity establishment in cells. Interestingly, both modules are known to rely on distinct theoretical paradigms of pattern formation. Mechanochemistry is considered to be the driving influence in self-organization in cortical cytoskeletal networks, whereas reaction-diffusion models are primarily used to explain

symmetry breaking for polarization. For this reason, much of the basic concepts pertaining to these systems are described in the individual chapters.

II

RECONSTITUTION OF A BIOMIMETIC MINIMAL CORTEX WITH ACTIN TURNOVER

1 Introduction

Rapid and controlled modulation of cell shape provides the foundation for various cellular functions, such as division, growth, migration and adhesion. In eukaryotic cells, much of this modulation can be attributed to changes in the actomyosin cortex that lines the inner surface of the plasma membrane. The cortex is a thin network of actin filaments associated with myosin motors (reviewed in [Salbreux et al., 2012]). It is further reinforced by a collection of actin binding proteins that mediate filament-filament and filament-membrane interactions. Myosin motors drive contractility of the actin meshwork, generating forces at different length scales that enable fast remodeling of the cell surface.

Another factor that imparts fast dynamics to the cortex is continuous turnover of all the protein components of this network. Relative rates of turnover can determine the mechanistic properties of the cortex. For example, the observed faster turnover of a cross-linker as compared to actin filaments may determine how long stresses persist in the network. Turnover rates are therefore subject to local regulation; a fact elucidated by the observation that the rate of actin turnover within the same cell can vary between functionally distinct regions of the cortex [Murthy and Wadsworth, 2005]. Actin turnover has significant consequences on cortical tension [Tinevez et al., 2009] and various network elements are implicated in imparting different turnover rates to subpopulations of actin [Fritzsche et al., 2013]. Turnover can be tuned by manipulation of either assembly or disassembly processes. Lipids in the bilayer can orchestrate local polymerization via activation of nucleators such as the Arp2/3 complex [Higgs and Pollard, 2000]. Besides dedicated actin severing proteins, myosin activity has also been implicated in contributing to disassembly. Inhibition of myosin activity was shown to reduce actin turnover in a range of cellular contexts, such as during mammalian cytokinesis [Guha et al., 2005, Murthy and Wadsworth, 2005], at the base of the neuronal growth cones [Medeiros et al., 2006, Yang et al., 2012] and at the rear end of motile keratocytes [Wilson et al., 2010]. Due to the complexity of cellular environments, *in vitro* experiments have proved more amenable for direct observa-

tion of myosin-II driven severing of actin filaments [Haviv et al., 2008, Murrell and Gardel, 2012, Vogel et al., 2013] as well as network disassembly [Reymann et al., 2012].

Reconstitution studies have, in general, been instrumental in providing deeper insights to the factors affecting self-organization of cytoskeletal networks (reviewed in [Mullins and Hansen, 2013]). Particularly for actin networks, an early drive towards simplified systems resulted in a profound mechanistic insight into emergent pattern formation, such as that observed during actin-based motility [Loisel et al., 1999, Cameron et al., 1999, Bernheim-Groswasser et al., 2002, Kawska et al., 2012]. Interestingly, the force generation in this process could occur independently of motor-induced contractility. Biomimetic cortices have served a great role in understanding the interplay between actin assembly and myosin contractility that determines tensile properties and network-level reorganization [Kohler et al., 2011, Bussonnier et al., 2014, Carvalho et al., 2013a, Carvalho et al., 2013b]. A direct investigation of myosin's role in network turnover has however been lacking in *in vitro* studies so far. There are multiple reasons contributing to this gap in our knowledge. The observation of filament turnover has often been limited by features of experimental design like stabilized actin filaments, strong surface adhesion and restricted polymerization [Vogel et al., 2013, Reymann et al., 2012, Murrell and Gardel, 2012, Linsmeier et al., 2016, Stam et al., 2017, Koster et al., 2016, Backouche et al., 2006]. In studies not affected by such limitations, the focus has usually been on mesoscopic effects of myosin contractility on restructuring of actin networks, with most studies done in solution [Kohler et al., 2011, Smith et al., 2007, Soares e Silva et al., 2011].

We designed a biomimetic cortex where strong assembly coexists with contraction-based disassembly to understand the consequences of these opposing effects on self-organization in membrane-bound actomyosin networks. Further, minimal restraints on the mobility of components allowed us to use this system for a direct observation of myosin-assisted network turnover. The essential features of such a system are thus– 1) catalytic polymerization localized at the membrane and 2) no additional anchoring of either myosin or the actin. The catalytic polymerization is provided by a network of proteins that builds branched actin filaments, also known as "dendritic" networks.

Figure II.1 presents a schematic representation of our basic experimental design. To proceed with the reconstitution of a biomimetic minimal cortex with the potential for actin turnover, we required a strong catalyst of actin polymerization to oppose the myosin activity. We chose to anchor this catalyst to the lipid bilayer with the stable interaction of a 10xHistidine tag to nickelated lipids [Nye and Groves, 2008]. The membrane adhesion of

the catalyst is a simplification of the cellular scenario, but also allows us to preferentially focus on the polymerization process in a complex environment, by using Total Internal Reflection Fluorescence (TIRF) microscopy. We used the constitutively active version of the murine N-Wasp, also known as "VCA", as the catalyst[1]. The VCA has been extensively studied *in vitro* and has been shown to promote the growth of a branched actin network, when combined with the Arp2/3 complex[2] [Rohatgi et al., 1999]. Muscle myosin-II motors are introduced into the system after actin assembly to observe the effects of contractility.

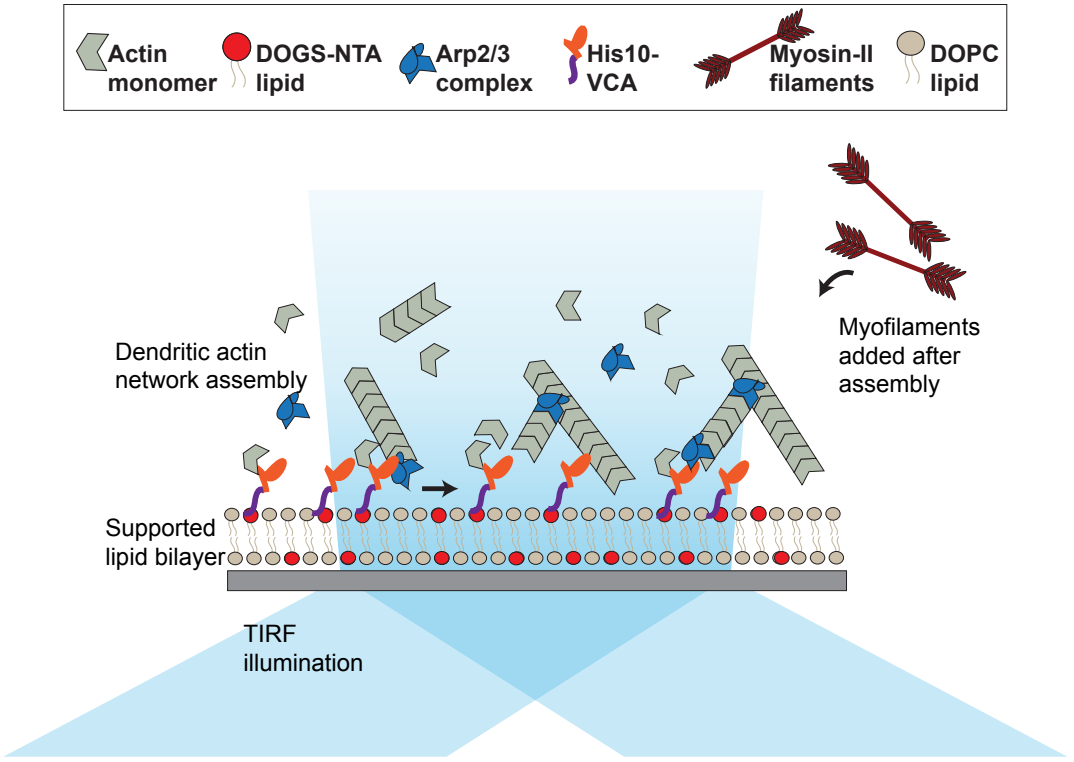

Figure II.1: Schematic representing design of the dynamic minimal cortex

In the process of building this dynamic cortex, we found that this molecular network of actin assembly inherently had the potential to generate discernible spatial heterogeneity that allows emergent actin patterns to form. These features had so far not been observed on membrane-associated networks in *in vitro* assays. In this chapter, we compare and contrast

[1] verpolin homology, cofilin, and acidic domain (VCA)
[2] Actin-related proteins 2/3 (Arp2/3)

our results with previous observations and present a novel paradigm for the study of both assembly-driven and motor-driven self-organization of membrane-bound actin networks[3].

2 Arp2/3-dependent self-organization in membrane-bound dendritic networks

In this section, we describe our investigation into the Arp2/3-dependent self-assembly of actin structures and elucidate some factors influencing the formation and transitions of these structures.

In brief, our general protocol comprised of preparing a Supported Lipid Bilayer (SLB) with a 99:1 molar ratio of DOPC to nickelated lipid DGS-NTA[4]. These membranes were incubated with 200 nM 10xHis-VCA and excess protein was washed off. Actin growth was then initiated by adding a reaction mix consisting of actin monomers, Arp2/3 complex, ATP and ATP regeneration system (see Appendix for details). A typical experiment consisted of 1 µM actin monomers and 10 nM Arp2/3, unless otherwise specified. The samples were then observed with TIRF microscopy.

2.1 Elucidating the positive feedback in dendritic network assembly

The mechanism by which VCA activates Arp2/3 complex to form a dendritic actin network has been well-described in literature [Ti et al., 2011, Padrick et al., 2011, Dayel and Mullins, 2004, Padrick et al., 2008, Smith et al., 2013a]. The Arp2/3 complex, upon activation, associates to the side of an actin filament forming a platform for the assembly of an actin branch. The branch angle is tightly regulated at 70° by the structure of the Arp2/3 complex that has a pocket mimicking an actin dimer, on which the new branch starts to assemble [Rouiller et al., 2008]. As the process results in generation of new actin barbed ends, each of which can grow independently and trigger a new branching event, the actin network shows autocatalytic growth dynamics [Pantaloni et al., 2000]. There are many molecules that can enhance this positive feedback and such protein networks can result in

[3] This project was carried out in collaboration with Dr. Kristina Ganzinger, Dr. Sven Vogel, Jonas Mücksch and Philipp Blumhardt. Individual contributions will be highlighted with the corresponding datasets.

[4] 1,2-Dioleoyl-sn-glycero-3-phosphoethanolamine (DGS-NTA)

spontaneous symmetry breaking on a bead or vesicle surface in motility assays [Cameron et al., 1999, Giardini et al., 2003].

A mixture of VCA, Arp2/3 complex and actin monomers was, on the other hand, sufficient to show formation of defined actin structures in solution [Haviv et al., 2006] as well as on the surface of a bead [Vignjevic et al., 2003]. These structures are described as actin "clouds" on the beads and "asters" in solution and are formed due to the dense growth of branched actin network. However, the effect of the autocatalysis on patterning of dendritic networks on membranes has so far not been described or demonstrated on a microscopic scale.

We found that the experimental conditions we used, allowed us to explicitly observe heterogeneity in actin assembly resulting from the positive feedback in Arp2/3 nucleation. Upon adding the actin and Arp2/3 mix to membranes pre-incubated with VCA, a sharp increase in intensity was observed due to the binding of actin monomers to the VCA. A considerable lag period was observed before the initiation of visible actin assembly in most cases, ranging from 5 to 15 minutes between different samples. Isolated nucleation points could thereafter be observed on the membrane and the actin network grew radially outwards from these points (Figure II.2). The growth of the actin network was relatively fast (1.30 $\pm$ 0.27 µm/min) as compared to the frequency of initiation events, therefore enabling us to observe heterogeneous assembly across the membrane[5]. In stark contrast, actin intensity increased steadily in the absence of Arp2/3 (dotted line in graph). We will discuss this further in the following section 2.2.

The radial symmetry of these actin networks was reminiscent of the actin asters or clouds described previously. These assemblies also showed a distinct decay in actin density moving outwards from the center (Figure II.3). Solution asters appeared to have a sharper decay from the center, but the asters on membranes resembled the corresponding Monte Carlo simulations in the same study quite closely [Haviv et al., 2006]. This radial decay was believed to result from the combination of fast growth at outward-facing barbed ends, and Arp2/3-nucleated branching along the filament that increased the density in the core region. The orientation of filaments was identified by virtue of branches at the periphery making a characteristic 70° angle to the outward radiating filament. Distinct branches were, however, harder to spot in our samples. No enrichment of VCA on the membrane was observed corresponding to the sites of autocatalytic growth (Figure II.4), presumably since the attachment of the VCA to actin filaments is transient.

[5]Rate of growth was calculated from Kymographs.

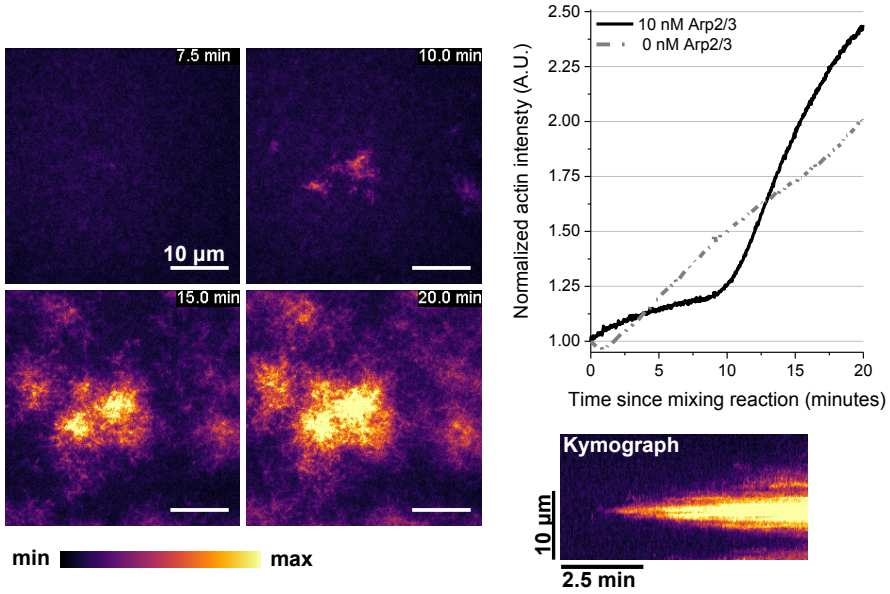

Figure II.2: Heterogeneous growth of actin reveals positive feedback

Frames showing actin with time starting at mixing of reaction. The graph shows normalized mean actin intensity on the membrane. An example kymograph from one of growth regions is shown.

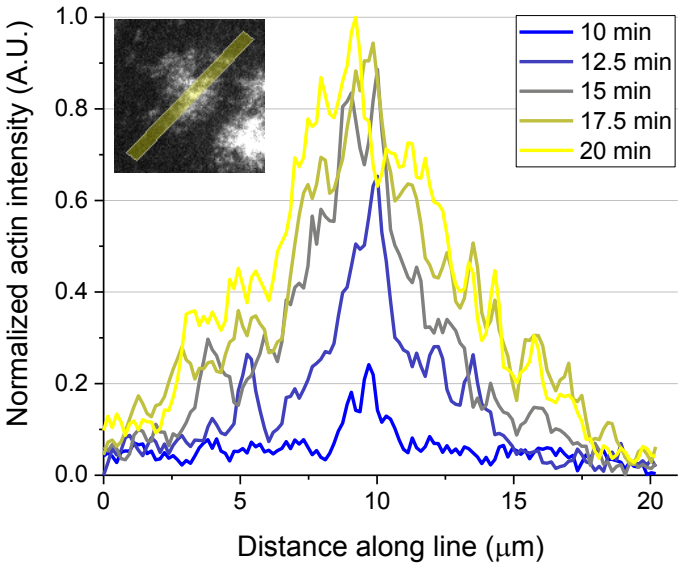

Figure II.3: Line profile across an actin patch shows radial decay in actin intensity

Actin intensities averaged over a 10-pixel width were plotted at different time points across a growing aster. Time is in reference to the start of the reaction.

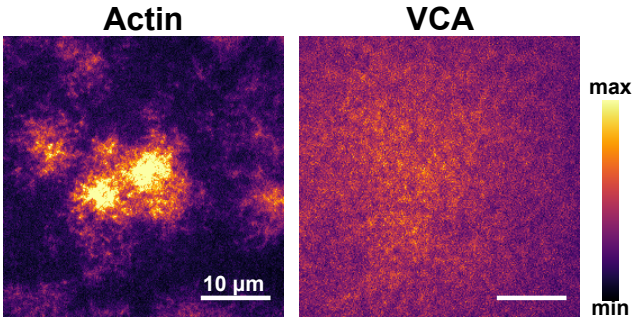

Figure II.4: VCA is uniformly distributed on the membrane while actin grows heterogeneously

2.2 Factors affecting spatial heterogeneity in assembly

The significance of Arp2/3 for formation of these actin asters was conceptually evident and the graph in Figure II.2 further confirmed this notion. Accordingly, in the absence of Arp2/3, no dense mesh was observed but elongation of individual filaments could be followed on the membrane (Figure II.5, white arrows). We attributed this to the ability of the VCA to promote elongation of actin filaments on surfaces, presumably by increasing the local concentrations of monomers available for filament growth [Bieling et al., 2018]. Addition of Arp2/3 to such a sample could immediately trigger the growth of a denser network (Figure II.6). This observation, along with the lag in initiation described previously, indicated that the limiting step in the actin network assembly was the availability of actin filaments on the membrane to serve as nucleation seeds for branching. As expected, reducing the Arp2/3 concentration from 10 to 5 nM resulted in more instances of homogeneous actin assembly (Figure II.7). Since Arp2/3 is incorporated in the branches, reducing its availability could weaken the positive feedback. The heterogeneity of initial assembly was often transient, as the spreading of the asters along with new nucleation events eventually led to a more or less homogeneous distribution of actin. However, in some cases, the heterogeneity was visible throughout the period of observation, up to an hour after initiation.

The limited availability of nucleation seeds on the membrane could result either from slow spontaneous filament assembly in solution or from diffusion-related delays in filaments reaching the membrane. To better understand this aspect, we changed the dimensions of our experimental chambers. Silicone separators served as wells on the coverglass for our reactions. By using wider wells, we could increase the membrane surface area to volume ratio in our samples by a factor of 2.5. This should increase the accessibility of filaments

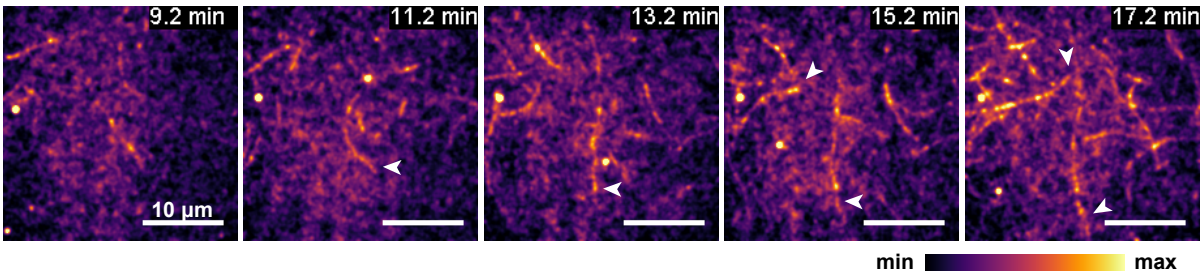

Figure II.5: Elongation of actin filaments is observed on the membrane in the absence of Arp2/3 complex

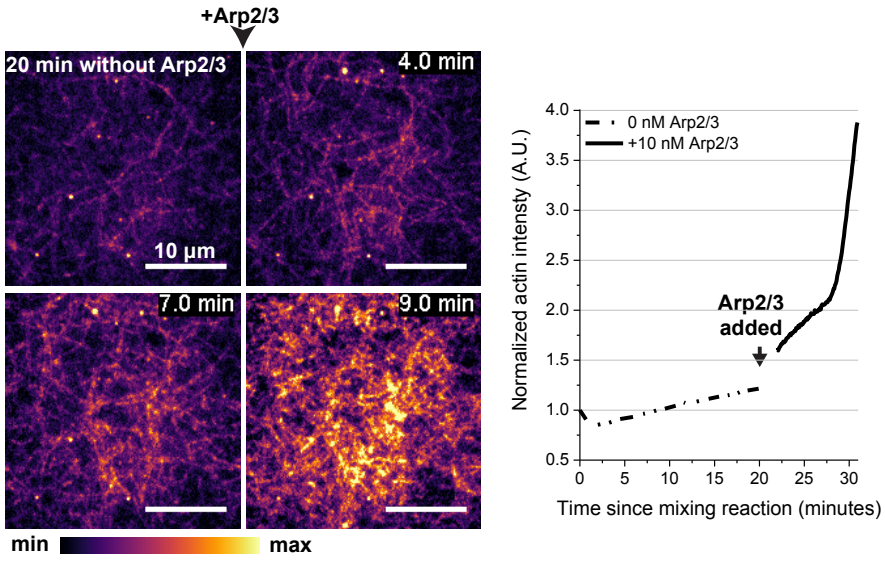

Figure II.6: Addition of Arp2/3 to the sample in Figure II.5 immediately results in dense actin growth

to the membrane, but have no obvious impact on the filament nucleation in solution. We found that use of wider chambers markedly reduced both the lag in initiation as well as the evident heterogeneity of assembly (Figure II.8). Individual nucleation sites were only rarely distinguishable before growing into a homogeneous network on the observed region of the membrane.

Another possible way of manipulating the pattern formation was to enhance the positive feedback by increasing the rate of branching. We tested this notion by introducing the capping protein CapZ (10 nM) to the homogeneous assembly in wider chambers. Capping of barbed ends by CapZ increases the incidence of branching at the expense of elongation of pre-existing branches. CapZ could not induce persistent heterogeneity, but fast growth of isolated nucleation sites could usually be observed during initiation (Figure II.9, white

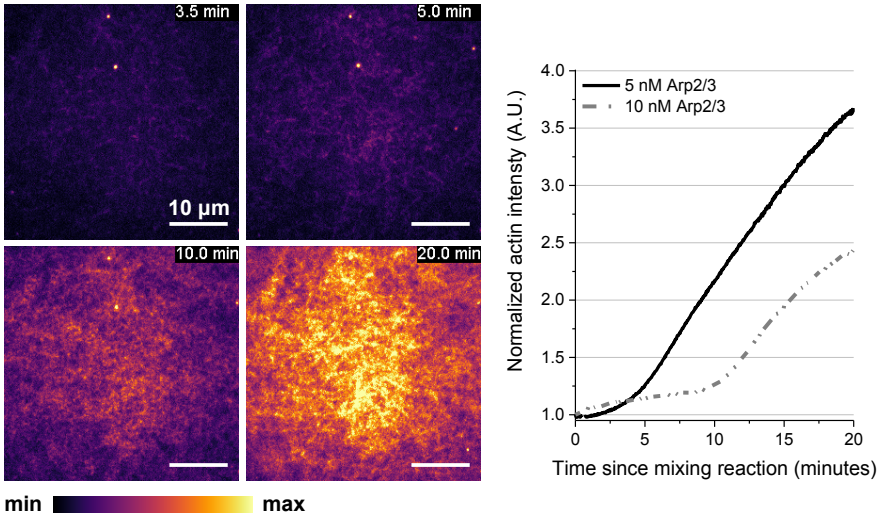

Figure II.7: Growth is more homogeneous at a lower Arp2/3 concentration of 5 nM

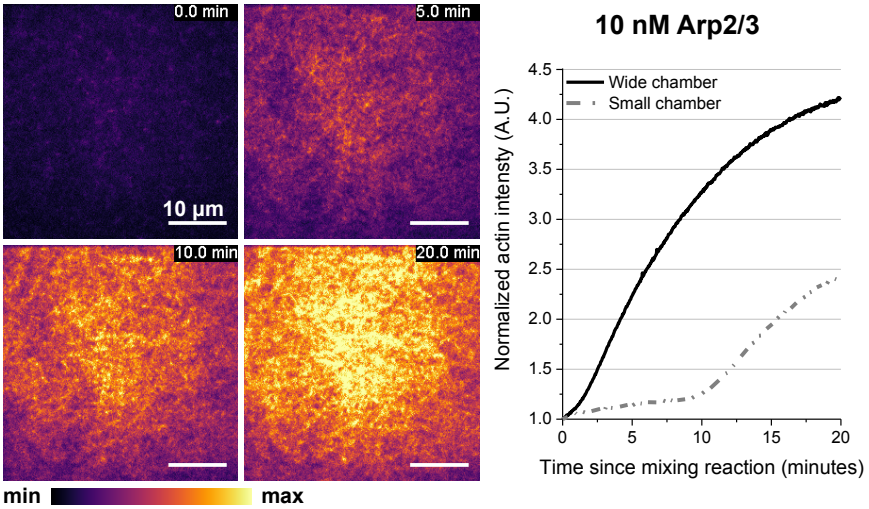

Figure II.8: Increased membrane surface area results in faster and homogeneous actin assembly

arrows). In contrast with 10 nM Arp2/3 sample in wider chambers (dotted gray line), the lag phase was much more pronounced in the presence of CapZ. Dense actin assembly thereafter resulted in a very homogeneous carpet of actin on the membrane[6].

[6]CapZ data was acquired by Dr. Kristina Ganzinger

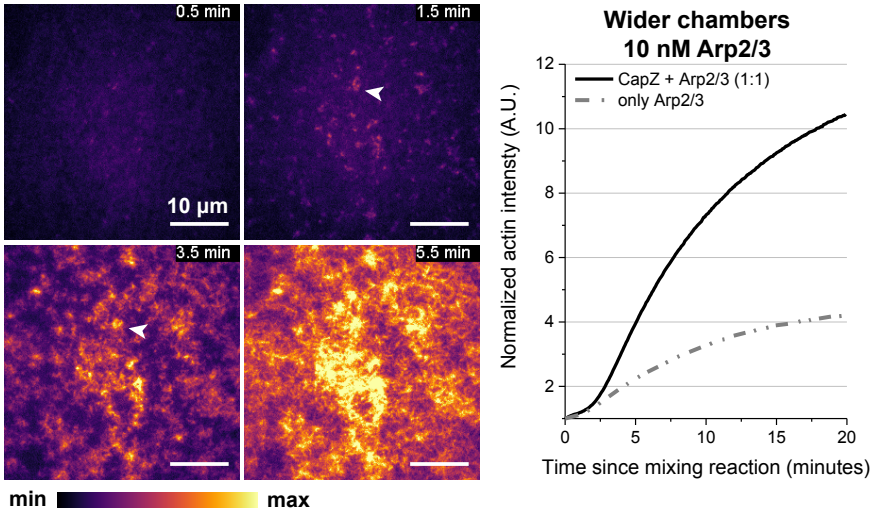

Figure II.9: Capping enhances the initial lag to reveal individual initiation events

2.3 Bundling-induced aster to star transition in actin structures

Since diffusion had appeared consequential in limiting the nucleation process of actin assembly, we tested whether reducing diffusion could lead to observable spatial heterogeneity in the wider chambers. To this end, we used the crowding agent methylcellulose (0.2%) that is also known to slow down diffusive processes. As predicted, isolated nucleation events were clearly discernible on the membrane in this condition (Figure II.10). Most strikingly, aster-like growth at these sites turned into "stars" over half an hour. According to convention, the distinguishing feature of the star from the aster is that the radiating arms are bundled actin and the length scales are usually larger. Previous studies have reported the transition of actin asters or clouds to stars in the presence of the actin bundling protein filamin [Haviv et al., 2006, Ideses et al., 2008, Vignjevic et al., 2003]. Additionally, the solution stars also showed growth of the radiating bundles with time, in accordance with our observations of the membrane-associated actin stars (Figure II.10, yellow arrows).

Interestingly, methylcellulose is also known to induce a membrane association of actin filaments due to its crowding effect (example- [Murrell and Gardel, 2012]). With slow diffusion and the flattening of actin filaments against the membrane, we could get improved imaging of asters. In Figure II.11, we follow the changes in a single aster with time. The signal is more diffused in the beginning with faintly visible branching along the edge. Since distinguishing between bundles and filaments is difficult in this set up, a clear demarcation of the aster to star transition is unlikely. Some bundles can however be

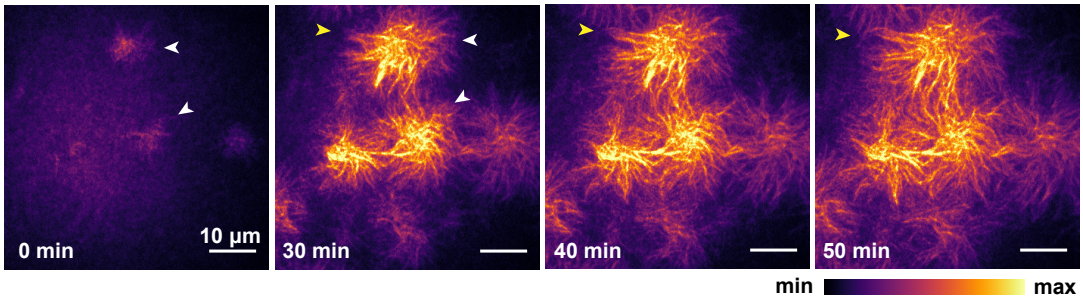

Figure II.10: Actin asters transition to stars under the influence of bundling
White arrows indicate asters that appear as stars at later points. Yellow arrows highlight a bundle that grows with time.

seen in the "600 sec" frame. The asters in this sample eventually form large stars as well (Supplementary figure A.1).

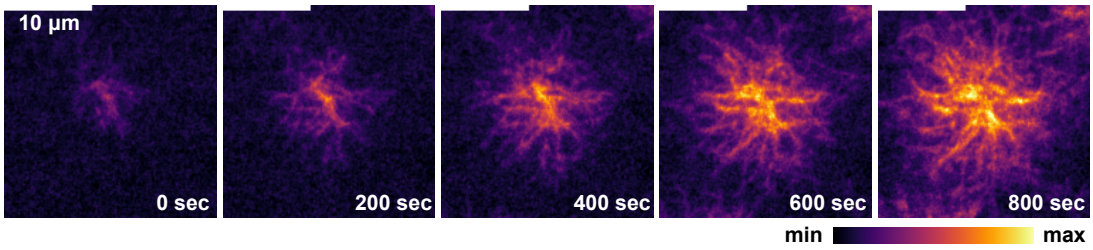

Figure II.11: Growth of a single aster can be observed in the presence of methylcellulose
The initiation and progression of an aster is followed. Time is an internal reference here. The first bundles are visible at 600 sec. Image processing was used to highlight features (see Appendix).

Further, we were also able to capture individual events of filament growth from a nucleation seed (Figure II.12). Distinct branches could be observed as the fractal-like growth of actin filaments proceeded (white arrows). The outward orientation of the branches confirms that, at least in the influence of crowding, the orientation of the filaments in our structures was as previously described for actin asters in solution [Haviv et al., 2006].

An aster to star transition in *in vitro* systems is considered analogous to a lamellipodia to filopodia transition observed in migratory cells. It was long known that Arp2/3 was required for building both structures, but the idea of parallel, bundled actin emerging from branched architecture was counterintuitive. A recent paper describing Arp2/3-dependent self-organization of actin *in vivo* also revealed actin asters and stars close to the membrane through super-resolution microscopy [Fritzsche et al., 2017]. What distinguishes our experiments from previous *in vitro* studies, and arguably makes it an even more relevant approximation of biology, is that the formation and transition of Arp2/3-dependent actin

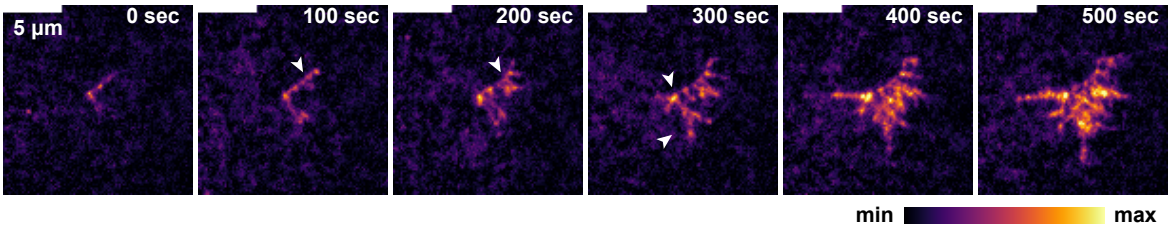

Figure II.12: Nucleation of an aster from a single seed is observed in detail
Branching events are highlighted with white arrows. Image processing was used to highlight features (see Appendix).

structures is observed in a quasi-2D system against a lipid bilayer. This characteristic makes our reconstituted network closer to the actin cortex, where both the structural transitions have been reported in cells.

3 Myosin activity induces turnover in a dynamic minimal cortex

As mentioned in section 1, one of our main aims for this project was to elucidate the role of myosin in actin turnover in this minimal cortex. With our characterization of dendritic actin growth in the previous section, we proceeded to optimize conditions such that inherent heterogeneities in the assembly process are minimized. The effect of myosin on actin patterning could then be studied independently.

3.1 Optimization of assembly conditions for homogeneous actin networks

As described in section 2.2, assembly of membrane-associated dendritic networks proceeded reliably and fairly homogeneously with our usual reaction mix containing 1 µM actin and 10 nM Arp2/3 in the wider chambers. Longer observations of such assembly showed that increase in surface actin intensity was fast with a lag in the beginning, characteristic of autocatalytic processes (Figure II.13). The initiation was almost instantaneous upon mixing, so the initial lag was often missed while setting up image acquisition.

We compared this growth process with reactions where either VCA or Arp2/3 had been excluded to better understand the molecular dependencies of the actin growth (Figure II.13, II.14). In the full reaction, i.e. including both VCA and Arp2/3 complex, dense

actin growth resulted in appearance of bundle-like organization with time (Figure II.14, lower panel). Interestingly, considerable growth was also observed in the absence of the Arp2/3 complex, though much slower and with a sparser meshwork (Figure II.14, middle panel). As expected, in the absence of VCA, no actin was observed on the lipid bilayer because VCA is required to bridge the membrane association of both monomers and filaments. Adding VCA to this sample immediately resulted in increased surface actin intensities (Figure II.14, lower panel). Despite some variability between samples, the trend in actin assembly in different conditions was conserved, with the full reactions tending towards saturation at later time points (Supplementary figure A.2). VCA intensity on the membrane remains considerably stable during the growth process (Supplementary figure A.3). The mobility provided by the membrane appeared to be essential for the actin network growth we observed, as holes in the lipid bilayer were largely devoid of actin, even though VCA accumulated there (Supplementary figure A.4).

Altogether, the fast dynamics of dendritic actin growth seemed suitable for counterbalancing myosin activity. Assembly was allowed to proceed for considerably longer periods of 1-2 hours for myosin experiments. The aim behind this was to saturate the growth process and minimize the amount of free monomers in the sample at the end of actin assembly.

Muscle myosin-II motors were allowed to assemble into filaments by incubation in a suitable buffer for 10 minutes before adding them to the pre-assembled actin network. TIRF microscopy was used for observation, as in the previous section.

3.2 Different length scales of actomyosin contraction in the dynamic minimal cortex

Consistent with previous studies on disordered actin networks on membranes [Koster et al., 2016,Linsmeier et al., 2016,Murrell and Gardel, 2012,Vogel et al., 2013], addition of myofilaments resulted in contraction in the membrane-bound dendritic network (Figure II.15)[7]. The initial stages of myosin contraction showed bundling of actin filaments, followed by a compaction of the actin network. As the actin condenses during the compaction, rips in the network can be observed. Finally, a decreased actin intensity indicated breakdown of the actin network. Myofilaments were seen associated with the bundles as well as the condensed actin (white arrows, lower panel). They, however, accumulated on the membrane even as the actin was lost. This process is specific and requires ATP as lack of available

[7]Images shown here have been background subtracted to highlight features.

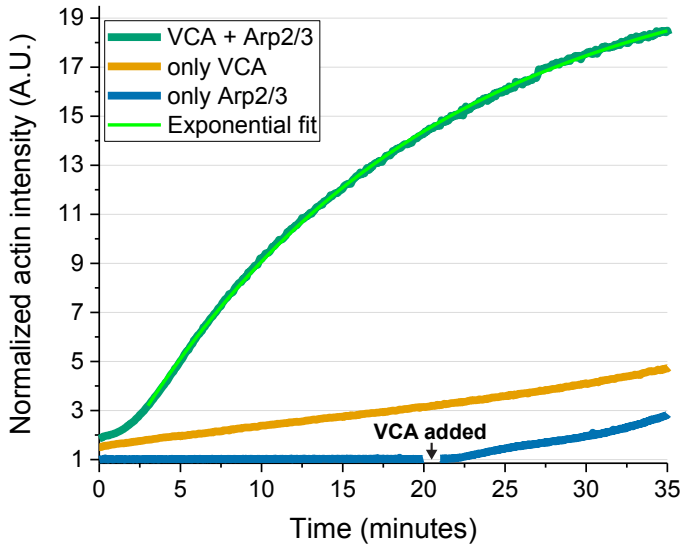

$y = y0 + A*\exp\hat{}(R0*x)$

y0	21.7259 ± 0.04272
A	-21.81604 ± 0.02867
R0	-0.05446 ± 2.69964E-4
Reduced Chi-Sqr	0.00782
R-Square(COD)	0.99958
Adj. R-Square	0.99958

Figure II.13: Effect of VCA and Arp2/3 on actin network assembly
Time profiles of actin intensity on the SLB in different reactions

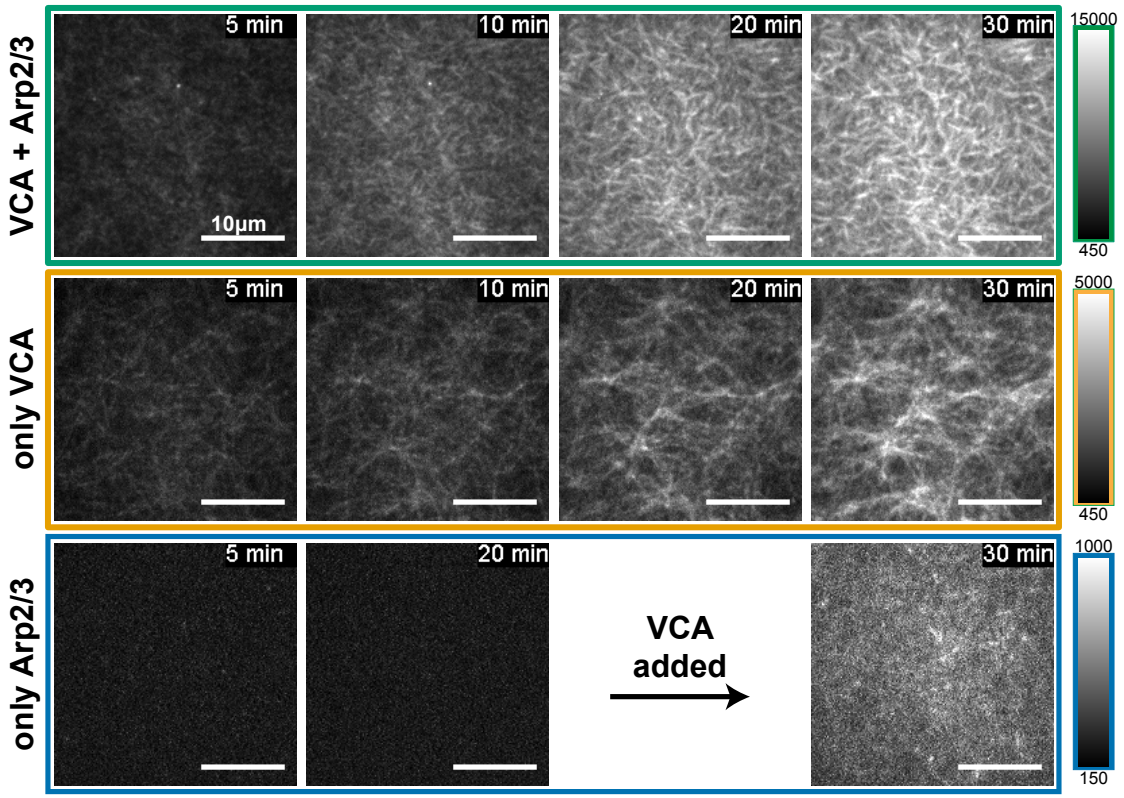

Figure II.14: Effect of VCA and Arp2/3 on actin network organization
Images corresponding to the time profile in Fig. II.13. Intensities are set differently between reactions to highlight actin organization

ATP stalled the process at bundling (Supplementary figure A.5). The bundles disappeared very quickly once new ATP was provided by the addition of an ATP regeneration mix.

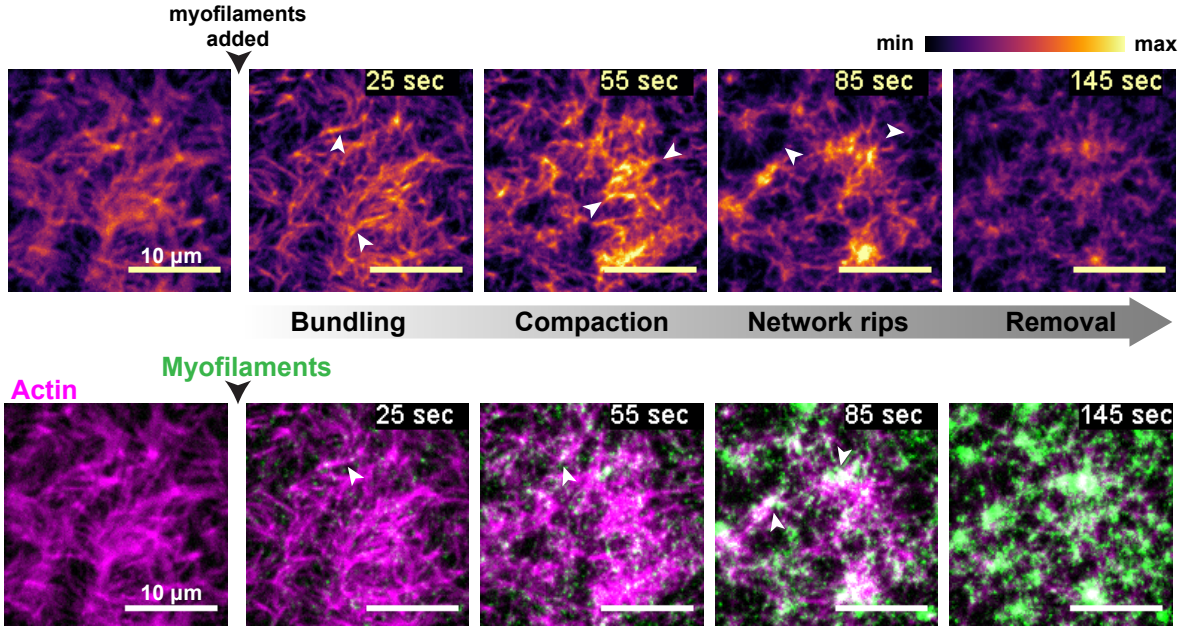

Figure II.15: Stages of myosin contraction in dendritic actin networks

Interestingly, we saw two distinct modes of initial actomyosin contraction in our experimental conditions. The condensation of actin, and therefore the rips in the actin network, occurred over different length scales. In some samples, the contraction foci are distributed homogeneously with short length scales (9.1±2.2 µm) and less pronounced condensation. In other cases, we observed a distinct multistage coarsening process, with dense actin condensates distributed over a much larger length scale (20.3±7.4 µm)[8]. Further fusion of these condensates could be observed occasionally. Figure II.16 shows representative images for both these modes and the length scales calculated as nearest neighbor distance of contraction foci from four samples each. A similar multistage coarsening has been described in other studies on disordered actin networks, both membrane-associated and in solution [Backouche et al., 2006, Kohler et al., 2011, Soares e Silva et al., 2011, Murrell and Gardel, 2012, Linsmeier et al., 2016, Vogel et al., 2013, Stam et al., 2017, Smith et al., 2007].

Length scale of actomyosin contraction is a complex phenomenon regulated by many variables such as membrane adhesion and filament cross-linking [Murrell and Gardel, 2012]. In dendritic actin networks, we found corresponding dependencies by manipulating the surface density of VCA, Arp2/3 concentration, myosin concentration and introducing branch

[8]Differences are significant by ANOVA analysis

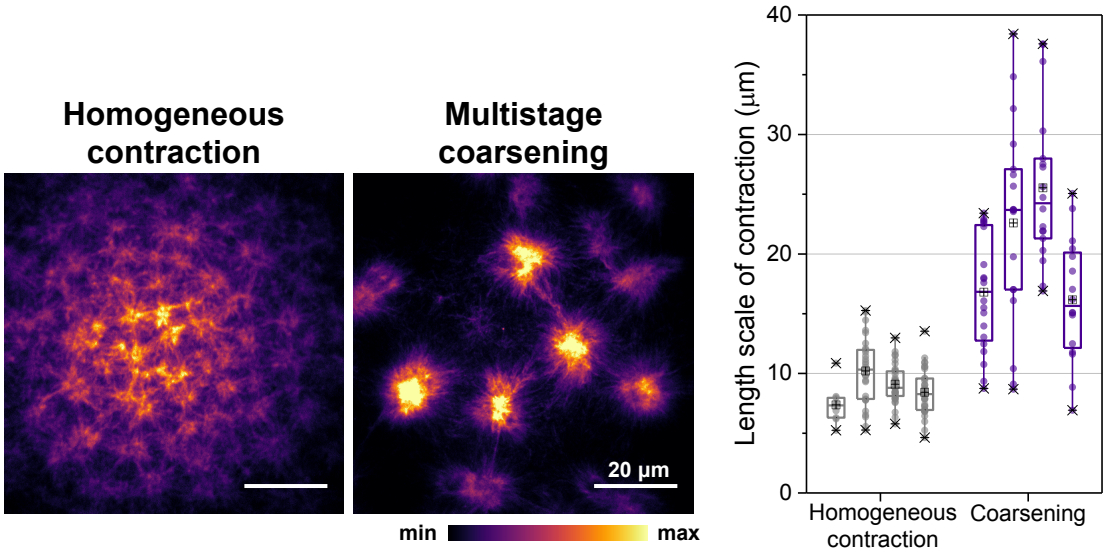

Figure II.16: Two modes of actomyosin contraction

capping. Higher mol% of DGS-NTA in the lipid bilayer resulted in lower length scales (6.0±1.2 µm, Figure II.17A)[9], presumably because the corresponding increased VCA surface density will lead to an increase in the net adhesion of the actin network to the membrane. When branching density was increased by growing the actin networks in higher Arp2/3 concentrations, the observed length scale decreased (Figure II.17B). The lower Arp2/3 concentrations (0, 5, 10 nM) had more variability due to incidences of coarsening. Coarsening also appeared to occur more frequently at higher myosin concentrations (Figure II.17C). Finally, we included the capping protein CapZ during network assembly[10].Capping increases branching density at the expense of filament elongation, resulting in shorter filament lengths. We observed no discernable foci in the presence of capping (Figure II.17D), which could indicate that the filaments are too short to form foci of observable length scales. Altogether, this analysis implied that net membrane adhesion and structural features of the actin network such as branching densities and filament length are crucial determinants of length scale of actomyosin contraction in this dynamic minimal cortex.

We hypothesized that our experimental conditions lie on a critical point in the complex phase space of factors affecting contraction length scales, thus giving rise to the bistable outcome. However, we favored these experimental conditions as the coarser contraction

[9]Differences are significant by ANOVA analysis
[10]CapZ data was acquired by Dr. Kristina Ganzinger

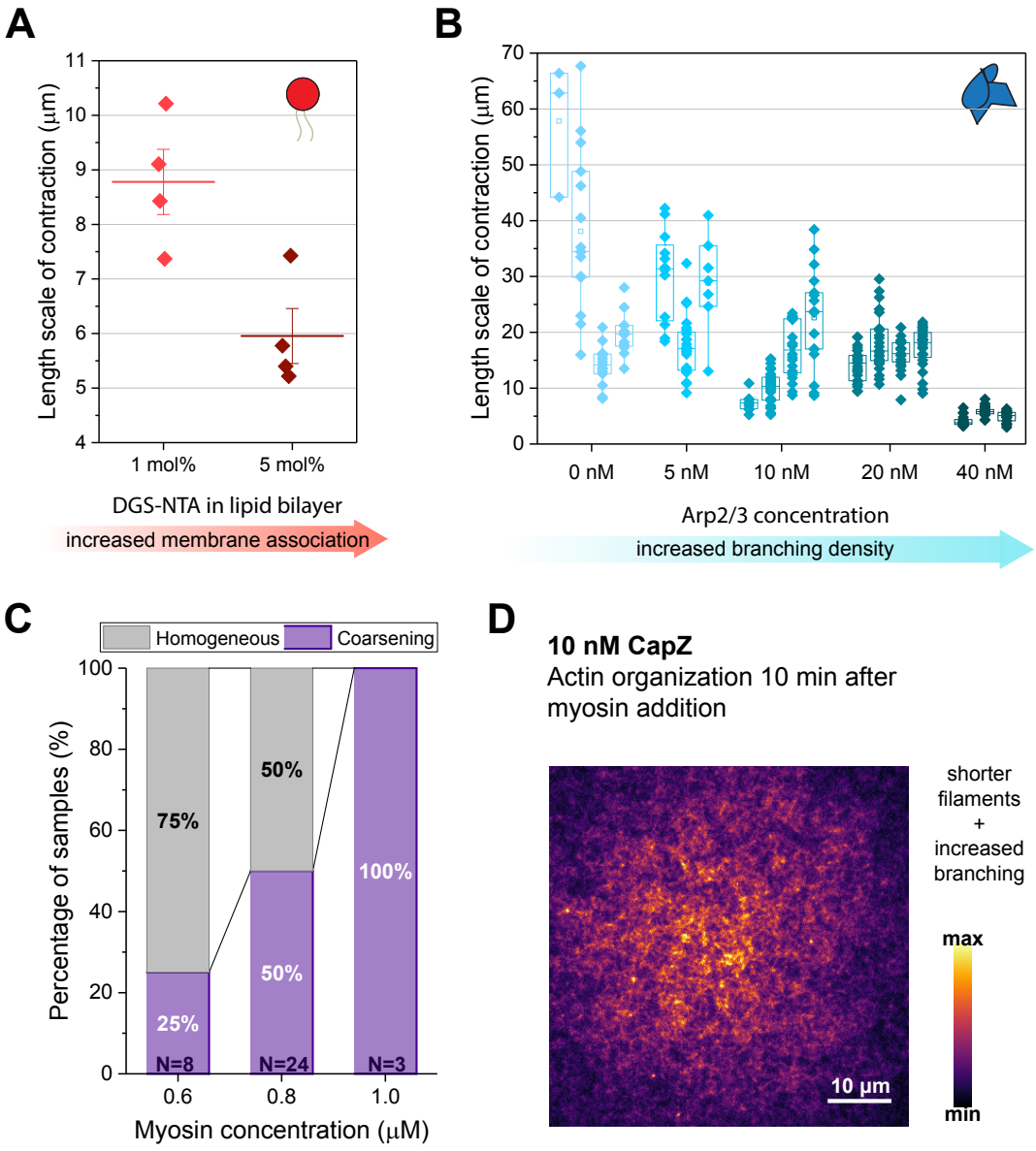

Figure II.17: Factors affecting length scale of contraction

provided a better contrast to investigate breakdown and redistribution of actin network upon myosin contraction, as described in subsequent sections.

3.3 Myosin contraction results in breakdown of actin network

Independent of the length scale of actomyosin contraction followed, a net loss of actin filaments was observed on the membrane after addition of myofilaments. An average profile of actin surface intensity in presence of myofilaments reveals that approximately 70 % of the

actin on the surface is lost within the first 10 minutes of contraction (Figure II.18). Myofilaments simultaneously accumulated on the membrane, as could also be seen in Figure II.15 (inset).

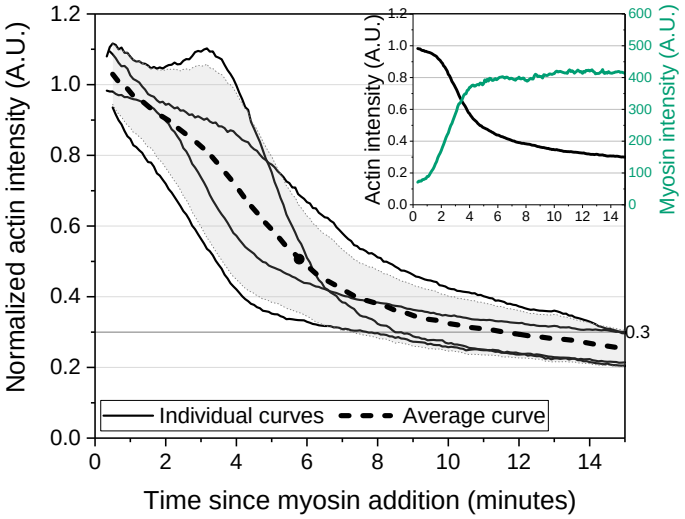

Figure II.18: Myosin activity results in reduced surface actin density
Time profiles from 4 experiments with homogeneous contraction. Inset shows corresponding myosin intensity changes for one of the curves.

The breakdown of actin was distinctly observed in the dense actin foci formed during coarsening. This is illustrated by the temporal progression of the radial intensity profile of actin and myosin in one of these foci (Figure II.19). Myofilaments also condensed with actin initially in these foci. Subsequently, a hollowing of the foci is observed, with the actin intensity at the core decreasing drastically, whereas the myosin intensity showed a minor reduction. This indicates that as contraction continues in the condensed actin, the actin filaments disintegrate rapidly under the stresses generated by the enriched myosin motors. Previous observations of filament fragmentation on membrane by myosin activity reinforce this notion [Murrell and Gardel, 2012, Vogel et al., 2013].

Individual events of filament or bundle fragmentation were difficult to observe in the dense network. However, as actin condensed into coarser foci, bundles of actin were occasionally observed distinctly linking the foci. As the contraction proceeded these bundles ruptured abruptly and recoiled, revealing the extensile stresses acting on them. Myofilaments were seen along the bundles, presumably responsible for cross-linking the actin filaments (Figure II.20 right, lower panel). This explicit shows one mode of filament breakage occurring during contraction in the dendritic network. Alternately, breaking of short filament segments could also be observed when the actin network was doped with

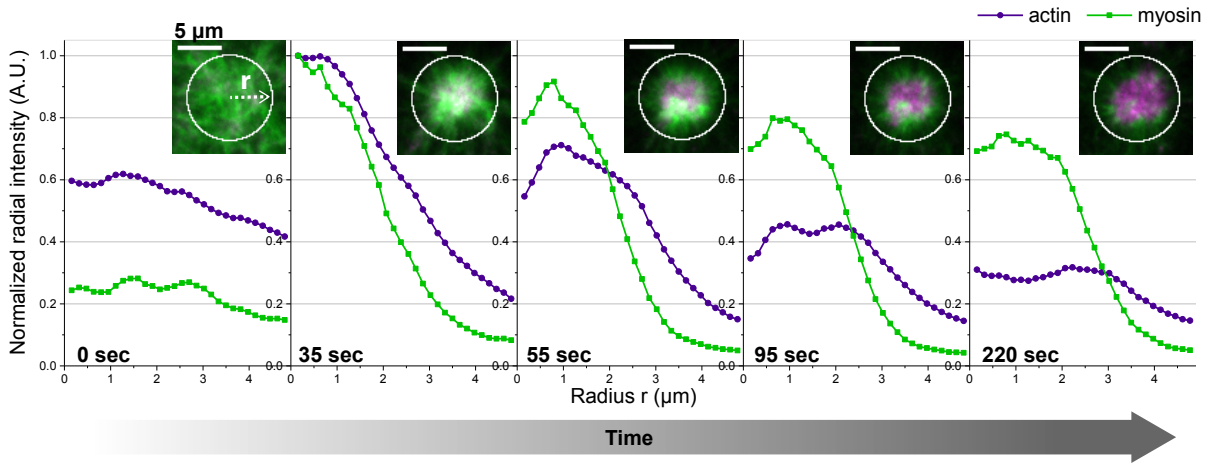

Figure II.19: Breakdown of actin filaments in contraction foci

monomers of a second label during assembly (Figure II.21). These short filaments were formed stochastically before the dilution of the labeled actin and were consequently only rarely observed.

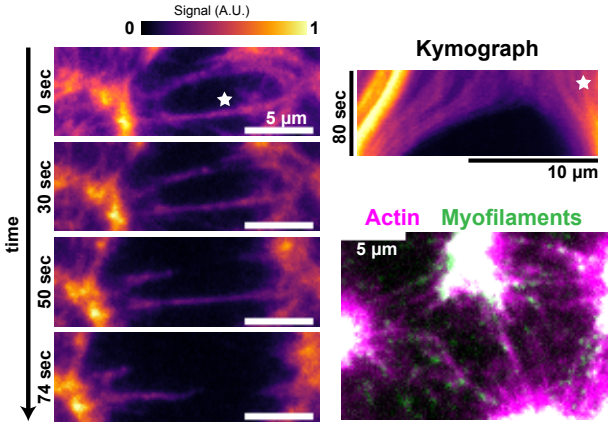

Figure II.20: Rupture and recoil of actin bundles during contraction

3.4 Redistribution of active network components restores homogeneous length scales

The stark contrast in actin distribution generated during the coarsening process also enabled us to observe phenomena, which are otherwise not visible during homogeneous contraction. In these instances, the actin distribution on the membrane recovered from the heterogeneity of coarsening and restored a seemingly uniform organization. In the graph

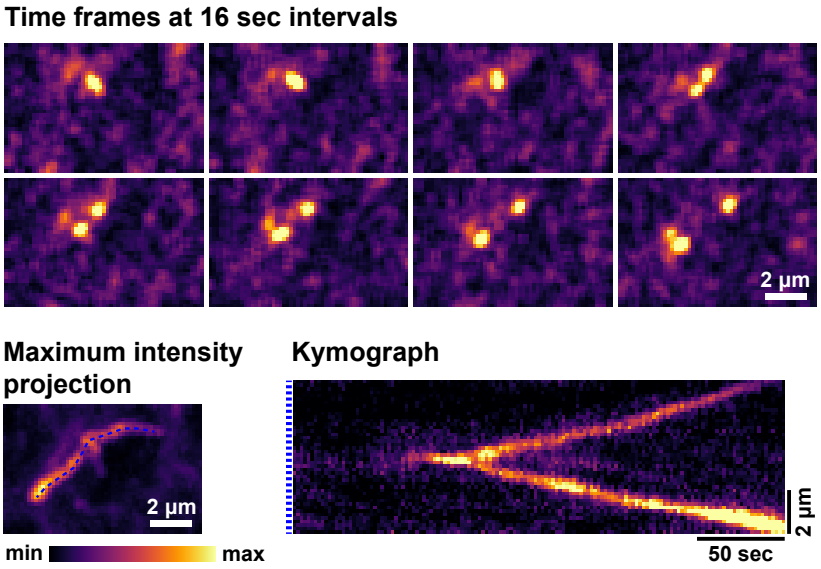

Figure II.21: Individual events of filament break

The actin mix was doped with 1:10000 of Alexa488-labeled actin to observe individual breakage events. A maximum intensity projection was used to trace the path of the filament fragments (blue dotted line) and a kymograph was plotted along this path to highlight the splitting event and the subsequent motion of the two fragments away from each other.

in Figure II.22, we use the Coefficient of Variance (CV)[11] of the actin intensity distribution as an indicator of the heterogeneity in the distribution of actin on the membrane in each time frame. The increase in CV coincides with the contraction process upon addition of myofilaments, peaking with coarsening (Figure II.22, images a-d). The CV then drops as the actin is redistributed and finally results in an actin distribution nearly as homogeneous as before the addition of myosin. The final heterogeneity in the system is comparable to that achieved when contraction proceeds homogeneously, as described in section 3.2 (Figure II.22, graph).

The restored uniformity in actin distribution can be attributed to two phenomena- the loss of actin from contraction foci and the recovery of actin filaments on the remaining regions of the membrane. These two processes occur simultaneously, as can be illustrated by plotting the changes in actin intensity in these two regions of the sample (Supplementary figure A.6). The loss of actin resulted from breakdown of condensed actin in the foci as explained in the previous section. The simultaneous reappearance of actin in other regions was accompanied by formation of new myosin foci in these parts (Figure II.23, white arrows). A kymograph of a stretch between two contraction foci shows that both actin

[11] Coefficient of Variance is the standard deviation divided by the mean of the distribution

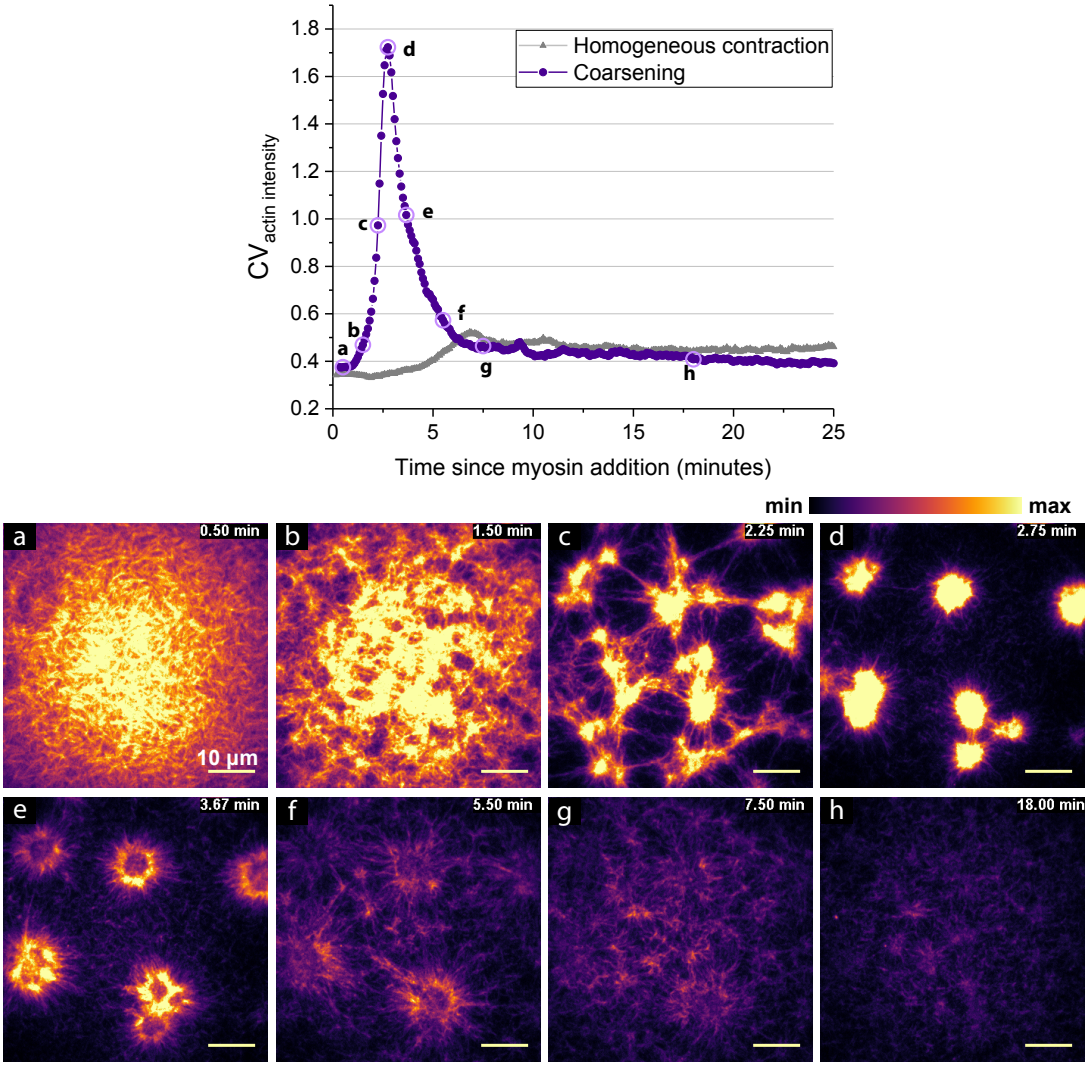

Figure II.22: Heterogeneity in actin distribution reverts after initial coarsening
Graph shows Coefficient of Variance of actin intensity plotted against time. The images corresponding to the encircled points in the graph are shown underneath.

and myosin appeared simultaneously as the new foci emerged between them (Figure II.24). The source of the material for growth of the new foci could not be distinctly discerned. However, both actin and myosin appeared to be exchanged with the neighboring foci (Figure II.24, white arrows). Myosin accumulated in the new foci with time (Figure II.24, middle image), whereas actin intensity remained stable (Figure II.24, right image). This observation, along with the previously noted slower reduction of myosin intensity in the foci (Figure II.19), suggests that the redistribution of myosin is much more limited than that of actin.

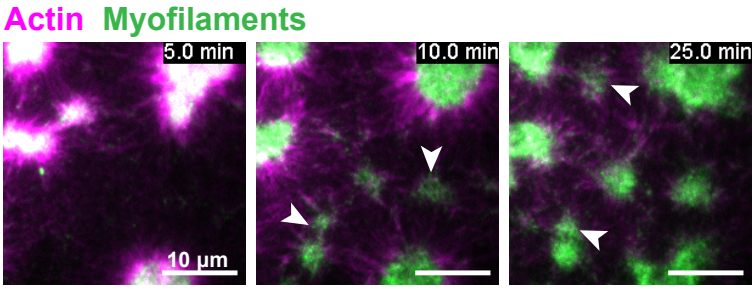

Figure II.23: Emergence of new actomyosin foci between the initial foci
White arrows highlight new foci. Time is counted from the addition of myosin

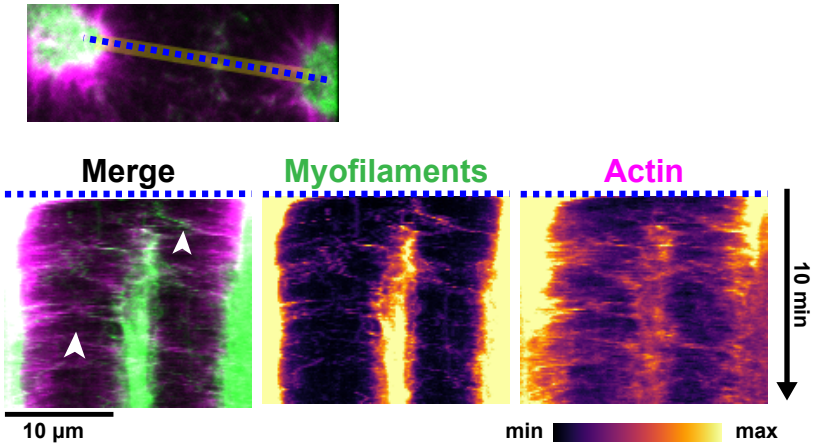

Figure II.24: Kymograph showing emergence of new foci
Kymographs were drawn from a track between two foci shown in Figure II.23 (dotted blue line). White arrows indicate some traces showing transfer of material. Individual kymographs for actin and myosin are shown with applied LUT to highlight details.

As can be expected, this reorganization resulted in a reduction of the length scales of contraction we previously measured during coarsening (Figure II.25). The final values approached those observed during homogeneous contraction (dotted line in graph), indicating that this actomyosin network has a favored length scale that is restored in spite of initial disturbances. The resultant distribution resembled a dynamic steady state with filament exchange between the foci observed for over an hour (Figure II.26). The late-stage foci thus appear to serve as local potential wells between the opposing forces acting in this active network.

In order to inspect whether new actin growth had a contribution to the recovery of actin, we also looked at the localization of the VCA on the membrane. Unlike myosin,

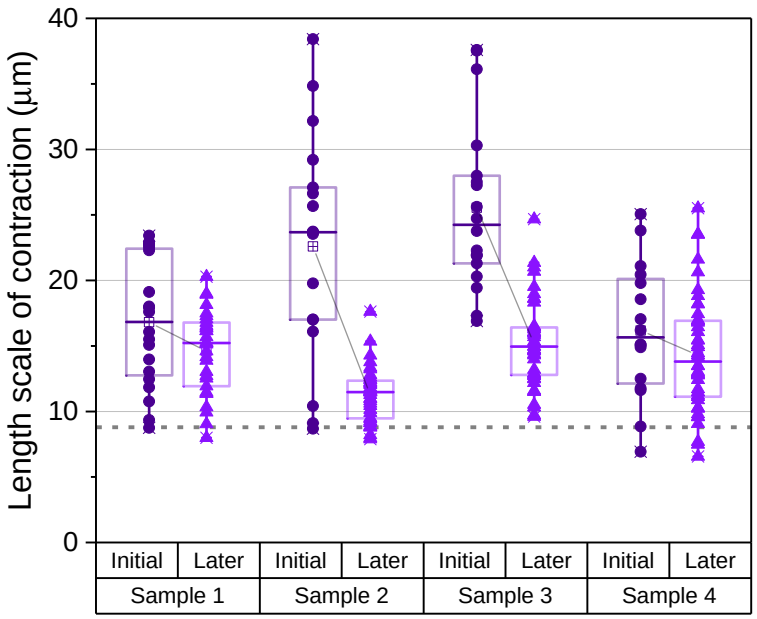

Figure II.25: Restoration of lower length scales after redistribution

Graph shows the change in length scales for 4 coarsening samples after redistribution. Dotted gray line marks the average value for homogeneous contraction

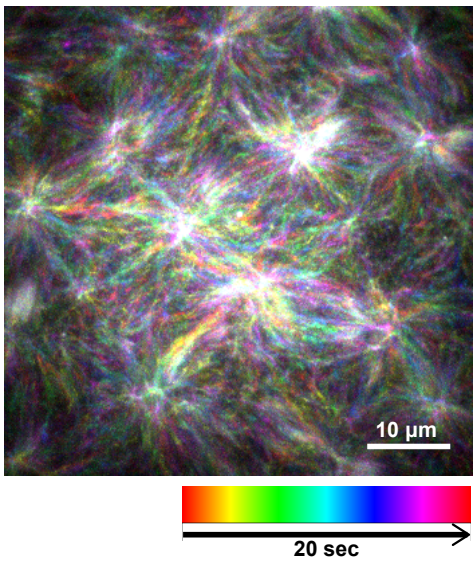

Figure II.26: Actin dynamics on the membrane 1 hour after myosin addition

Temporal color coding is used to show the dynamics of actin in a 20 second window. Static regions will appear white in this color code due to overlap of all colors. Actin bundles appear to keep moving between the late-stage foci.

VCA localization on the membrane is stable during contraction (Figure II.27A) and unaffected by coarsening (Figure II.27B, left panel). Interestingly, VCA also enriches in the late-stage actomyosin foci formed on the membrane, raising the possibility of enhanced polymerization at these sites (Figure II.27B, right panel).

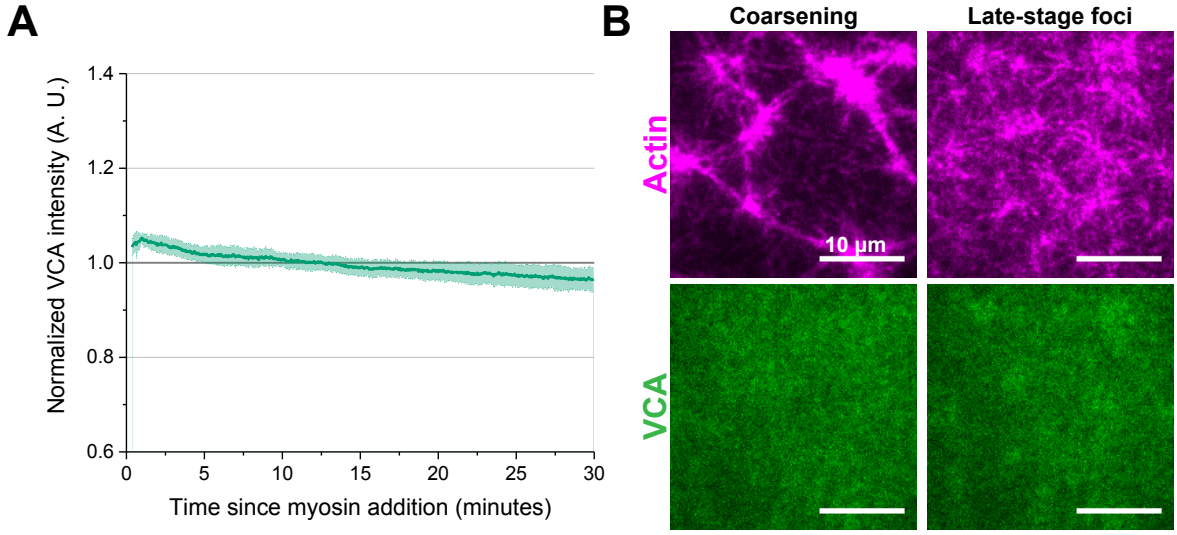

Figure II.27: Organization of VCA during myosin activity
Note that the graph axis does not start at zero to indicate that small changes in VCA intensity are observed.

On an average, not much increase was observed in actin intensity on the membrane after the initial reduction during contraction (Figure II.28). A considerable proportion of the actin network that is lost from the surface appeared as aggregates in solution (Figure II.29A), reminiscent of previously described solution condensates (Soares e Silva et al., 2011). The shape dynamics of these blobs indicated that myosin is active in them (Figure II.29B), possibly trapping the actin filaments by cross-linking and recapture.

3.5 Actin undergoes turnover in the dynamic minimal cortex

In order to investigate the role of myosin-driven fragmentation in actin filament turnover, we asked whether the network components released during myosin contraction can be reused for new polymerization. Excess monomers were washed off from the actin network before addition of myofilaments. After the initial fragmentation and redistribution, myosin-II activity was blocked using the inhibitor blebbistatin and actin growth was followed as usual. We found that surface intensity of actin increased gradually after the inactivation of myosin (Figure II.30), confirming that myosin breaks down the actin network to the level of

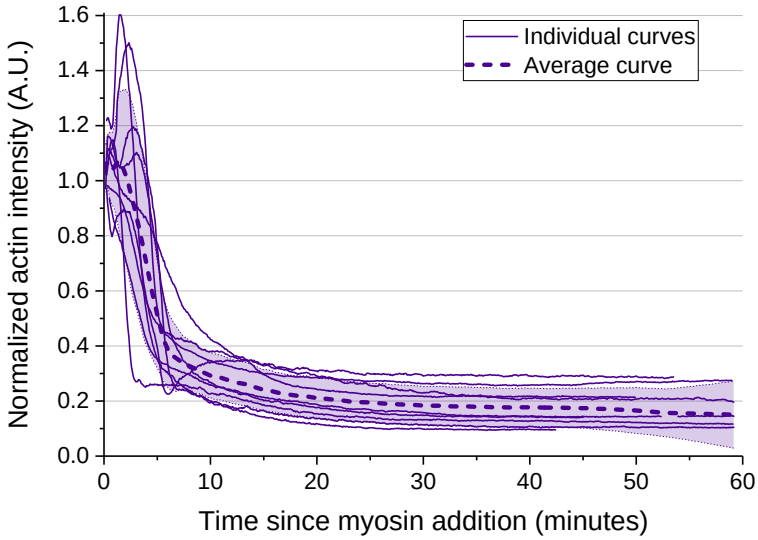

Figure II.28: Myosin activity leads to a net loss of actin from the membrane

Over longer observation periods, the net actin intensity on the membrane remains unchanged after the initial decrease upon myosin addition.

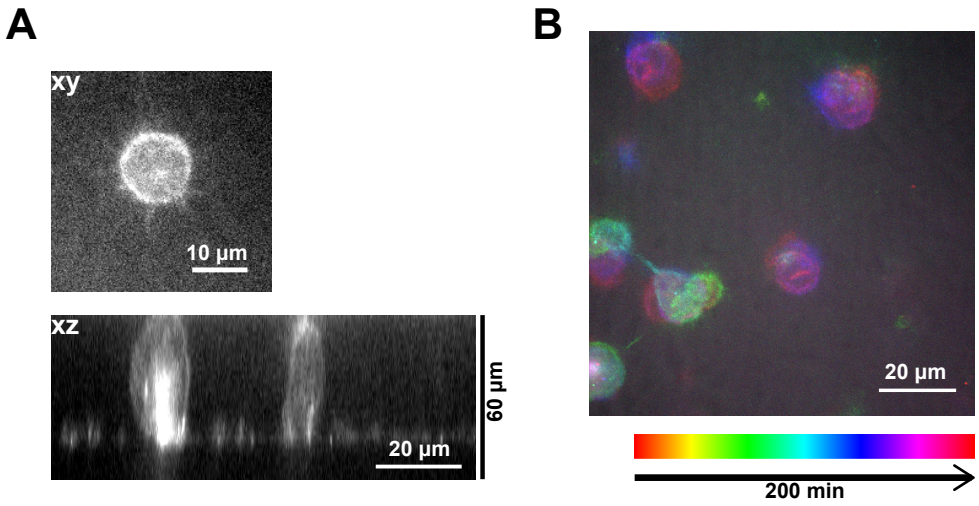

Figure II.29: Actomyosin aggregates in solution

A. An aggregate in solution in shown in xy and xz planes. B. Temporal color code shows dynamics of the solution aggregates in a 200 minute interval.

monomers which are then competent for new polymerization. Interestingly, if blebbistatin was added before myosin could break down the actin network, no increase was observed (Figure II.30, dotted line). The intensity, in fact, decreased from apparent bleaching. This indicates that the breakdown is needed to facilitate new actin assembly.

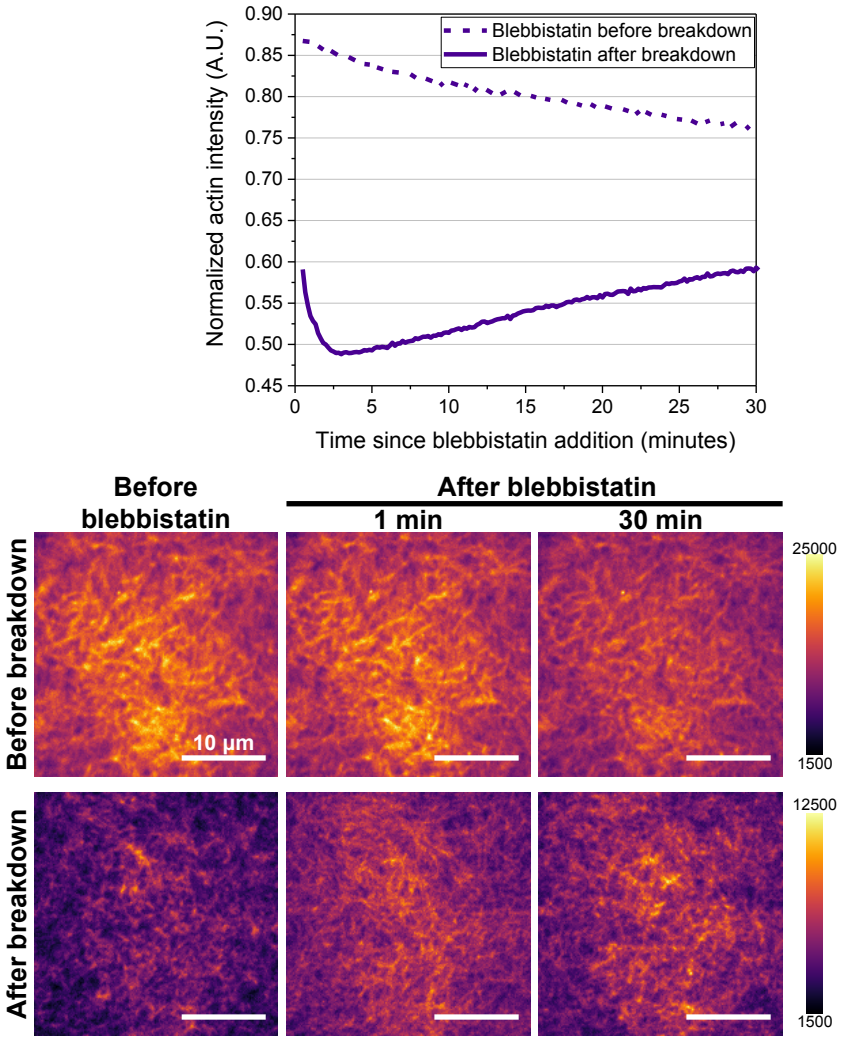

Figure II.30: Actin intensity increases when myosin activity is blocked after network breakdown

Graph shows the change in actin intensity after blebbistatin is used to block myosin activity. Intensities are normalized to values before addition of myosin. Each line represents a single sample, with blebbistatin added either before or after breakdown of actin by myosin. Intensity settings are set differently between conditions to highlight structures, but are comparable within a condition.

To follow the formation of new filaments in the presence of myosin activity in greater detail, we designed a pulse-chase type experiment with two differently labeled actin monomers

(Figure II.31). Actin network was assembled as usual with 10% Alexa568-labeled actin (Label1). Excess monomers in solution were then removed by extensive washing. Along with myofilaments, additional actin monomers were added to the system, 10% of which were labeled with Alexa488 (Label2). Additional Arp2/3 complex was also provided so that the process of reassembly is not limited by its availability. We then observed the actin on the membrane for mixing of the two labels.

We observed that the proportion of Label2 in the membrane-associated actin increased over time, after the initial breakdown of the Label1-network (Figure II.32). This gradual change confirms that the actin filaments observed on the membrane are undergoing constant turnover in the presence of myosin activity. The steady increase in Label2 intensity on the membrane is accompanied by a gradual decrease in Label1 intensity, as can be better observed in the kymograph. The difference in the rates of change is probably due to the increase in total amount of actin on the membrane in this period and the total amount of Label2-actin in the system being higher.

In the intermediate stages of label mixing, filaments with uniform distribution of Label1 show a speckled occurrence of Label2 (Figure II.33). Such filaments of mixed, interspersed labeling would only be observed if monomers of both Label1 and Label2 are available for polymerization, i.e. only if Label1 monomers were released from the pre-assembled network upon myosin contraction. Since the actin on the membrane appeared bundled in the presence of myosin, individual filaments cannot be distinguished. However, single pixel line profiles along two distinct bundles show that the intensities of the two labels appear to be anti-correlated (Figure II.34). This supports the idea that the filaments we observed on the membrane have an interspersed distribution of monomers of both labels.

3.6 Preliminary results from non-muscle myosin-II

The experiments described so far in this section were performed with myosin-II purified from rabbit muscle. This was purely due to practical considerations as muscle myosin purifications result in very high yield. On the other hand, members of our lab have struggled with the efficient replication and establishment of protocols for the purification of myosin-II from non-muscle sources, such as *Dictyolstelium*. However, we succeeded in purifying enough protein to be able to replicate a few experiments in this section with non-muscle Myosin-II (NMM-II)[12]. A detailed purification protocol is described in the appendix.

[12]Results are preliminary, with only one sample analyzed for each condition.

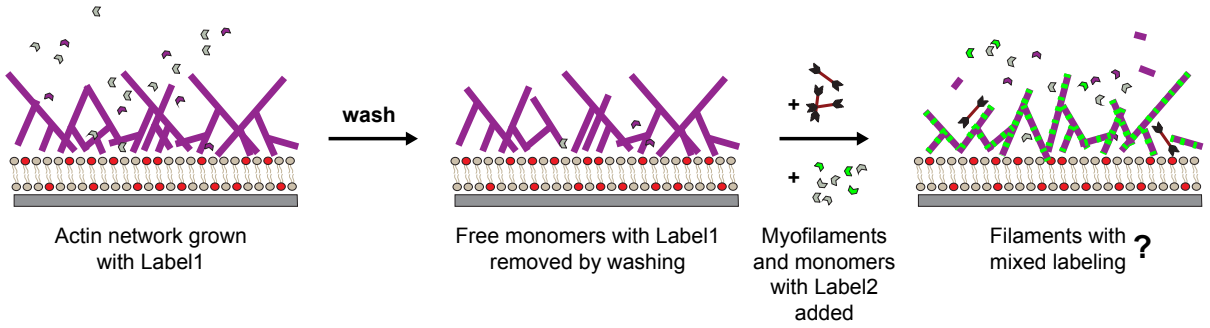

Figure II.31: Schematic of experiment to investigate actin turnover

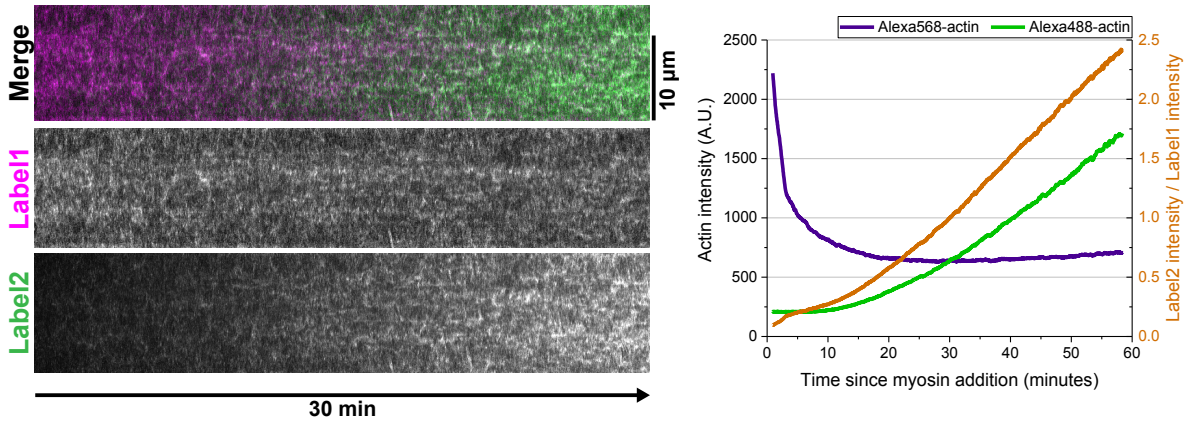

Figure II.32: Turnover of actin filaments observed in dual labeling experiment
Kymograph shows change of actin on the membrane from Label1 to Label2 over a 30 minute period. The graph plots the intensity changes as well as the ratio of label intensities (right axis).

Interestingly, contraction process with NMM-II showed many similar features to the muscle myosin (Figure II.35). Actin filaments bundled in the initial phases of contraction and a net loss of actin intensity was observed as the process proceeded, indicating that breakdown of actin networks also occurs during NMM-II activity. Contraction, however, always proceeded with a homogeneous length scale due to which breakdown and redistribution could not be distinctly observed in detail. The yield and concentration of purified NMM-II was relatively low. We were therefore unable to test if large scale coarsening could be induced by higher concentrations of the motor[13].

Some features were distinctly different in the case of NMM-II activity, when contrasted with muscle myosin. The contraction foci appeared as very sharp points, compared to

[13]These experiments were done with 0.5 µM non-muscle myosin-II, as opposed to 0.8 µM for most experiments with muscle myosin

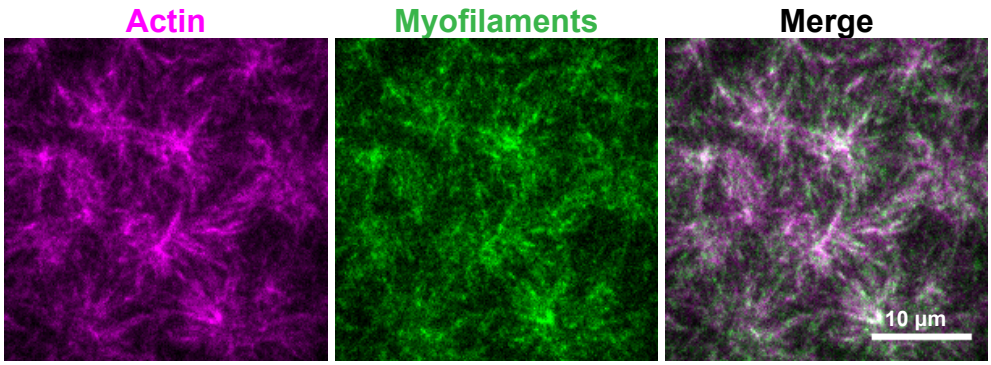

Figure II.33: Filaments of mixed labeling are visible in intermediate stages

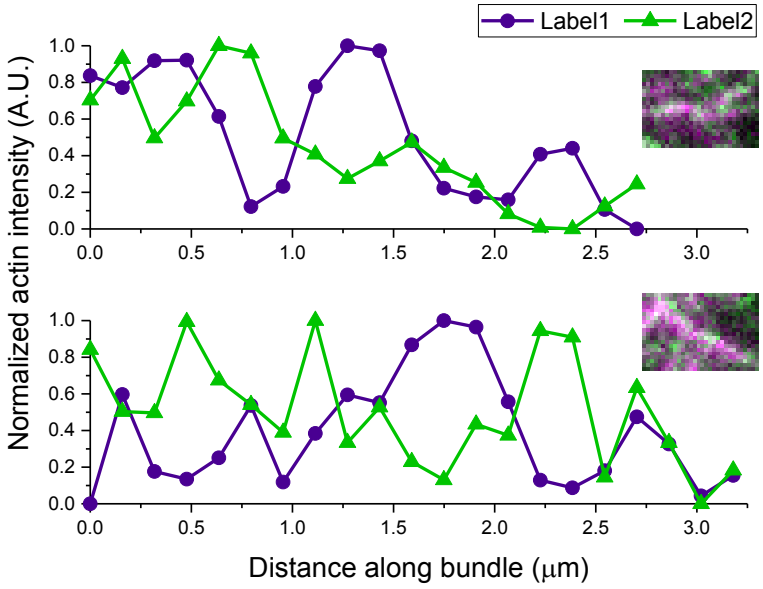

Figure II.34: Line profiles of intensities along the length of two bundles from Figure II.33

the actin condensates previously described for muscle myosin in section 3.2. Additionally, instead of a steep drop in actin intensity on the membrane, a slower decrease was observed for NMM-II (Figure II.36A). Figure II.36B shows that length scales were lower than that observed for homogeneous contraction with muscle myosin (value marked with dashed gray line).

Most strikingly, in agreement with muscle myosin results, a dynamic exchange of filaments between the foci could be observed long after the addition of the motor (Figure II.37). This suggests that a dynamic steady state with constant turnover of filaments could also

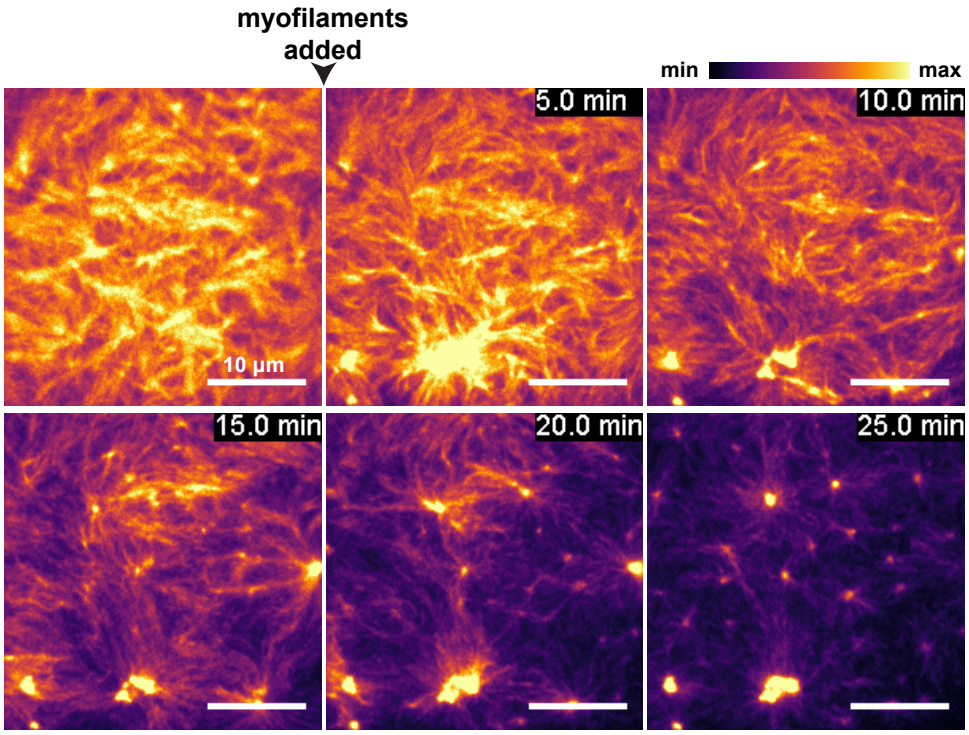

Figure II.35: Effect of NMM-II contraction on membrane-associated dendritic actin network

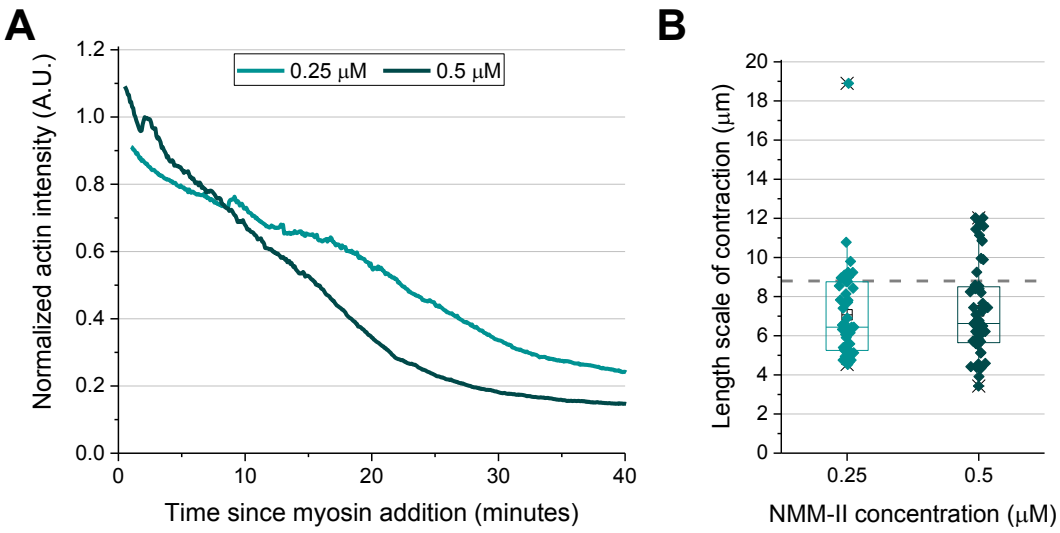

Figure II.36: Characterization of NMM-II contraction

A. A slower decrease in surface actin intensity is observed B. Length scale of contraction calculated as nearest neighbour distance

be established with NMM-II. However, this notion can only be ascertained in the future with further experiments and improved yield of NMM-II purification.

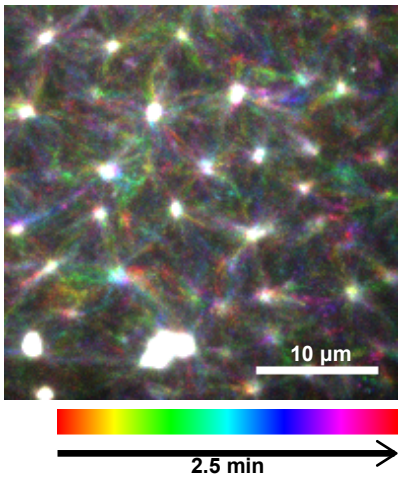

Figure II.37: Actin filament dynamics 30 minutes after addition of NMM-II
A. Temporal color code shows dynamics of actin on the membrane in a 2.5 minute interval, 30 minutes since the addition of 0.5 µM NMM-II. Foci appear white as intensity there is largely static

4 Discussion

This study explores the bottom-up reconstitution of a dynamic minimal cortex, where the process of branched actin network assembly coexists and counterbalances disassembly by myosin motors. Firstly, we showed that the mechanism of Arp2/3-dependent branching itself provides a strong positive feedback, which can lead to the self-organization of actin patterns on the membrane, even without motor activity. Secondly, the introduction of actomyosin contractility results in the formation of an emergent dynamic steady state in this minimal cortex, with the actin undergoing continuous turnover. We, therefore, present the first explicit demonstration that myosin can contribute to recycling of actin network components.

4.1 Arp2/3 facilitates actin self-organization in membrane-associated networks

The effect of motor activity has always predominated the discussion on pattern formation in actin networks. While the autocatalytic behavior of branched actin growth has been

thoroughly demonstrated through biochemistry, the actual impact of it on self-organization of cortical actin is not well understood. One reason for this is that the actin structures in a cell are controlled by many redundant pathways of regulation. The genetic manipulation of a certain pathway often results in triggering compensatory mechanisms, confounding a clear understanding of cause and effect in cell studies. A second reason is that the actin cortex, being only a few microns in thickness, is not particularly amenable to light microscopy. A recent study successfully demonstrated some of the actin structures long predicted by *in vitro* and *in silico* analysis, by using a sophisticated super-resolution imaging approach [Fritzsche et al., 2017].

While countless studies have used Arp2/3-based nucleation in combination with a Nucleation Promoting Factor (NPF) to elucidate various aspects of actin assembly, our study is distinct in its design. The key distinguishing features, with respect to investigation of self-organization by assembly, is that TIRF microscopy enables us to provide microscopic details of fractal-like actin assembly on membranes. Most previous studies have focused on these reactions in bulk [Backouche et al., 2006, Haviv et al., 2008] or a mesoscale description on surfaces like beads [Bernheim-Groswasser et al., 2002, Kawska et al., 2012] or vesicles [Giardini et al., 2003, Pontani et al., 2009, Liu and Fletcher, 2006]. Where higher resolution analysis is attempted [Reymann et al., 2012], the significance of the membrane as a dynamic scaffold is overlooked. The growth processes we observed in our experiments depend on the mobile substrate that a lipid bilayer provides (Supplementary figure A.4). It can be envisaged that since fractal branching benefits from a dynamic capture and dissociation of VCA by actin filaments, a mobile pool of the VCA increases its catalytic action.

These features have enabled us to elucidate self-organization of actin patterns on a membrane in dendritic networks. We found, as expected, that Arp2/3 is essential for aster-like actin growth on membranes and the extent of this heterogeneity can be manipulated by increasing filament access on the membrane or capping. While capping is commonly observed in cellular actin networks, regulation of filament-membrane association could indirectly be brought about by many pathways. For instance, even myosin activity described in the latter half of this project could locally increase availability of filament fragments. A motor-independent means of regulating cytoskeletal structures could allow cells to manipulate local form, uncoupled from stress-generation. In fact, the autocatalytic dendritic network assembly itself can generate forces on membrane [Giardini et al., 2003, Carvalho et al., 2013a], providing a bimodal regulation of critical cortical features.

The transition between actin structures depending on filament-filament adhesion is another important result in our study. Bundling-induced aster to star transition is considered to be the equivalent of the structural changes that dynamically regulate lamellipodia and filopodia structures on the leading edge of a migratory cell. Since filopodia are highly polar bundled structures, whereas lamellipodia are flat, disordered meshes, this transformation has been puzzling. Studies on beads and in solution have shown that branch actin networks can transform to polar bundles in the presence of bundling proteins like fascin [Haviv et al., 2008, Ideses et al., 2008, Vignjevic et al., 2003]. However, this transition has so far not been reported on a mobile lipid surface; where it actually localizes in the context of a cell. We confirmed the formation of stars with bundling as well as the subsequent growth of the radiating arms. The orientation of filaments in membrane-associated asters appears to be similar to that observed in solution asters, as opposed to beads. However, a comparison of the actual images indicates that the concentration of actin in the centre is much less pronounced on the membrane. The core also appears to be less sharply defined in the actin stars. Since we have validated the behavior of our quasi-2D system to have similarities with the 3D system, it would be interesting to further delve into the differences to understand the role of the membrane better. Our set up is amenable to both detailed manipulations as well as higher resolution analysis to be able to address this factor in the future.

4.2 Myosin activity induces turnover in a dynamic miminal cortex

Our study further proceeds to provide a direct demonstration of the role of myosin activity in actin network turnover. The key distinguishing feature of the minimal actin cortex described in this study is the coexistence of catalytic actin polymerization with the contractile activity of myosin. This enabled us to demonstrate all essential aspects of filament turnover in our system- 1) the disassembly of pre-existing actin network, 2) the redistribution of released network components, and 3) the re-use of these components for new network assembly (Figure II.38).

On a lipid bilayer, fragmentation of individual actin filaments by myofilaments, in isolation or within a dense network, has been demonstrated [Vogel et al., 2013, Linsmeier et al., 2016, Murrell and Gardel, 2012]. However, the breakdown and release of membrane-bound actin after initial compaction was presumably impaired by strong membrane adhesion of the actin filaments or crowding agents in solution. In contrast, only the nucleation promoting factor (VCA) is firmly bound to the nickelated lipids in the membrane in our system.

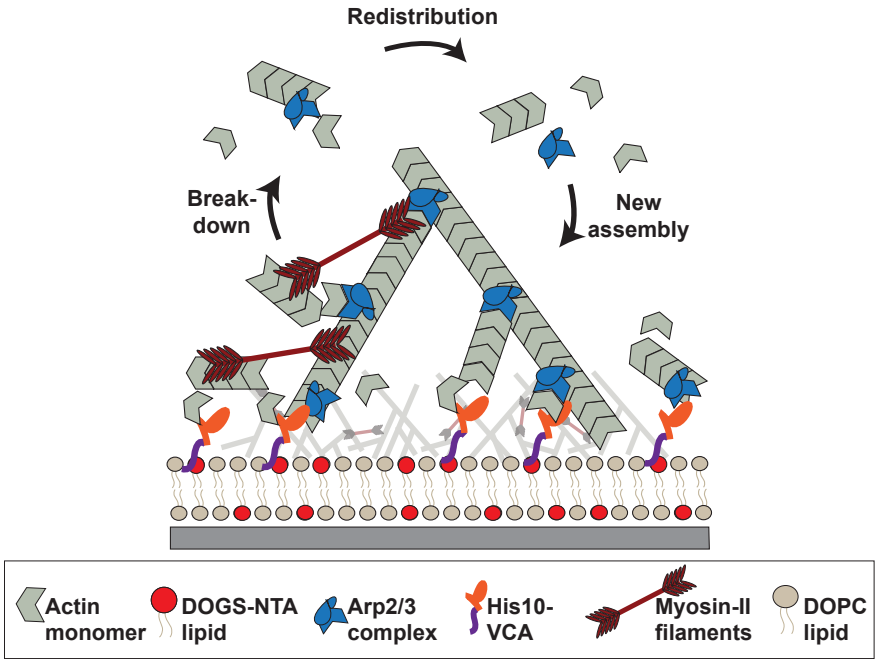

Figure II.38: Schematic depicting the three essential aspects of network turnover observable in the dynamic minimal cortex

The membrane association of the actin, resulting from the cumulative effect of multivalent interactions between the actin filaments and the VCA, is persistent but dynamic. Disassembly could similarly be observed in dendritic networks adhered to a glass surface via related nucleation promoters [Reymann et al., 2012]. Condensates in solution have also reported a hollowing of the actin core [Soares e Silva et al., 2011]. This set-up is a reasonable approximation of cellular environments, where proteins linking actin networks to membrane undergo fast turnover [Fritzsche et al., 2014], making the association highly dynamic.

Lack of surface adhesion also aids observation of redistribution, as has been previously demonstrated by the emergence of a dynamic steady state in solution clusters [Backouche et al., 2006,Kohler et al., 2011]. In our case, the samples where contraction proceeded with coarsening provided us a unique opportunity to observe the redistribution of network components distinctly on the membrane. It is interesting to note that the synergistic relocation of actin and myosin tended towards a more homogeneous distribution of contraction foci. The active network then continued to show long-term filament dynamics over this preferred length scale, indicative of a dynamic steady state of network distribution. Such fluidization of membrane-associated actin networks by motor activity has mechanistic implications for

the rheological properties of the cell cortex and its liquid-like behavior [Etienne et al., 2015].

While we relied on coarsening for a lot of our analysis, the observations of homogeneous contraction were also interesting. Previous studies on actomyosin networks have seen a distinct coarsening process, usually multistage, both in solution [Backouche et al., 2006, Kohler et al., 2011, Soares e Silva et al., 2011] or on a membrane [Murrell and Gardel, 2012, Linsmeier et al., 2016, Vogel et al., 2013, Stam et al., 2017, Smith et al., 2007]. Further study is needed to determine why our cortical network shows a bimodal outcome. However, we suspect that it results from an intricate interplay of many parameters. An array of factors affected the length scale of the emergent distribution in this dynamic minimal cortex. We observed a dependence on net membrane association, branching densities and possibly filament length and active motor concentration. Previous studies had also found a dependence of membrane adhesion and inter-filament interaction [Murrell and Gardel, 2012]. These are all factors that are subject to extensive biochemical regulation in cells, suggesting a mechanism by which cortical properties could be coordinated over varying length scales in developmental phenomena such as cortical flows [Bray and White, 1988, Munro et al., 2004].

Finally, we elucidate the contribution of myosin activity in actin filament turnover in this dynamic minimal cortex. The notion of myosin enhancing actin turnover rates has been suggested in various cellular contexts [Guha et al., 2005, Medeiros et al., 2006, Murthy and Wadsworth, 2005, Wilson et al., 2010, Yang et al., 2012], but the inhibition of myosin activity is a fairly complex perturbation due to the many roles of myosin-II motors in the cell. Myosin activity in the cell is locally regulated by signaling, for example via the Rho pathway regulation of myosin light chains. By disassembly of actin networks, it can amplify local cortical remodeling by providing fast access to a pool of network components for new assembly. In our assay, the delay in the appearance of Label2 actin suggested that the actin filaments observed initially are re-formed from the broken down Label1 network. Since actin organization is to be coordinated over large distances in the cell from a limited pool of components, this suggests an interesting mechanism by which myosin activity could support faster dynamics on a shorter scale. Furthermore, the negative feedback on contractility due to disassembly might have mechanistic implications on the pulsatory dynamics observed during certain developmental processes [Martin et al., 2009, Nishikawa et al., 2017].

An obvious future direction to our work would be to compare and contrast out observations with non-muscle myosin-II. A coarsening process has also been reported for NMM-II contractility on membrane-adhering disoredered actin networks [Linsmeier et al., 2016]. We show that at least some basic features of our observations could be corroborated with NMM-II, such as breakdown of actin network and formation of foci with dynamic actin flows between them. Even though the concentrations we used were not comparable due to practical limitations, small structural differences in the actomyosin foci were apparent and the dynamics had distinct trends. A detailed comparison of the two types of myosin-II with respect to the turnover assay would be interesting to pursue.

There are many other factors that are implicated in redundant mechanisms for actin turnover in the cell, such as the severing protein cofilin [Chan et al., 2009, Blanchoin et al., 2000]. These pathways obfuscate the contribution of myosin in cellular studies. In our simplified cortex, we chose to include only the minimal components required for dendritic network assembly and contraction. This allows us to gain a clearer understanding of the role of each participating component. We could independently perturb myosin activity with temporal precision and follow the passage of a fraction of the actin monomers because of this reconstitution assay, allowing an explicit demonstration of actin turnover. We also gained a nascent understanding of how other network components can manipulate actomyosin contractility. This demonstrates that our platform is by no means restrictive to increasing complexity and will still allow intricate, but controlled, manipulations. The dynamic minimal cortex described in this study therefore has immense potential for providing insights into the functioning of its biological inspiration.

III

TOWARDS RECONSTITUTION OF A MINIMAL MODULE FOR EUKARYOTIC POLARIZATION

1 Introduction

Cellular polarity refers to a regulated and reproducible asymmetry in the distribution of molecules observed in various cell types. Polarization is essentially the selection of a morphological axis, whereby different parts of the cell acquire different function. The relative spatial position of these regions would be similar in cells of the same type. This is akin to the positional assignment of the limbs versus the head during animal development. Cells polarize in response to various environmental and physiological cues. During multicellular development, such cues can be inherited from parent cells. However, single cells sometimes will select a random polarization axis in the absence of any explicit cue. This process is referred to as spontaneous polarization and it reveals that the directional cues only provide a positional bias to an inherent symmetry-breaking machinery present in these cells.

The observation of spontaneous polarization leads us to believe that there is an inherent molecular network in cells that may be isolated *in vitro* to study symmetry breaking. This section begins with an introduction to the basic concepts of yeast polarization. This is followed by a primer on reaction-diffusion models of pattern formation. Finally, the two parts are consolidated to give an overview of the theoretical paradigm that motivated our attempts to build the minimal module for eukaryotic polarization.

1.1 Basic concepts in yeast polarization

Spontaneous polarization has been reported from various models of single cell polarity such as bud site selection in yeast or migration of neutrophils and *Dictyostelium* [Petrie et al., 2009, Wedlich-Soldner et al., 2003, Irazoqui et al., 2003]. Yeast cells will select a random bud site if the polarity machinery is genetically uncoupled from cue-detection. Migrating cells also show random axis selection when they are kept in homogeneous environments. Studies from various model systems have revealed conserved molecular networks involved in polarity establishment and maintenance. For this study, we will focus on the process of bud site selection in *S. cerevisiae*.

Budding yeast have two phases in their life cycle- a diploid phase and a haploid phase. In both phases, reproduction is carried out by the formation of buds on a yeast cell that grow and eventually dissociate to form individual cells. The process of selecting a new bud site is highly regulated. In haploid cells, each new bud appears with a precise orientation to the scar of the previous bud, whereas budding occurs in a bipolar orientation in diploids. Extensive genetic and biochemical research has revealed the intricate mechanism that regulate the haploid bud site selection.

As one of the earliest proteins to appear at the presumptive bud site, the RhoGTPase Cdc42 is believed to have a directive role in the process of bud site selection [Ozbudak et al., 2005, Tong et al., 2007, Okada et al., 2013]. Rho-family GTPases belong to a superfamily of small GTPases, most of which are involved in critical signaling processes in cells [Van Aelst and D'Souza-Schorey, 1997, Hall, 1998] , and particularly in polarity [Park and Bi, 2007]. These are nucleotide-binding proteins, which show reversible membrane binding in response to their nucleotide status, resulting in a switch-like behavior. The GTP-bound state is considered the "ON" state in terms of its signaling roles in the cell. Cdc42 will preferentially bind to the membrane when associated with a GTP. Conversely, the "OFF" state is when Cdc42 is associated with GDP. This results in a lowering of membrane affinity leading to the extraction of Cdc42 from the membrane by the Guanosine nucleotide dissociation inhibitor (GDI) [Johnson et al., 2009, DerMardirossian and Bokoch, 2005]. Additional regulatory proteins exist to manipulate the nucleotide status of Cdc42 (Figure III.1). There are GTPase-activating proteins (GAPs) that enhance the inherently weak rate of GTP hydrolysis of the GTPase [Smith et al., 2002]. The Guanine nucleotide Exchange Factors (GEFs) facilitate the renewal of a GTP-bound state by weakening the nucleotide association and enhancing the propensity for nucleotide exchange in the GTP-rich environment of the cell [Rossman et al., 2005]. This cycle is crucial to the regulation of Cdc42 proteins.

In budding yeast, Cdc42 interacts with certain proteins that serve as landmark for identifying the previous bud site. These eventually result in the local recruitment of the Cdc42 GEF, Cdc24. This, in turn, causes local activation of Cdc42. Cdc42 can then trigger a series of events such as formation of actin cables that increase directional delivery of material to the bud site. In genetic manipulations where this pathway linking the landmark complexes to GEF activation are compromised, Cdc42 foci were observed to randomly localize on the membrane [Wedlich-Soldner et al., 2003, Irazoqui et al., 2003]. This spontaneous

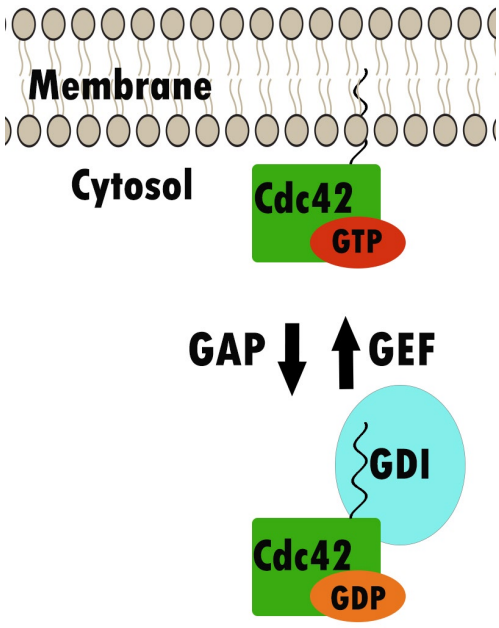

Figure III.1: Schematic depicting the network of proteins that regulate Cdc42 activity

polarization suggests that Cdc42 has the potential to orchestrate symmetry breaking in the absence of positional molecular cues.

Various theoretical paradigms have attempted to explain the phenomenon of Cdc42-dependent symmetry breaking [Goryachev and Pokhilko, 2008, Altschuler et al., 2008, Klunder et al., 2013, Mori et al., 2008]. A predominant notion in the field is that the spontaneous polarization of Cdc42 is a two-step process [Wedlich-Soldner et al., 2004, Ayscough et al., 1997]. In the first step, a reaction-diffusion based mechanism results in the formation of a dominant Cdc42 foci. This is the actual step where symmetry is broken. However, the formation of a stable Cdc42 foci needs the second step, which is a trafficking-dependent feedback into the local Cdc42 enrichment. As mentioned earlier, Cdc42 can enhance local transport by leading to the nucleation of actin cables. It has been reported that Cdc42 could also serve as cargo on these transportation routes resulting in a positive feedback. Since cellular trafficking is a complex network, our intention for the reconstitution study was to focus on the initial reaction-diffusion based mechanism.

1.2 A primer on reaction-diffusion models of pattern formation

At this point, a brief introduction to reaction-diffusion models might be beneficial. These models are based on partial differential equations that describe the evolution of concentrations of one or more chemical species as a function of position and time. In the most basic scenario describing the concentration of a species $a(x,t)$ in one-dimensional space and time, these equations will have the form:

$$\frac{\partial a}{\partial t} = \underbrace{D_a \frac{\partial^2 a}{\partial x^2}}_{\text{Diffusion}} + \underbrace{f(a)}_{\text{Reaction}} \tag{III.1}$$

where D_a is the diffusion coefficient of a and $f(a)$ describes how the change in u depends on its own current concentration. The first term is, therefore, the "diffusion" term and the second is the "reaction" term.

In his 1952 paper, Turing made an illustration where a nearly homogeneous system could evolve into a polarized distribution if it had two species with very different diffusive properties and a particular set of interactions [Turing, 1952]. Small local fluctuations in concentration of the species would be sufficient to trigger an amplification leading to the "instability" in the system. Turing instability, therefore, refers to the diffusion-driven instability of an otherwise stable steady state.

Gierer and Meinhardt later revised Turing's model by defining the reactions in a less abstract form [Gierer and Meinhardt, 1972]. They described a reaction-diffusion system based on an activator-inhibitor interaction. The following two species are required:

1. the activator a is a short-range autocatalytic substance
2. the inhibitor h is a long-range antagonist of a

The evolution of these species in space and time is described by the following set of equations:

$$\frac{\partial a}{\partial t} = \rho \frac{a^2}{h} - \mu_a a + D_a \frac{\partial^2 a}{\partial x^2} + \rho_a \tag{III.2}$$

$$\frac{\partial h}{\partial t} = \rho a^2 - \mu_h h + D_h \frac{\partial^2 h}{\partial x^2} + \rho_h \tag{III.3}$$

where D_a and D_h are diffusion constants, ρ_a and ρ_h are baseline constant production rates, and μ_a and μ_h are decay rates of the two species. The first terms of each equation

are production terms that describe the interactions of the two species that introduce the non-linearity that is critical for the outcome. For a, the autocatalysis of a is depicted by its dependence on a^2 and the inhibition by h is depicted by the inverse proportionality of this term to the concentration of h. The production of the inhibitor h itself shows a non-linear dependence on a in the second equation and both these dependencies have a proportionality constant ρ. To simplify, a will lead to an increase in its own production, as well as the production of its inhibitor h. A delay in the response of a to inhibition is needed for the system to lead to instability. This condition is specified by the diffusion constants with a showing slower diffusion than h.

Gierer and Meinhardt also offered an alternative whereby no explicit inhibitor species is needed for the instability. This is called the activator-substrate depletion model, wherein the substrate s is needed for the autocatalysis of the activator a. The negative feedback in the process results from a local depletion of the substrate. The system of equations that could describe this scenario are as follows:

$$\frac{\partial a}{\partial t} = \rho s a^2 - \mu_a a + D_a \frac{\partial^2 a}{\partial x^2} + \rho_0 \tag{III.4}$$

$$\frac{\partial s}{\partial t} = \delta - \rho s a^2 - \mu_s s + D_s \frac{\partial^2 s}{\partial x^2} \tag{III.5}$$

where the diffusion coefficients D_a and D_s and decay constants μ_a and μ_s are as before. ρ_0 is the initial concentration of a and δ is that of h. The term $\rho s a^2$ defines the relationship, whereby substrate s is a reactant in the autocatalytic activation of a, with ρ again as the rate constant of this reaction. The term is negative for the time evolution of s as the substrate gets consumed in the reaction. Note that this implies that there is limited pool of substrate s that will get consumed as this process proceeds. Eventually, the lack of availability of s would lead to a tacit "inhibition" of the autocatalysis of a.

While this is an illustration of how reaction-diffusion class of equations can be used to describe pattern formation, individual models will vary on the terms in the equation, particularly the ones defining the "reaction" term.

1.3 Brief review of theoretical paradigm for yeast polarization

The gist of the equations described in the previous section is to describe a system where local enrichment of a species can occur, while suppressing the same enrichment in other regions. This is exactly the outcome of the formation of a Cdc42 "pole" in budding yeast.

The essential feature for emergent behavior in such systems is feedback [Novak and Tyson, 2008,Ferrell, 2013]. The next step is to recognize motifs in the regulatory network of Cdc42 that could relate to the interactions described in the reaction-diffusion models. Multiple scenarios can provide the necessary feedback, as has been recent reviewed in great detail in [Goryachev and Leda, 2017].

Multiple pathways serve as candidates for the positive feedback. One popular notion is through the Pak-Bem1-GEF axis. This suggests that autocatalysis can exist through a scaffolding protein Bem1 that puts the GEF downstream of an effector of Cdc42[1]. An effector of Cdc42, the Pak kinase Cla4, shares an indirect interaction with the GEF Cdc24 through the scaffolding protein Bem1[2] [Irazoqui et al., 2003,Butty et al., 2002,Kozubowski et al., 2008]. The use of an artifical GEF-Pak fusion could bypass the need for Bem1 for polarization in budding yeast [Kozubowski et al., 2008]. Since both Bem1 and Cla4 can bind Cdc42, this feedback could be nonlinear. Additionally, Bem1 also shares other interactors with Cdc42 such as proteins of the exocyst pathway [France et al., 2006, Liu and Novick, 2014], which could promote simultaneous multivalent interactions. Bem1 is, however, not essential for symmetry breaking in yeast [Smith et al., 2013b]. Additional sources of feedback must hence exist in the cellular environment (reviewed in [Martin, 2015, Goryachev and Leda, 2017]). Many studies have suggested the importance of a competition between the GEF and the GDI for the cytosolic GDP-bound Cdc42 as an additional source of feedback [Goryachev and Pokhilko, 2008,Freisinger et al., 2013,Robbe et al., 2003].

While there is no consensus in the field as to which feedbacks are crucial for spontaneous polarization in yeast, the collection of ideas discussed here provides sufficient material to envisage a minimal module for *in vitro* reconstitution.

2 Network design of a minimal module for symmetry breaking based on Cdc42

Based on the current understanding of the molecular regulation of polarity establishment in the budding yeast, we proposed to reconstitute a minimal molecular module that would be capable of spontaneously breaking symmetry in Cdc42 distribution. This module was based

[1]Effectors are proteins that interact directly with a signaling protein and mediate downstream signaling cascades.

[2]Scaffolding proteins form a base for multi-protein complexes by simultaneous interaction with many proteins.

on the concept of the activator-substrate depletion model subclass of reaction diffusion systems and was devised with input from Prof. Wedlich-Söldner and Prof. Erwin Frey. GTP-bound Cdc42 on the membrane serves as the hypothetical "activator" of the Gierer-Meinhardt model in this case (Figure III.2). This protein can recruit its own GEF protein through an engineered interaction explained shortly. GEF will activate more Cdc42 in the vicinity by enhancing nucleotide exchange to a GTP state, thereby serving as the autocatalytic feedback loop. Each stochastic site of Cdc42 binding could start to grow in this manner. No explicit inhibitor is required in the system as substrate depletion might sufficiently serve for suppressing the same reaction from occurring homogenously. The substrate in this case is the "inactive" GDP-bound Cdc42 that is used up during the GEF reaction. As GDP-Cdc42 binds to GDI and remains soluble, it diffuses freely towards sites of enhanced recruitment as a chemical gradient is created by the increased uptake of GDP-Cdc42. In a closed system, with a limited pool of molecules available, this process will deplete the remaining region from available substrate thus supressing the reaction there. It is to be noted that it is unlikely in this minimal state for the system to achieve singular polarization. However, we expected to see foci of Cdc42 formed on the membrane from a near homogenous situation.

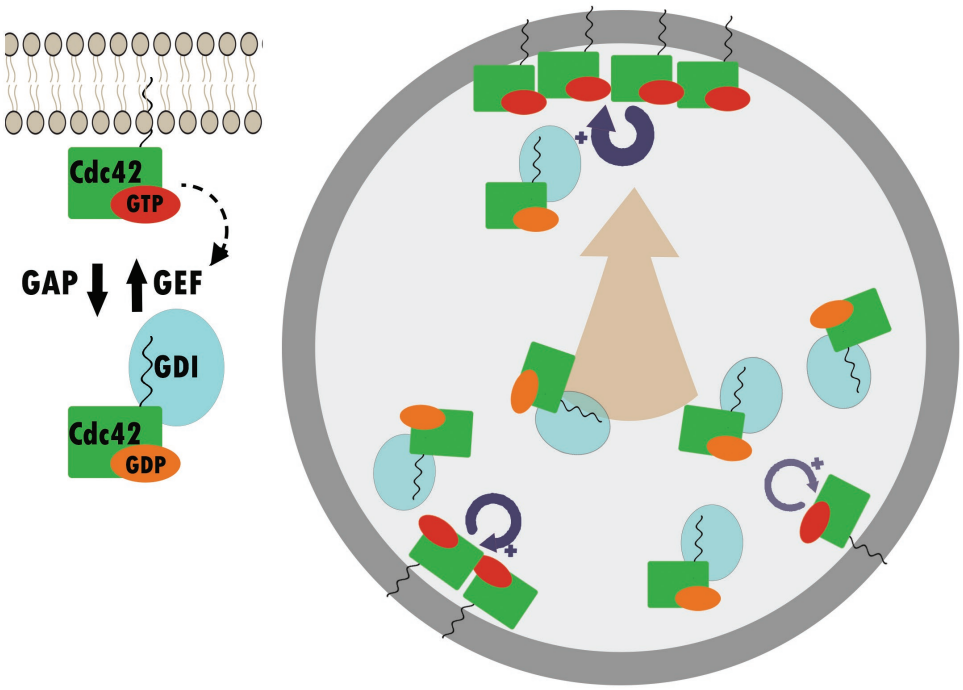

Figure III.2: Schematic explaining the design of the minimal module for spontaneous symmetry breaking

The basic requirements to be fulfilled were:

1. Reversible membrane attachment of Cdc42:

   Cdc42 binds to the membrane through a geranylgeranyl modification on a Cysteine close to the C-terminus. The hydrophibicity of this lipid-like moeity results in a strong membrane binding that can only be disrupted by association with GDI. The GDI has a hydrophobic pocket wherein the geranylgeranyl group can be sequestered to form a complex that is soluble. Since GDI has a preferential binding to the GDP-bound Cdc42, the membrane-binding switch is coupled to the nucleotide switching of the protein. This reversible membrane binding in response to nucleotide status is critical for the functioning of the minimal network. By virtue of including the GDI, we also have the possibility for the GEF-GDI competition to be observed and analyzed.

2. Autocatalysis in Cdc42 activation:

   The existence of a positive feedback loop for the activator is essential in this model of spontaneous symmetry breaking. In a yeast cell, various proteins have been implicated for this role. However, in order to minimize the number of elements in our network, we engineered a chimeric protein that should provide a function similar to the Bem1 scaffolding. As Cdc42 has a directive role in many signaling pathways, many proteins can be found to have a domain, known as the Cdc42- and Rac-interactive binding (CRIB) domain, that specifically recognizes GTP-Cdc42. We thus fused the CRIB domain with a minimal segment of Cdc24 with GEF activity. Note that we included the PH domain along with the GEF domain as this is believed to be important for GEF activity. The CRIB domain was chosen from the protein Gic2 as preliminary results from the group of Prof. Wedlich-Söldner had shown that this domain shows good binding to bud sites in *in vivo* analysis. Figure III.3 shows a schematic depicting the activity of the CRIB-GEF fusion.

3. Regeneration of substrate:

   Since there is explicit negative feedback in the minimal system, nucleotide turnover in Cdc42 needs to be maintained for system dynamics. GTPase activity of Cdc42 is inherent low and GAP proteins are needed to enhance it *in vivo*. We included a minimal GAP protein in our network design for this purpose.

4. Suitable membrane system:

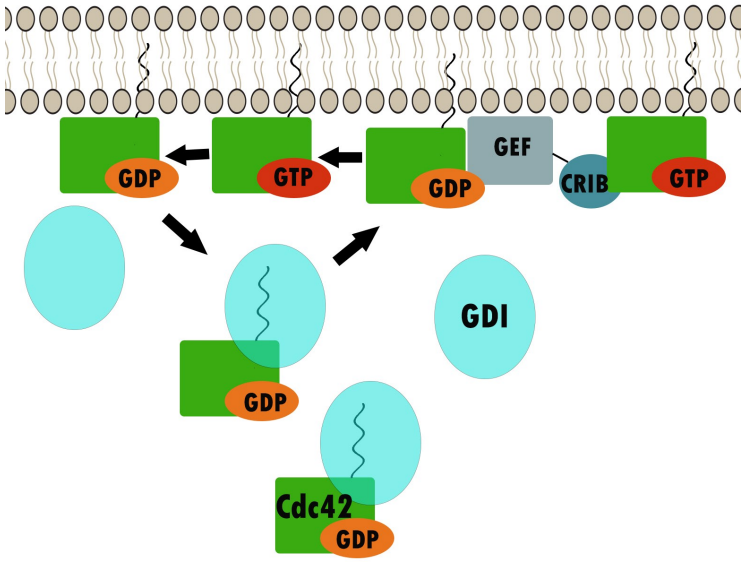

Figure III.3: Schematic explaining how CRIB-GEF fusion serves as a positive feedback for Cdc42 activation

For substrate depletion to set in, there must be a limited supply of Cdc42 proteins that should be less than the amount required to saturate the membrane. The most suitable technique for reconstitution on membranes would therefore be encapsulation of proteins in vesicles. However, since extensive titration of components was likely to be needed for finding the right regime for symmetry breaking, experiments were initiated on open systems like SLBs or the outside of Giant Unilamellar Vesicle (GUV)s. Both these systems are well-suited for light microscopy.

In summary, the minimal module for symmetry breaking would include prenylated Cdc42, GDI, CRIB-GEF fusion and GAP proteins reconstituted on a suitable membrane system. Once this is established, various avenues of manipulations could be envisaged by which reaction rates could be tuned to better understand this network of symmetry breaking. For instance, the prenylation of Cdc42 could be altered to produce weaker or stronger membrane association.

3 Reconstitution of network components from *S. cerevisiae*

To start with assembling the minimal network, we proceeded with purification of the protein components and testing the reversible membrane association of the Cdc42 proteins.

3.1 Purification of prenylated Cdc42

Cdc42 is a protein that undergoes a three-step post translational modification *in vivo*. The protein has a CAAX domain at the C-terminus [Roberts et al., 2008]. A geranylgeranyl transferase adds the prenyl group to the Cysteine in the CAAX motif. This is followed by a methylation of the Cys and a truncation of the last 3 amino acids by other enzymes. While the last two modifications are not necessary for membrane binding, the prenylation is. Since this modification does not occur in bacteria, Cdc42 was produced in eukaryotic expression systems like insect cells. Cdc42 is a ~20 kDa protein and the resulting prenylated protein is very prone to aggregation due to increased hydrophobicity. We initially found that the protein expression in insect cells is considerably enhanced when a bigger tag is present on the protein, possibly by increasing steric hindrance between molecules. Since we intended to use light microscopy for analysis, we added a enhanced Green Fluorescent Protein (eGFP) to the N-terminus of Cdc42 and an additional 6xHis tag for purification. We tested different conditions of production to optimize protein output such as expressing Cdc42 in the absence of GDI and purifying using detergents, or co-purifying with bacterially-expressed GDI. Alternatively, eGFP-Cdc42 could be co-expressed with the GDI and this approached provided the best protein preparation and has been used in all experiments in this section. The different approaches to reconstitution of Cdc42 on model membranes are summarized in Supplementary Figure B.1

The GDI (RDI1 in yeast) was expressed in bacteria independently for purification.

3.2 Reversible membrane interaction of eGFP-Cdc42

Using GUVs made with different lipid composition, we determined the charge- and nucleotide-specificity of the interaction of eGFP-Cdc42 with the membrane (Figure III.4). Binding was only observed when the membrane was negatively charged, e.g. containing 15% DOPS[3],

[3]The lipid composition for experiments in this section included 10 mol% DOPE. DOPS and sometimes PIP2 were included in varying concentrations where negative charge was desired. The rest was DOPC.

and a non-hydrolyzable GTP analog (GMPPNP) was provided in solution. This confirms the canonical idea of specificity of membrane interactions of Cdc42. Increasing charge on the membrane showed a slight increase in the amount of Cdc42 on the membrane but there was considerable variability in the samples. An alternate method of including the protein in the sucrose medium of the GUVs before dilution into buffer yielded higher binding and overcame the problem of aggregation of negatively charged vesicles in the presence of Mg^{2+} ions.

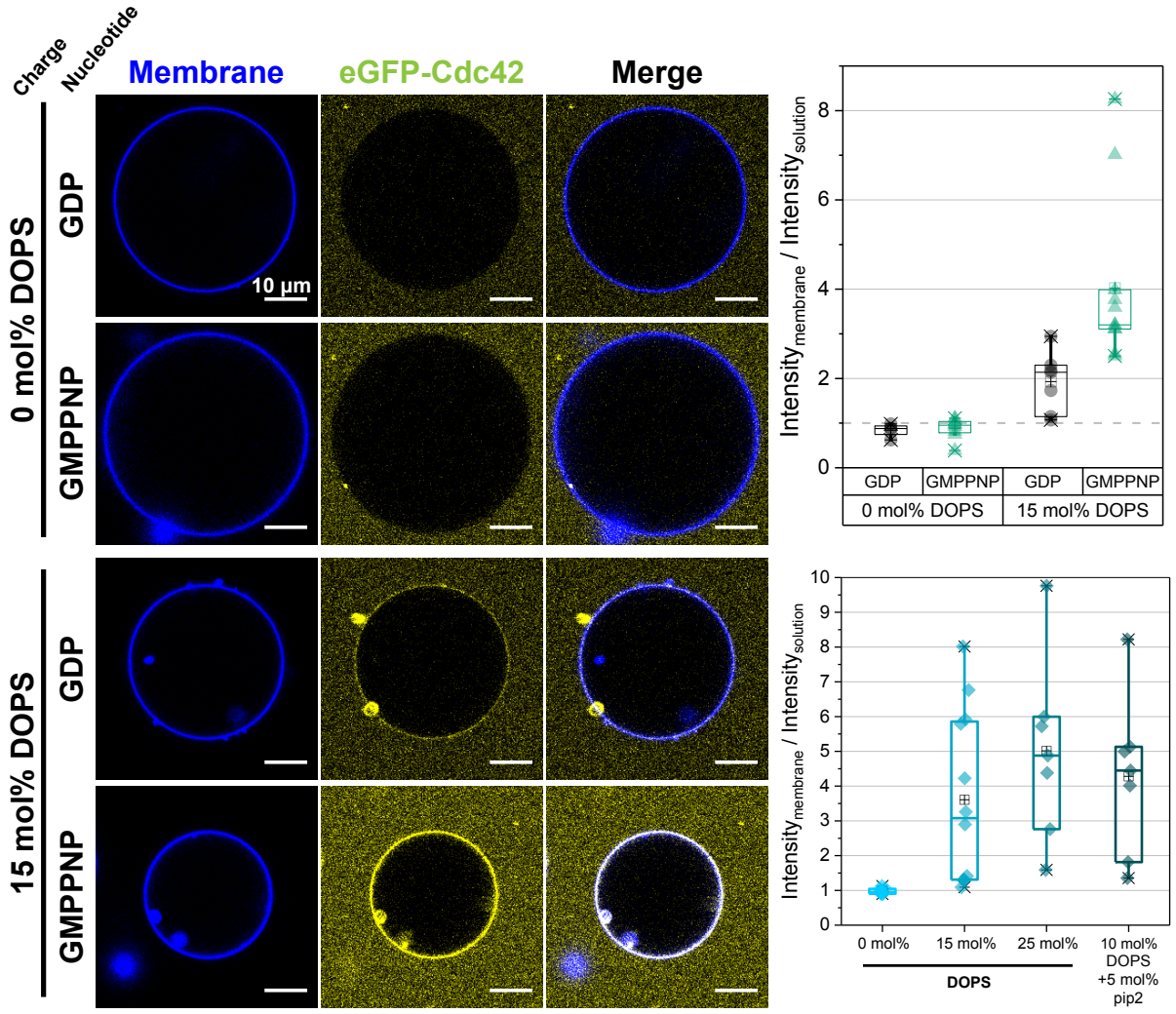

Figure III.4: Nucleotide- and charge-specificity of membrane interaction of Cdc42

After 15 mol% DOPS containing vesicles were preloaded eGFP-Cdc42 in sucrose, excess GDP and GDI were introduced to look for extraction. Addition of GDI appeared to lead to a reduction in the surface density of eGFP-Cdc42 (Figure III.5). However,

aggregates of Cdc42 were visible on the membrane during the extraction. These seemed to cause membrane deformations of the GUVs, making a quantitative analysis of these effects impractical. This observation was independent on whether the protein was added directly in the sucrose or added to the buffer. Binding of eGFP-Cdc42 was also observed on membranes but the mobility of the protein was significantly impaired presumably due to substrate interactions. Consequently, GDI also did not have much effect of membrane localization of Cdc42.

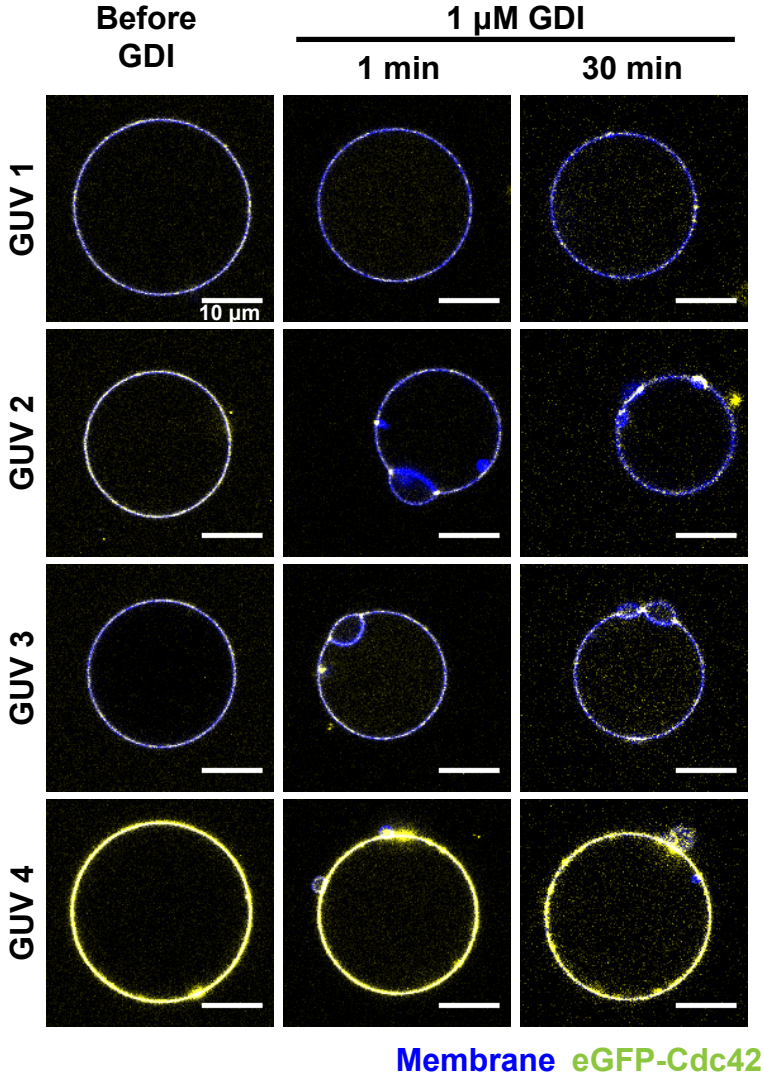

Figure III.5: Effect of addition of GDI to vesicles loaded with eGFP-Cdc42
Data from 4 vesicles depicts the variability in response to GDI as well as membrane deformations resulting from it

There were multiple indications that the quality of the eGFP-Cdc42 protein preparation was suboptimal. Considerable aggregation effects were observed in the assays such as high variability in solution fluorescence. Artifacts of aggregation also appeared in Microscale Thermophoresis measurements which confounded calculation of binding constants. No considerable improvement was observed in the conditions we tested for buffer optimization. This could be the reason behind the aggregates retained on the membrane after GDI extraction.

3.3 Optimization of CRIB-GEF design

The intitial design of the CRIB-GEF fusion included these three parts:

1. CRIB domain from Cla4p (amino acid (aa) 1-241): This domain was tested in the lab of Prof. Wedlich-Söldner as a GFP fusion and showed good colocalization with active Cdc42 sites.

2. DHPH domain from Cdc24p (aa 272-682): These domains were impicated in GEF activity [Cerione and Zheng, 1996]

3. A linker with 5x repeats of Glycine-Serine

We proceeded to analyze the effect of inclusion of CRIB-GEF in the membrane binding of eGFP-Cdc42. Membranes for this experiment included 10 mol% DOPS and 5 mol% PIP2 as this may aid the functionality of the PH-motif containing CRIB-GEF fusion. While inclusion on membrane was not increased in the presence of CRIB-GEF, large aggregates were observed close to the membrane. These aggregates were observed both on SLBs and GUVs and showed association with the membrane at certain points. If GDI was included additionally, larger aggregates were seen.

Formation of such aggregates could result from multiple problems. In general, this observation suggests that the CRIB-GEF fusion acts as a cross-linker for individual Cdc42 proteins. While persistent binding may be expected for the CRIB domain, the enzymatic activity of the GEF domain should be processive and the binding to Cdc42 should therefore be transient. A persistent association could result from compromised functionality of either the Cdc42 or the GEF domain in the fusion construct. As the CRIB-GEF is a chimeric construct, various aspects of its design could be optimized for better stability and functionality of its constituents. These included:

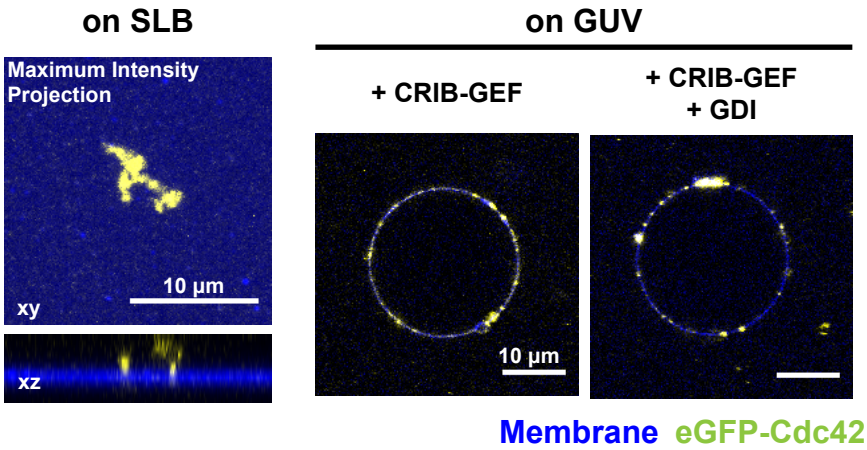

Figure III.6: Effect of CRIB-GEF on membrane binding of eGFP-Cdc42

1. Alternate truncation of DHPH (GEF) domain
2. Alternate linker design
3. Alternate truncation of CRIB domain
4. Reverse order of CRIB and GEF domains on the fusion construct

To optimize the GEF domain, we planned to purify DHPH domain in isolation to test the enzymatic activity. This domain, however, proved to be unstable in isolation. We also failed to express a slightly different truncation of the DHPH domain from Cdc24p (aa 285-681), that was reported to have activity in a study on aggregation of these domains [Mionnet et al., 2008].

We also redesigned the constructs with longer linker lengths of 10x or 15x repeats of Glycine-Serine. Alternatively, two linker designs were selected from literature to provide a rigid or a flexible linker [Waldo et al., 1999]. Studies have suggested that rigid linkers may be much better for protein functionality where a certain separation of domains is desired [Chen et al., 2013]. These constructs are, however, still to be tested.

3.4 Stability concerns in yeast proteins

While the observed eGFP-Cdc42 organization in the presence of CRIB-GEF superficially resembles the pattern formation we were seeking, the results are clearly confounded by protein aggregation and therefore, unreliable. In order to tackle the aggregation problems in the purified eGFP-Cdc42, we considered other options such as *in vitro* prenylation of

protein expressed in bacteria. We had considerable difficulty in expressing the protein, even in the absence of prenylation. A comparison of expression between the *S. cerevisiae* version and the human Cdc42 in cell-free expression reactions revealed that the human protein expressed considerably better. Thermal denaturation studies also indicated that the human protein had higher stability, with transition temperatures higher by 10-15°C. It is known that the unstructured C-terminus of small GTPases contributes significantly to the aggregation tendencies of these proteins. For this reason, these regions are often excluded in crystallization studies [Morreale et al., 2000]. Small differences in the sequence in this region could therefore impart different stabilities to the resulting protein. Additionally, we observed that the stability of both Cdc42 proteins would be slightly improved by the addition of excess GDP in the buffers (transition temperatures increased by 5-6°C).

Due to cumulative problem of expression of various network components from the yeast system, we considered redesigning the network with homologous parts from human proteins. Besides the higher stability of the human protein, and presumably partially due to it, many more protocols were available in literature for purification of this protein [Johnson et al., 2009]. Additionally, the human versions of most of the interacting proteins in the network had also been characterized better both *in vivo* and *in vitro*, and were even used to get parameters for yeast polarization model [Freisinger et al., 2013].

Importantly, we were only interested in the functional modularity of the components in our network and not the actual protein, as a principle of synthetic biology. For further studies, excess nucleotide (usually GDP) was included in all buffers for purification, storage and experiments with Cdc42.

4 Developing new methodologies for synthetic protein networks on membranes

While assays of *in vitro* reconstitution of the revised polarization module with human proteins could not be completed within the time frame of this thesis, we incorporated various new approaches in our work flow to streamline the optimization of network components. In this section, we will discuss these methodologies from a technical perspective to highlight their significance as general tools for development of synthetic protein networks, particularly those with membrane association. We will elucidate the usefulness of these techniques with examples from the eukaryotic polarization module.

The key approaches we will discuss are as follows:

1. Fast screening of DNA constructs for stability of the resultant protein using cell-free expression techniques

2. Using *in vitro* prenylation as a tool to engineer membrane association of proteins

3. Fast screening of functionality of chimeric proteins using a combination of cell-free expression and microscopy-based readouts

Experiments in this section were conducted in collaboration with Dr. Lei Kai, with assistance from Dr. Katharina Nakel.

4.1 Stability screening using cell-free expression

The big advantage of using cell-free expression systems for production of proteins has always been the ease of screening of stabilizing compounds and expression conditions. Additionally, the time between having a DNA construct and obtaining information on protein expression can be reduced to a single day, bypassing the tedious processes of transforming bacterial cells and growing colonies or cultures for propagation.

Using small volume cell-free expression, we screened a variety of tags and expression conditions for the yeast Cdc42 and RDI1. An example screen shown in Supplementary Figure B.2 displays how this approach can be useful for gaining insights into protein stability. The yeast Cdc42 would largely go to insoluble aggregates at the end of expression. As mentioned earlier, this lead us to redesign the polarization modules using human orthologs.

After cell-free screening, we used the selected constructs for over-expression in bacteria as usual. Through this workflow, we found that human Cdc42 expressed considerably well in bacteria both with a 10xHis tag and with additional bulkier tags like superfolder Green Fluorescent Protein (sfGFP), mCherry and GST. Purification resulted in high yields and quality tests of the proteins were favorable. Human RhoGDI, DHPH (GEF) and GAP proteins could also be purified with good yield from bacteria.

4.2 Engineering membrane binding through *in vitro* prenylation

Various potential advantages lead us to investigate if *in vitro prenylation* could be used to functionalize Cdc42. This method has been extensively used for another Rho family

GTPase, RhoA [Tnimov et al., 2012]. Since *in vitro* prenylation could be carried out directly on top of an SLB, we could bypass the use of aggregation-prone high concentration stock solutions of prenylated Cdc42.

Using sfGFP-Cdc42 (human version) purified from bacteria, we tested the prenylation reaction on top of an SLB[4]. Note that a full reaction mix would comprise of the prenylation enzyme Geranylgeranyl transferase-I (GGTase-I) and the prenyl substrate Geranylgeranyl pyrophosphate (GGPP). We found that sfGFP-Cdc42 enriched on the membrane after 20 minutes since reaction initiation. This enrichment was not observed in the control without prenyl substrate in the reaction mix (Figure III.7). Reactions included GTP to favor membrane binding.

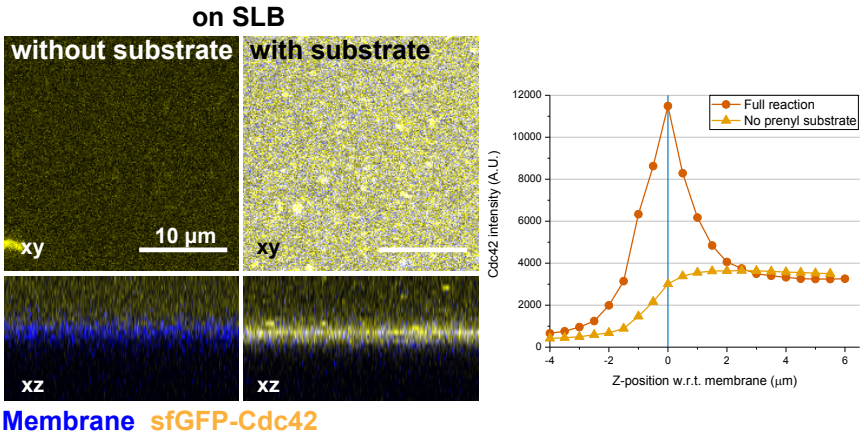

Figure III.7: *In vitro* prenylation of sfGFP-Cdc42 (human) on SLBs

We went on to test the membrane interaction of Cdc42 using this experimental set-up. Inclusion of GDI in the reaction mix resulted in significantly less membrane binding of sfGFP-Cdc42. GDP was standardly included in prenylation buffer, so we added a GTP regeneration system (see Appendix) to induce the formation of GTP. As expected from the known GTP-dependence of Cdc42 membrane binding, protein enrichment was seen on the membrane (Figure III.8). However, there is a noticeable drop in the solution intensity in the sample and large aggregates can be observed. It is therefore hard to distinguish whether more protein is incorporated into the membrane or the protein in solution has aggregated resulting in an apparent membrane "enrichment".

We then tested whether protein bound to the membrane by the reaction could be extracted by GDI. For this, we did the reaction on the SLB in presence of GTP to allow

[4]We included 0.4 mg/ml Bovine Serum Albumin (BSA) in buffers to reduce substrate interactions and saw that mobility of the protein was higher.

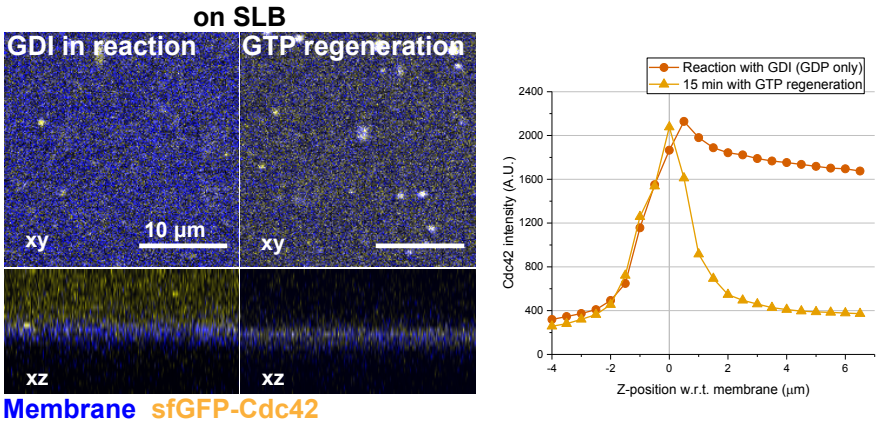

Figure III.8: Inclusion of GDI during *in vitro* prenylation reduces membrane enrichment of sfGFP-Cdc42 (human) on SLBs

loading of sfGFP-Cdc42 onto the membrane. We then washed the sample to remove soluble fraction of the protein as well as replace the buffer with excess GDP. Addition of GDI to this washed sample resulted in a decrease in the intensity of sfGFP-Cdc42 on the SLB (Figure III.9). However, we noticed a curious effect in these experiments due to which the region that is imaged increases slightly in brightness over time. We attribute this to phototoxicity induced by the laser. For this reason, the intensity after GDI extraction in other regions was much lower than the one imaged. Again, it is noticeable that the solution intensity does not increase when GDI is added, and is even slightly lower. Aggregation is also observed in some regions of the sample.

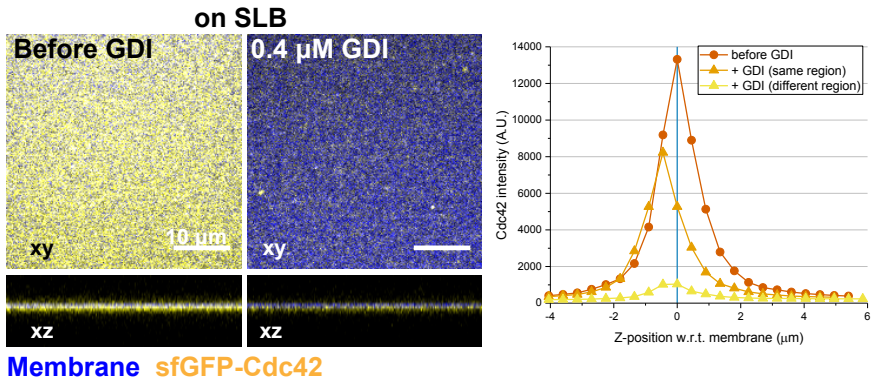

Figure III.9: GDI mediates membrane extraction of prenylated sfGFP-Cdc42 (human)

In vitro prenylation on SLBs was also tested for the yeast Cdc42. Prenylation reaction for mCherry-Cdc42[5] showed the characteristic charge dependence of the protein with binding only observed when DOPS was present in the membrane (Figure III.10).

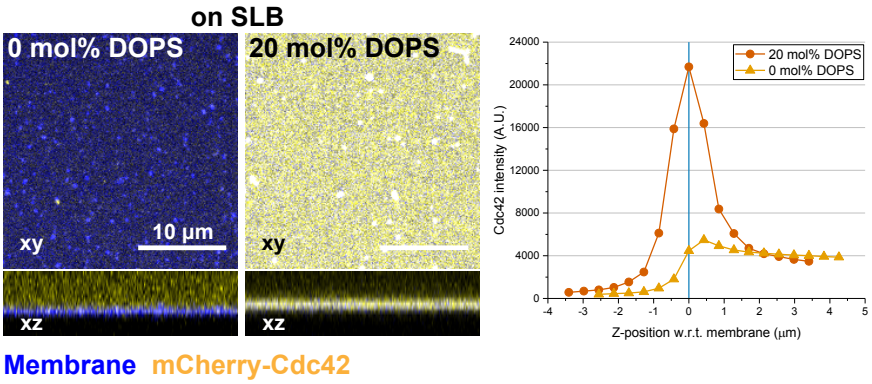

Figure III.10: Charge-dependent membrane binding of mCherry-Cdc42 (yeast) upon *in vitro* prenylation

Altogether, these results indicate that the prenylation reactions and membrane incorporation of Cdc42 proteins are effective using this approach. However, aggregation problems in the Cdc42 protein network still need to be addressed.

A second advantage of this approach is that the membrane affinity of the resulting protein can be tuned. There are three classes of prenylation enzymes that operate on small GTPases [Maurer-Stroh et al., 2003]. Each of these enzymes favors a certain type of prenyl substrate as well as the corresponding CAAX motifs on the protein substrate [Roberts et al., 2008]. Therefore, by making mutations in the CAAX motif and using the appropriate enzyme, we could adjust the strength of membrane binding. For instance, pattern formation in our predicted polarization module relies on reversible membrane binding of Cdc42. It would, therefore, be interesting to observe how the dynamics of the symmetry breaking could be affected by replacing the strongly hydrophobic geranylgeranyl moeity with a weaker farnesyl group.

Finally, such engineering also enables us to make completely artificial constructs with tuned membrane binding, as has been previously demonstrated [Fenz et al., 2014]. We tested two constructs where a GST tag was followed by a rigid linker and a C-terminal fragment from either a geranylgeranylation substrate (human Cdc42) or a farnesylation substrate (human KRasB). An mCherry with the KRasB CAAX motif CVIM[6] was used

[5]mCherry-Cdc42 with the yeast protein sequence was purified from cell-free production for this experiment

[6]CVIM refers to the amino acid sequence Cysteine-Valine-Isoleucine-Methionine

to demonstrate membrane binding on SLBs (Supplementary Figure B.3). This method has already been validated for creation of chimeric membrane binding proteins. For our experiments, we designed these artificial constructs to serve as controls for spatial patterning.

4.3 Fast functional screening of chimeric constructs

As described in 3.3, many factors need to be considered for designing a chimeric protein like the CRIB-GEF fusion. Purifying these different versions for testing functionality in microscopy-based assays can be a time- and effort-intensive workflow. Screening of potential CRIB-GEF constructs using cell-free expression offers an efficient alternative to overcome this problem. The constructs were expressed in batch mode with cell-free lysates. The expression can reach concentrations of 1 mg/ml in such a system. We pre-tested the expression to test stability of the various constructs.

A microscopy-based assay was set up using SLBs. *In vitro* prenylation was used to introduce sfGFP-Cdc42 to the membrane in each sample. The proteins in solution were washed off and replaced with GDI to make soluble Cdc42/GDI complexes. By adding a fraction of the lysate expressing any of the CRIB-GEF constructs, we can then test their activity by observing Cdc42 incorporation into the membrane. The distribution of Cdc42 could also provide hints on whether the construct is capable of positive feedback. Alternatively, this assay could be performed with purified Cdc42/GDI complexes by incubating membranes with the lysates before adding the complexes.

Only preliminary experiments of this approach were conducted before the writing of this document. For the yeast CRIB-GEF constructs, some influence of the linker lengths was observed in this test (Supplementary Figure B.4), but a thorough analysis with multiple repeats is necessary to verify these results.

5 Discussion and outlook

Due to stability issues of the proteins involved in this network, we failed to reconstitute a functional minimal module of eukaryotic polarization. Where hetergeneous distributions were observed, it was difficult to extract meaningful inferences because Cdc42 was itself prone to aggregation. However, there are various interesting aspects that were highlighted during our efforts in this direction.

Most significantly, one observation seems to indicate that our theoretically premise might be inadequate to produce symmetry breaking. Cdc42 from both yeast and human

appeared to have a high inherent rate of nucleotide exchange, even in the absence of GEF proteins. This is inferred by two observations- 1) the low stability of Cdc42 in the absence of excess nucleotide in solution, and 2) the immediate membrane incorporation observed in the presence of GTP. Elaborating the first point, Mg^{2+} is known to stabilize the nucleotide association of small GTPases [Zhang et al., 2000]. However, this stabilization is not sufficient for proteins with inherently weak nucleotide attachment and therefore higher exchange rates. In the absence of excess nucleotide in solution, these proteins quickly lose their bound nucleotide and this can lead to aggregation. Secondly, in all our membrane binding assays, we observed that excess GTP in solution was sufficient to deliver Cdc42 to the membrane from soluble GDI-complexes. A thorough investigation into the factor by which this rate is increased in the presence of a GEF protein could not be completed within the time frame of this thesis, but poses an interesting avenue for further investigation.

Importantly, our current model relies on the GEF activity for the positive feedback that is essential to the predicted symmetry breaking process. Theoretical simulation studies could be used to estimate what factor of rate enhancement in the nucleotide exchange would be minimally required for pattern formation.

Alternatively, other modes of positive feedback in such a network would be worth consideration. Studies have suggested that a second positive feedback may be necessary to introduce pattern formation in Cdc42 networks [Lo et al., 2014]. One possible source of non-linearity may be self-assembly of Cdc42 into higher order structures. This has previously been reported in some studies [Park et al., 2015, Zhang and Zheng, 1998]. In principle, this hypothesis could easily be tested *in vitro* using FRET-based techniques or Fluorescence Cross Correlation Spectroscopy. Interestingly, the C-terminal that is implicated in oligomerization is also the region known to cause aggregation. This provides a new, more positive, perspective to the issue of aggregation that should be considered for future experiments.

Additionally, there is a consistent observation in our studies that aggregation ensues whenever membrane extraction of Cdc42 by the GDI is attempted. The GDI is indeed notorious for its tendency to aggregate [Sheffield et al., 1999]. We often saw multimers of the protein during size exclusion chromatography, rather than aggregates in the void volume. It would be interesting to probe if GDI itself has a tendency to self-assemble and how this may impact the network design for a symmetry breaking module.

We consolidated many different techniques to try to stream the workflow of design and functional screening of the protein components in this system. These techniques were all

previously developed, but were only independently applied in *in vitro* studies so far, to the best of our knowledge. These included the incorporation of cell-free expression to test stability and possibly functionality of proteins, as well as *in vitro* prenylation to prepare membrane binding proteins. While some of these aspects were successfully implemented with proteins of our interest, we found them inadequate to counter the stability issues with Cdc42 and its interaction partners. Nevertheless, we hope that this repertoire of methods will be useful for future attempts in designing and implementing synthetic protein networks on model membranes.

Bibliography

[Altschuler et al., 2008] Altschuler, S. J., Angenent, S. B., Wang, Y., and Wu, L. F. (2008). On the spontaneous emergence of cell polarity. *Nature*, 454(7206):886–889.

[Ayscough et al., 1997] Ayscough, K. R., Stryker, J., Pokala, N., Sanders, M., Crews, P., and Drubin, D. G. (1997). High rates of actin filament turnover in budding yeast and roles for actin in establishment and maintenance of cell polarity revealed using the actin inhibitor latrunculin-a. *J Cell Biol*, 137(2):399–416.

[Backouche et al., 2006] Backouche, F., Haviv, L., Groswasser, D., and Bernheim-Groswasser, A. (2006). Active gels: dynamics of patterning and self-organization. *Phys Biol*, 3(4):264–273.

[Bernheim-Groswasser et al., 2002] Bernheim-Groswasser, A., Wiesner, S., Golsteyn, R. M., Carlier, M. F., and Sykes, C. (2002). The dynamics of actin-based motility depend on surface parameters. *Nature*, 417(6886):308–311.

[Bieling et al., 2018] Bieling, P., Hansen, S. D., Akin, O., Li, T. D., Hayden, C. C., Fletcher, D. A., and Mullins, R. D. (2018). Wh2 and proline-rich domains of wasp-family proteins collaborate to accelerate actin filament elongation. *EMBO J*, 37(1):102–121.

[Blanchoin et al., 2000] Blanchoin, L., Pollard, T. D., and Mullins, R. D. (2000). Interactions of adf/cofilin, arp2/3 complex, capping protein and profilin in remodeling of branched actin filament networks. *Curr Biol*, 10(20):1273–1282.

[Bray and White, 1988] Bray, D. and White, J. G. (1988). Cortical flow in animal cells. *Science*, 239(4842):883–888.

[Bussonnier et al., 2014] Bussonnier, M., Carvalho, K., Lemiere, J., Joanny, J. F., Sykes, C., and Betz, T. (2014). Mechanical detection of a long-range actin network emanating from a biomimetic cortex. *Biophys J*, 107(4):854–862.

[Butty et al., 2002] Butty, A. C., Perrinjaquet, N., Petit, A., Jaquenoud, M., Segall, J. E., Hofmann, K., Zwahlen, C., and Peter, M. (2002). A positive feedback loop stabilizes the guanine-nucleotide exchange factor cdc24 at sites of polarization. *EMBO J*, 21(7):1565–1576.

[Cameron et al., 1999] Cameron, L. A., Footer, M. J., van Oudenaarden, A., and Theriot, J. A. (1999). Motility of acta protein-coated microspheres driven by actin polymerization. *Proc Natl Acad Sci U S A*, 96(9):4908–4913.

[Carvalho et al., 2013a] Carvalho, K., Lemiere, J., Faqir, F., Manzi, J., Blanchoin, L., Plastino, J., Betz, T., and Sykes, C. (2013a). Actin polymerization or myosin contraction: two ways to build up cortical tension for symmetry breaking. *Philos Trans R Soc Lond B Biol Sci*, 368(1629):20130005.

[Carvalho et al., 2013b] Carvalho, K., Tsai, F. C., Lees, E., Voituriez, R., Koenderink, G. H., and Sykes, C. (2013b). Cell-sized liposomes reveal how actomyosin cortical tension drives shape change. *Proc Natl Acad Sci U S A*, 110(41):16456–16461.

[Cerione and Zheng, 1996] Cerione, R. A. and Zheng, Y. (1996). The dbl family of oncogenes. *Curr Opin Cell Biol*, 8(2):216–222.

[Chan et al., 2009] Chan, C., Beltzner, C. C., and Pollard, T. D. (2009). Cofilin dissociates arp2/3 complex and branches from actin filaments. *Curr Biol*, 19(7):537–545.

[Chen et al., 2013] Chen, X., Zaro, J. L., and Shen, W. C. (2013). Fusion protein linkers: property, design and functionality. *Adv Drug Deliv Rev*, 65(10):1357–1369.

[Cross and Hohenberg, 1993] Cross, M. C. and Hohenberg, P. C. (1993). Pattern-formation outside of equilibrium. *Reviews of Modern Physics*, 65(3):851–1112.

[Dayel and Mullins, 2004] Dayel, M. J. and Mullins, R. D. (2004). Activation of arp2/3 complex: addition of the first subunit of the new filament by a wasp protein triggers rapid atp hydrolysis on arp2. *PLoS Biol*, 2(4):E91.

[DerMardirossian and Bokoch, 2005] DerMardirossian, C. and Bokoch, G. M. (2005). Gdis: central regulatory molecules in rho gtpase activation. *Trends Cell Biol*, 15(7):356–363.

[Etienne et al., 2015] Etienne, J., Fouchard, J., Mitrossilis, D., Bufi, N., Durand-Smet, P., and Asnacios, A. (2015). Cells as liquid motors: mechanosensitivity emerges from collective dynamics of actomyosin cortex. *Proc Natl Acad Sci U S A*, 112(9):2740–2745.

[Fenz et al., 2014] Fenz, S. F., Sachse, R., Schmidt, T., and Kubick, S. (2014). Cell-free synthesis of membrane proteins: tailored cell models out of microsomes. *Biochim Biophys Acta*, 1838(5):1382–1388.

[Ferrell, 2013] Ferrell, J. E., J. (2013). Feedback loops and reciprocal regulation: recurring motifs in the systems biology of the cell cycle. *Curr Opin Cell Biol*, 25(6):676–686.

[France et al., 2006] France, Y. E., Boyd, C., Coleman, J., and Novick, P. J. (2006). The polarity-establishment component bem1p interacts with the exocyst complex through the sec15p subunit. *J Cell Sci*, 119(Pt 5):876–888.

[Freisinger et al., 2013] Freisinger, T., Klunder, B., Johnson, J., Muller, N., Pichler, G., Beck, G., Costanzo, M., Boone, C., Cerione, R. A., Frey, E., and Wedlich-Soldner, R. (2013). Establishment of a robust single axis of cell polarity by coupling multiple positive feedback loops. *Nature Communications*, 4.

[Fritzsche et al., 2013] Fritzsche, M., Lewalle, A., Duke, T., Kruse, K., and Charras, G. (2013). Analysis of turnover dynamics of the submembranous actin cortex. *Mol Biol Cell*, 24(6):757–767.

[Fritzsche et al., 2017] Fritzsche, M., Li, D., Colin-York, H., Chang, V. T., Moeendarbary, E., Felce, J. H., Sezgin, E., Charras, G., Betzig, E., and Eggeling, C. (2017). Self-organizing actin patterns shape membrane architecture but not cell mechanics. *Nat Commun*, 8:14347.

[Fritzsche et al., 2014] Fritzsche, M., Thorogate, R., and Charras, G. (2014). Quantitative analysis of ezrin turnover dynamics in the actin cortex. *Biophys J*, 106(2):343–353.

[Giardini et al., 2003] Giardini, P. A., Fletcher, D. A., and Theriot, J. A. (2003). Compression forces generated by actin comet tails on lipid vesicles. *Proc Natl Acad Sci U S A*, 100(11):6493–6498.

[Gierer and Meinhardt, 1972] Gierer, A. and Meinhardt, H. (1972). A theory of biological pattern formation. *Kybernetik*, 12(1):30–39.

[Goryachev and Leda, 2017] Goryachev, A. B. and Leda, M. (2017). Many roads to symmetry breaking: molecular mechanisms and theoretical models of yeast cell polarity. *Mol Biol Cell*, 28(3):370–380.

[Goryachev and Pokhilko, 2008] Goryachev, A. B. and Pokhilko, A. V. (2008). Dynamics of cdc42 network embodies a turing-type mechanism of yeast cell polarity. *FEBS Lett*, 582(10):1437–1443.

[Guha et al., 2005] Guha, M., Zhou, M., and Wang, Y. L. (2005). Cortical actin turnover during cytokinesis requires myosin ii. *Curr Biol*, 15(8):732–736.

[Hall, 1998] Hall, A. (1998). Rho gtpases and the actin cytoskeleton. *Science*, 279(5350):509–514.

[Haviv et al., 2006] Haviv, L., Brill-Karniely, Y., Mahaffy, R., Backouche, F., Ben-Shaul, A., Pollard, T. D., and Bernheim-Groswasser, A. (2006). Reconstitution of the transition from lamellipodium to filopodium in a membrane-free system. *Proc Natl Acad Sci U S A*, 103(13):4906–4911.

[Haviv et al., 2008] Haviv, L., Gillo, D., Backouche, F., and Bernheim-Groswasser, A. (2008). A cytoskeletal demolition worker: myosin ii acts as an actin depolymerization agent. *J Mol Biol*, 375(2):325–330.

[Higgs and Pollard, 2000] Higgs, H. N. and Pollard, T. D. (2000). Activation by cdc42 and pip(2) of wiskott-aldrich syndrome protein (wasp) stimulates actin nucleation by arp2/3 complex. *J Cell Biol*, 150(6):1311–1320.

[Ideses et al., 2008] Ideses, Y., Brill-Karniely, Y., Haviv, L., Ben-Shaul, A., and Bernheim-Groswasser, A. (2008). Arp2/3 branched actin network mediates filopodia-like bundles formation in vitro. *PLoS One*, 3(9):e3297.

[Irazoqui et al., 2003] Irazoqui, J. E., Gladfelter, A. S., and Lew, D. J. (2003). Scaffold-mediated symmetry breaking by cdc42p. *Nat Cell Biol*, 5(12):1062–1070.

[Johnson et al., 2009] Johnson, J. L., Erickson, J. W., and Cerione, R. A. (2009). New insights into how the rho guanine nucleotide dissociation inhibitor regulates the interaction of cdc42 with membranes. *Journal of Biological Chemistry*, 284(35):23860–23871.

[Kai et al., 2012] Kai, L., Roos, C., Haberstock, S., Proverbio, D., Ma, Y., Junge, F., Karbyshev, M., Dotsch, V., and Bernhard, F. (2012). Systems for the cell-free synthesis of proteins. *Methods Mol Biol*, 800:201–225.

[Kawska et al., 2012] Kawska, A., Carvalho, K., Manzi, J., Boujemaa-Paterski, R., Blanchoin, L., Martiel, J. L., and Sykes, C. (2012). How actin network dynamics control the onset of actin-based motility. *Proceedings of the National Academy of Sciences of the United States of America*, 109(36):14440–14445.

[Klunder et al., 2013] Klunder, B., Freisinger, T., Wedlich-Soldner, R., and Frey, E. (2013). Gdi-mediated cell polarization in yeast provides precise spatial and temporal control of cdc42 signaling. *Plos Computational Biology*, 9(12).

[Kohler et al., 2011] Kohler, S., Schaller, V., and Bausch, A. R. (2011). Structure formation in active networks. *Nat Mater*, 10(6):462–468.

[Koster et al., 2016] Koster, D. V., Husain, K., Iljazi, E., Bhat, A., Bieling, P., Mullins, R. D., Rao, M., and Mayor, S. (2016). Actomyosin dynamics drive local membrane component organization in an in vitro active composite layer. *Proc Natl Acad Sci U S A*, 113(12):E1645–1654.

[Kozubowski et al., 2008] Kozubowski, L., Saito, K., Johnson, J. M., Howell, A. S., Zyla, T. R., and Lew, D. J. (2008). Symmetry-breaking polarization driven by a cdc42p gef-pak complex. *Curr Biol*, 18(22):1719–1726.

[Linsmeier et al., 2016] Linsmeier, I., Banerjee, S., Oakes, P. W., Jung, W., Kim, T., and Murrell, M. P. (2016). Disordered actomyosin networks are sufficient to produce cooperative and telescopic contractility. *Nat Commun*, 7:12615.

[Liu and Fletcher, 2006] Liu, A. P. and Fletcher, D. A. (2006). Actin polymerization serves as a membrane domain switch in model lipid bilayers. *Biophys J*, 91(11):4064–4070.

[Liu and Novick, 2014] Liu, D. and Novick, P. (2014). Bem1p contributes to secretory pathway polarization through a direct interaction with exo70p. *J Cell Biol*, 207(1):59–72.

[Lo et al., 2014] Lo, W. C., Park, H. O., and Chou, C. S. (2014). Mathematical analysis of spontaneous emergence of cell polarity. *Bull Math Biol*, 76(8):1835–1865.

[Loisel et al., 1999] Loisel, T. P., Boujemaa, R., Pantaloni, D., and Carlier, M. F. (1999). Reconstitution of actin-based motility of listeria and shigella using pure proteins. *Nature*, 401(6753):613–616.

[Martin et al., 2009] Martin, A. C., Kaschube, M., and Wieschaus, E. F. (2009). Pulsed contractions of an actin-myosin network drive apical constriction. *Nature*, 457(7228):495–499.

[Martin, 2015] Martin, S. G. (2015). Spontaneous cell polarization: Feedback control of cdc42 gtpase breaks cellular symmetry. *Bioessays*, 37(11):1193–1201.

[Maruta et al., 1983] Maruta, H., Baltes, W., Dieter, P., Marme, D., and Gerisch, G. (1983). Myosin heavy chain kinase inactivated by ca2+/calmodulin from aggregating cells of dictyostelium discoideum. *EMBO J*, 2(4):535–542.

[Maurer-Stroh et al., 2003] Maurer-Stroh, S., Washietl, S., and Eisenhaber, F. (2003). Protein prenyltransferases. *Genome Biol*, 4(4):212.

[Medeiros et al., 2006] Medeiros, N. A., Burnette, D. T., and Forscher, P. (2006). Myosin ii functions in actin-bundle turnover in neuronal growth cones. *Nat Cell Biol*, 8(3):215–226.

[Mionnet et al., 2008] Mionnet, C., Bogliolo, S., and Arkowitz, R. A. (2008). Oligomerization regulates the localization of cdc24, the cdc42 activator in saccharomyces cerevisiae. *J Biol Chem*, 283(25):17515–17530.

[Mori et al., 2008] Mori, Y., Jilkine, A., and Edelstein-Keshet, L. (2008). Wave-pinning and cell polarity from a bistable reaction-diffusion system. *Biophys J*, 94(9):3684–3697.

[Morreale et al., 2000] Morreale, A., Venkatesan, M., Mott, H. R., Owen, D., Nietlispach, D., Lowe, P. N., and Laue, E. D. (2000). Structure of cdc42 bound to the gtpase binding domain of pak. *Nat Struct Biol*, 7(5):384–388.

[Mullins and Hansen, 2013] Mullins, R. D. and Hansen, S. D. (2013). In vitro studies of actin filament and network dynamics. *Curr Opin Cell Biol*, 25(1):6–13.

[Munro et al., 2004] Munro, E., Nance, J., and Priess, J. R. (2004). Cortical flows powered by asymmetrical contraction transport par proteins to establish and maintain anterior-posterior polarity in the early c. elegans embryo. *Dev Cell*, 7(3):413–424.

[Murrell and Gardel, 2012] Murrell, M. P. and Gardel, M. L. (2012). F-actin buckling coordinates contractility and severing in a biomimetic actomyosin cortex. *Proc Natl Acad Sci U S A*, 109(51):20820–20825.

[Murthy and Wadsworth, 2005] Murthy, K. and Wadsworth, P. (2005). Myosin-ii-dependent localization and dynamics of f-actin during cytokinesis. *Curr Biol*, 15(8):724–731.

[Nishikawa et al., 2017] Nishikawa, M., Naganathan, S. R., Julicher, F., and Grill, S. W. (2017). Controlling contractile instabilities in the actomyosin cortex. *Elife*, 6.

[Novak and Tyson, 2008] Novak, B. and Tyson, J. J. (2008). Design principles of biochemical oscillators. *Nat Rev Mol Cell Biol*, 9(12):981–991.

[Nye and Groves, 2008] Nye, J. A. and Groves, J. T. (2008). Kinetic control of histidine-tagged protein surface density on supported lipid bilayers. *Langmuir*, 24(8):4145–4149.

[Okada et al., 2013] Okada, S., Leda, M., Hanna, J., Savage, N. S., Bi, E., and Goryachev, A. B. (2013). Daughter cell identity emerges from the interplay of cdc42, septins, and exocytosis. *Dev Cell*, 26(2):148–161.

[Ozbudak et al., 2005] Ozbudak, E. M., Becskei, A., and van Oudenaarden, A. (2005). A system of counteracting feedback loops regulates cdc42p activity during spontaneous cell polarization. *Dev Cell*, 9(4):565–571.

[Padrick et al., 2008] Padrick, S. B., Cheng, H. C., Ismail, A. M., Panchal, S. C., Doolittle, L. K., Kim, S., Skehan, B. M., Umetani, J., Brautigam, C. A., Leong, J. M., and Rosen, M. K. (2008). Hierarchical regulation of wasp/wave proteins. *Mol Cell*, 32(3):426–438.

[Padrick et al., 2011] Padrick, S. B., Doolittle, L. K., Brautigam, C. A., King, D. S., and Rosen, M. K. (2011). Arp2/3 complex is bound and activated by two wasp proteins. *Proc Natl Acad Sci U S A*, 108(33):E472–479.

[Pantaloni et al., 2000] Pantaloni, D., Boujemaa, R., Didry, D., Gounon, P., and Carlier, M. F. (2000). The arp2/3 complex branches filament barbed ends: functional antagonism with capping proteins. *Nat Cell Biol*, 2(7):385–391.

[Park and Bi, 2007] Park, H. O. and Bi, E. (2007). Central roles of small gtpases in the development of cell polarity in yeast and beyond. *Microbiol Mol Biol Rev*, 71(1):48–96.

[Park et al., 2015] Park, S. Y., Yang, J. S., Schmider, A. B., Soberman, R. J., and Hsu, V. W. (2015). Coordinated regulation of bidirectional copi transport at the golgi by cdc42. *Nature*, 521(7553):529–532.

[Petrie et al., 2009] Petrie, R. J., Doyle, A. D., and Yamada, K. M. (2009). Random versus directionally persistent cell migration. *Nat Rev Mol Cell Biol*, 10(8):538–549.

[Pontani et al., 2009] Pontani, L. L., van der Gucht, J., Salbreux, G., Heuvingh, J., Joanny, J. F., and Sykes, C. (2009). Reconstitution of an actin cortex inside a liposome. *Biophys J*, 96(1):192–198.

[Reymann et al., 2012] Reymann, A. C., Boujemaa-Paterski, R., Martiel, J. L., Guerin, C., Cao, W., Chin, H. F., De La Cruz, E. M., Thery, M., and Blanchoin, L. (2012). Actin network architecture can determine myosin motor activity. *Science*, 336(6086):1310–1314.

[Robbe et al., 2003] Robbe, K., Otto-Bruc, A., Chardin, P., and Antonny, B. (2003). Dissociation of gdp dissociation inhibitor and membrane translocation are required for efficient activation of rac by the dbl homology-pleckstrin homology region of tiam. *J Biol Chem*, 278(7):4756–4762.

[Roberts et al., 2008] Roberts, P. J., Mitin, N., Keller, P. J., Chenette, E. J., Madigan, J. P., Currin, R. O., Cox, A. D., Wilson, O., Kirschmeier, P., and Der, C. J. (2008). Rho family gtpase modification and dependence on caax motif-signaled posttranslational modification. *J Biol Chem*, 283(37):25150–25163.

[Rohatgi et al., 1999] Rohatgi, R., Ma, L., Miki, H., Lopez, M., Kirchhausen, T., Takenawa, T., and Kirschner, M. W. (1999). The interaction between n-wasp and the arp2/3 complex links cdc42-dependent signals to actin assembly. *Cell*, 97(2):221–231.

[Rossman et al., 2005] Rossman, K. L., Der, C. J., and Sondek, J. (2005). Gef means go: turning on rho gtpases with guanine nucleotide-exchange factors. *Nat Rev Mol Cell Biol*, 6(2):167–180.

[Rouiller et al., 2008] Rouiller, I., Xu, X. P., Amann, K. J., Egile, C., Nickell, S., Nicastro, D., Li, R., Pollard, T. D., Volkmann, N., and Hanein, D. (2008). The structural basis of actin filament branching by the arp2/3 complex. *J Cell Biol*, 180(5):887–895.

[Salbreux et al., 2012] Salbreux, G., Charras, G., and Paluch, E. (2012). Actin cortex mechanics and cellular morphogenesis. *Trends Cell Biol*, 22(10):536–545.

[Sheffield et al., 1999] Sheffield, P., Garrard, S., and Derewenda, Z. (1999). Overcoming expression and purification problems of rhogdi using a family of "parallel" expression vectors. *Protein Expr Purif*, 15(1):34–39.

[Smith et al., 2013a] Smith, B. A., Padrick, S. B., Doolittle, L. K., Daugherty-Clarke, K., Correa, I. R., J., Xu, M. Q., Goode, B. L., Rosen, M. K., and Gelles, J. (2013a). Three-color single molecule imaging shows wasp detachment from arp2/3 complex triggers actin filament branch formation. *Elife*, 2:e01008.

[Smith et al., 2007] Smith, D., Ziebert, F., Humphrey, D., Duggan, C., Steinbeck, M., Zimmermann, W., and Kas, J. (2007). Molecular motor-induced instabilities and cross linkers determine biopolymer organization. *Biophys J*, 93(12):4445–4452.

[Smith et al., 2002] Smith, G. R., Givan, S. A., Cullen, P., and Sprague, G. F., J. (2002). Gtpase-activating proteins for cdc42. *Eukaryot Cell*, 1(3):469–480.

[Smith et al., 2013b] Smith, S. E., Rubinstein, B., Mendes Pinto, I., Slaughter, B. D., Unruh, J. R., and Li, R. (2013b). Independence of symmetry breaking on bem1-mediated autocatalytic activation of cdc42. *J Cell Biol*, 202(7):1091–1106.

[Soares e Silva et al., 2011] Soares e Silva, M., Depken, M., Stuhrmann, B., Korsten, M., MacKintosh, F. C., and Koenderink, G. H. (2011). Active multistage coarsening of actin networks driven by myosin motors. *Proc Natl Acad Sci U S A*, 108(23):9408–9413.

[Stam et al., 2017] Stam, S., Freedman, S. L., Banerjee, S., Weirich, K. L., Dinner, A. R., and Gardel, M. L. (2017). Filament rigidity and connectivity tune the deformation modes of active biopolymer networks. *Proc Natl Acad Sci U S A*, 114(47):E10037–E10045.

[Ti et al., 2011] Ti, S. C., Jurgenson, C. T., Nolen, B. J., and Pollard, T. D. (2011). Structural and biochemical characterization of two binding sites for nucleation-promoting factor wasp-vca on arp2/3 complex. *Proc Natl Acad Sci U S A*, 108(33):E463–471.

[Tinevez et al., 2009] Tinevez, J. Y., Schulze, U., Salbreux, G., Roensch, J., Joanny, J. F., and Paluch, E. (2009). Role of cortical tension in bleb growth. *Proc Natl Acad Sci U S A*, 106(44):18581–18586.

[Tnimov et al., 2012] Tnimov, Z., Guo, Z., Gambin, Y., Nguyen, U. T., Wu, Y. W., Abankwa, D., Stigter, A., Collins, B. M., Waldmann, H., Goody, R. S., and Alexandrov, K. (2012). Quantitative analysis of prenylated rhoa interaction with its chaperone, rhogdi. *J Biol Chem*, 287(32):26549–26562.

[Tong et al., 2007] Tong, Z., Gao, X.-D., Howell, A. S., Bose, I., Lew, D. J., and Bi, E. (2007). Adjacent positioning of cellular structures enabled by a cdc42 gtpase-activating protein–mediated zone of inhibition. *The Journal of Cell Biology*, 179(7):1375–1384.

[Turing, 1952] Turing, A. M. (1952). The chemical basis of morphogenesis. *Philosophical Transactions of the Royal Society of London Series B-Biological Sciences*, 237(641):37–72.

[Van Aelst and D'Souza-Schorey, 1997] Van Aelst, L. and D'Souza-Schorey, C. (1997). Rho gtpases and signaling networks. *Genes Dev*, 11(18):2295–2322.

[Vignjevic et al., 2003] Vignjevic, D., Yarar, D., Welch, M. D., Peloquin, J., Svitkina, T., and Borisy, G. G. (2003). Formation of filopodia-like bundles in vitro from a dendritic network. *J Cell Biol*, 160(6):951–962.

[Vogel et al., 2013] Vogel, S. K., Petrasek, Z., Heinemann, F., and Schwille, P. (2013). Myosin motors fragment and compact membrane-bound actin filaments. *Elife*, 2.

[Waldo et al., 1999] Waldo, G. S., Standish, B. M., Berendzen, J., and Terwilliger, T. C. (1999). Rapid protein-folding assay using green fluorescent protein. *Nat Biotechnol*, 17(7):691–695.

[Wedlich-Soldner et al., 2003] Wedlich-Soldner, R., Altschuler, S., Wu, L., and Li, R. (2003). Spontaneous cell polarization through actomyosin-based delivery of the cdc42 gtpase. *Science*, 299(5610):1231–1235.

[Wedlich-Soldner et al., 2004] Wedlich-Soldner, R., Wai, S. C., Schmidt, T., and Li, R. (2004). Robust cell polarity is a dynamic state established by coupling transport and gtpase signaling. *J Cell Biol*, 166(6):889–900.

[Wilson et al., 2010] Wilson, C. A., Tsuchida, M. A., Allen, G. M., Barnhart, E. L., Applegate, K. T., Yam, P. T., Ji, L., Keren, K., Danuser, G., and Theriot, J. A. (2010). Myosin ii contributes to cell-scale actin network treadmilling through network disassembly. *Nature*, 465(7296):373–377.

[Yang et al., 2012] Yang, Q., Zhang, X. F., Pollard, T. D., and Forscher, P. (2012). Arp2/3 complex-dependent actin networks constrain myosin ii function in driving retrograde actin flow. *J Cell Biol*, 197(7):939–956.

[Zhang et al., 2000] Zhang, B., Zhang, Y., Wang, Z., and Zheng, Y. (2000). The role of mg2+ cofactor in the guanine nucleotide exchange and gtp hydrolysis reactions of rho family gtp-binding proteins. *J Biol Chem*, 275(33):25299–25307.

[Zhang and Zheng, 1998] Zhang, B. and Zheng, Y. (1998). Negative regulation of rho family gtpases cdc42 and rac2 by homodimer formation. *J Biol Chem*, 273(40):25728–25733.

A

SUPPORTING INFORMATION FOR ACTOMYOSIN PROJECT

1 Preparation of proteins

Unlabeled actin monomers from rabbit skeletal muscle (AKL99) and Arp2/3 complex from porcine brain (RP01P) were purchased from Cytoskeleton, Inc. Actin monomers conjugated with Alexa Fluor 568 (A12374) and Alexa Fluor 488 (A12373) were from ThermoFischer Scientific. Capping protein CapZ (non-muscle, human recombinant) was purchased from HYPERMOL EK, Germany.

Myosin-II purification from rabbit muscle, as well as labeling with Alexa Fluor 488, was carried out by Dr. Sven Vogel, as described in [Vogel et al., 2013]. The other purifications are described in detail.

Preparation of 10xHis-tagged VCA- This purification was performed with Dr. Kristina Ganzinger.

10xHis-tagged VCA was expressed in a 1 L culture of Rosetta T1 strain of BL21 cells by inducing with 0.5 mM IPTG and growing the cells for 16 hours. For purification, cells were lysed by sonication.

The purification was carried out by a combination of affinity chromatography, followed by anion exchange. A standard phosphate buffer saline (PBS) was supplemented with an additional 150 mM of NaCl, 20 mM Imidazole and 1 mM TCEP for loading onto a HisTrap HP column (GE Healthcare) via a chromatography system. Protease inhibitors (Roche complete) and Sm DNase were included in the lysis buffer. The protein was washed on column with 40 column volumes of the loading buffer and eluted with step concentrations of Imidazole. For ion exchange chromatography, a monoQ column from GE Healthcare was used. The loading was done in 20 mM Tris-HCl buffer (pH 8.0) and the salt concentration gradient went from 0 to 1 M NaCl. All buffers included 1 mM TCEP. The peak fractions from anion exchange were identified on a SDS-PAGE, combined and concentrated on Amicon concentrators. Buffer exchange was done on a PD-10 column into PBS, supplemented with 10 % Glycerol and 1 mM TCEP.

The protein was then tested on LC-MS as well as DLS for quality control. Protein was labeled with Atto 488 maleimide (28562) from Sigma-Aldrich. The dye was used in at fold 20-fold excess of the protein (by mass). The protein was mixed with dye aliquot in 1 mM TCEP containing buffer and incubated overnight in a cold room with gentle rotation. Buffer exchange was done on a small volume Sephadex G-25 column. This was followed by dialysis for complete removal of the dye. The final storage buffer of the protein was 50 mM Tris-HCl (pH 7.5), 150 mM NaCl, 10% Glycerol and 1 mM TCEP. Labeling efficiency was quantified by spectrophotometric analysis.

Preparation of non-muscle Myosin-II from Dictyostelium- This purification was performed with Dr. Kristina Ganzinger, with critical input from Dr. Sven Vogel and Gosia Poczopko. *Dictyostelium* cells were grown and kindly provided by Maria Ecke and Prof. Günther Gerisch (Emeritus at Max Planck Institute of Biochemistry). The protocol was also provided by Gerisch lab [Maruta et al., 1983] and performed with some adaptations.

Besides the buffers listed below, a 1.2 M stock of KI, ammonium sulphate salt and Glycerol are needed for the protocol. Buffer recipes are as follows:

G-buffer (homogenization buffer): 30 mM Tris (pH 7.5), 1 mM DTT, 2 mM EGTA, 30% sucrose, 1 mM Mg-ATP, 10 mM Benzamidine, 0.5mM PMSF, Roche complete protease inhibitor mix

Extraction buffer: 30 mM Tris (pH 7.5), 1 mM DTT, 1 mM Mg-ATP, 1 M KCl, 10 mM Benzamidine

Gel filtration buffer:30 mM Tris (pH 7.5), 1 mM DTT, 0.1 mM Mg-ATP, 0.6 M KCl

TDA buffer: 20 mM Tris (pH 7.5), 1 mM DTT, 0.6 M KCl

TDAS buffer: 30 mM Tris (pH 7.5), 1mM DTT, 0.1mM Mg-ATP, 15% sucrose

Roughly 20-30 g cell mass was provided by the Gerisch lab, suspended in G-buffer (total volume 50 ml). Cells were grown with a 12 hour long starvation at 23°C. All steps are performed at 4°C or in the cold room.

Cell lysis was done on a French press with 5000 psi setting. Cell debris was removed by a 15 minute centrifugation at 23,000xg (JA25.5 rotor). The supernatant was ultracentrifuged at 100,000xg for 3 hours in a Ti70 rotor. The myosin-containing pellet was resuspended in Extraction buffer, with 10 passes in a glass douncer (pestle B). The resuspended pellet solution (volume 18 ml) was ultracentrifuged at 100,000xg for 18 hours in a Ti70 rotor. The protein was then precipitated by adding Ammonium sulphate salt to get to a concentration of 1.5 M, under gentle and continuous mixing (using glass pipette or

stirrer). The solution was allowed to stand for 15 minutes, after which it was centrifuged at 23,000xg for 15 minutes in a JA25.5 rotor. Supernatant was carefully removed and the pellet was resuspended in a 1:1 mix of Extraction buffer and 1.2 mM KI. Volume should be kept minimal at this stage, so we used 3-4 ml. Insoluble debris was removed by a 15 minute centrifugation at 23,000xg.

The supernatant was then loaded onto a customized Superose 6 colume (XK26/70, GE Healthcare), equilibrated with gel filtration buffer. The loading was done through a 5 ml loop, pre-filled with the Extraction buffer/KI mix. An extra 10 ml of this buffer was flushed into the column immediately after loading, after which elution was carried out in the usual gel filtration buffer. SDS-PAGE gels were run from the fractions. A large peak corresponding to the size of actin was visible on the chromatogram. The myosin-containing samples were spread over nearly 32 ml, with a much less prominent peak in the chromatogram.

The myosin-containing fractions were pooled and the ammonium sulphate precipitation was repeated for concentrating the protein. The precipitate was collected by a 15 minute 23,000xg centrifugation. The protein was resuspended in TDA buffer and dialyzed overnight in TDAS buffer. Equal volume of Glycerol was added to the protein solution for storage at -20°C. SDS-PAGE shows a double band near 250 kDa, which is the approximate size of the myosin heavy chain.

2 Material and methods

Preparation of lipid bilayers- All lipids were purchased from Avanti Polar Lipids, Inc. This includes 1,2-dioleoyl-sn-glycero-3-phospho-L-serine (DOPS), 1,2-Dioleoyl-sn-glycero-3-phosphoethanolamine (DOPE), 1,2-Dioleoyl-sn-glycero-3-phosphocholine (DOPC), Phosphatidylinositol 4,5-bisphosphate (PIP2) and DGS-NTA. Small unilamellar vesicles with desired proportion of DOPC:DGS-NTA lipids (with 0.005% Atto655-DOPE) were prepared by rehydrating a lipid film in SLB buffer (50 mM Tris pH 7.5, 150 mM KCl) followed by sonication. The composition was 99 mol% DOPC and 1 mol% DGS-NTA in all cases unless otherwise mentioned. High precision coverglass (no. 1.5, Marienfeld-Superior) was treated with Piranha cleaning and a short exposure to O_2 plasma treatment. Press-to-seal silicone isolators from Grace Bio-labs were used as chambers (smaller well-GBL664208, wider wells-GBL664206). All experiments in chapter II from section 2.3 onwards used the wider chambers. 0.1 mg/ml of vesicles were deposited in the silicone chambers with frequent

pipetting, followed by 15 minutes of incubation. The bilayers were gently washed first with SLB buffer and then with VCA buffer (10 mM Tris (pH 7.5), 50 mM NaCl, 1 mM DTT) and stored in this buffer till sample was to be prepared.

Sample preparation- A lipid bilayer was flushed again with VCA buffer and then incubated with 200 nM 10xHis-VCA in the same buffer. For experiments where labeled VCA was required, Atto488-labeled VCA was included in a 1 in 10 ratio with unlabeled VCA. Since VCA showed considerable drop in activity with time, the protein was stored in small aliquots and freshly thawed for each sample. A premix containing actin monomers (10 % Alexa568-labeled), Arp2/3 complex and ATP regeneration system (Phosphocreatine and Creatine Phosphokinase) was made at the same time in G-buffer (10 mM Tris (pH 8.0), 0.2 mM $CaCl_2$, 0.2 mM ATP, 1 mM DTT). After 20 minutes, the excess VCA was removed through multiple washes and the sample was loaded on the microscope. The membrane and VCA (when labeled) were checked before adding the actin pre-mix. An image was taken for the reference intensity value for normalization before triggering polymerization by adding the 5xG-to-F buffer (50 mM Tris pH 7.5, 250 mM KCl, 10 mM $MgCl_2$, 1 mM DTT with variable ATP). A typical sample finally contained 1 µM actin monomers and 10 nM Arp2/3, unless otherwise mentioned. Additionally, the sample also included the ATP regeneration system (20 mM Phosphocreatinine, 53 U/ml Creatine Phosphokinase), and an oxygen scavenger system (37 U/ml Pyranose Oxidase, 90 U/ml Catalase and 0.8 % Glucose)[1]. The final buffer conditions were 10 mM Tris (pH 7.5), 50 mM KCl, 1 mM $MgCl_2$, 1mM DTT with ATP adjusted to 0.1 mM. The sample volumes were 20 ml in small chambers and 40 ml in wider chambers.

Myofilaments were pre-assembled by making a 4x stock of the myosin in a buffer of 10 mM Tris (pH 7.5), 50 mM KCl, 2 mM $MgCl_2$, 1 mM DTT and incubating for 10 minutes before adding to the actin network by replacing ¼ of the sample volume. Where washing was required before addition of myosin, a 4-fold replacement of sample volume was carried out with mixing.

In all cases, evaporation was minimized by storing the samples in closed boxes with wet tissue till they were used. For putting on the microscope, a hydrophobic pen was used to draw a "moat" around the silicone well and this was filled with water. A small plastic lid was used to cover the sample, including the moat, during imaging.

[1]These reagents are from Sigma-Aldrich

Variations from this basic protocol have been mentioned in the text, where relevant. Methylcellulose (Sigma) was used at a final concentration of 0.2% and included in a 2x concentration in the VCA buffer before adding the actin mix. Blebbistatin (Sigma) was dissolved in DMSO and used at a concentration of 20 µM.

For experiments were a second label of actin was needed, Alexa488-labeled actin monomers were used. For data in Figure II.21, these monomers were included in a 1:1000 ratio to the Alexa568 monomers. For experiments in section 3.5, Alexa488-labeled monomers were mixed with unlabeled actin monomers at a 1 in 10 ratio. 1 µM of this 10 % labeled actin was added to the sample, as described in the text.

Image acquisition- For most of the data, fluorescence images were recorded on a home-built objective-type TIRF microscope, constructed around a Nikon Ti-S microscope body with oil immersion objective (Nikon SR Apo TIRF, 100x, NA 1.49). This set-up was built and maintained by Jonas Mücksch and Philipp Blumhardt[2]. Imaging was done with 490 nm, 561 nm and 640 nm wavelength lasers with corresponding bandpass filters of 525/50, 593/46 and 705/100, respectively. An Andor EMCCD camera (iXon Ultra 897) was used for detection. A custom-built focus stabilization eliminated drift of the focus position. Imaging interval was either 2 or 5 seconds, with exposure times of 50 or 100 msec.

For imaging in solution, as shown in Figure II.29, a Yokogawa scan head CSU10-X1 spinning disk system set up on a Nikon Eclipse Ti inverted microscope body was used. Detection was done with an Andor Ixon Ultra 512 × 512 EMCCD camera and a 3i solid state diode laser stack with 488 nm, 561 nm and 640 nm laser lines (3i, Denver, Colorado USA) was used for excitation. Imaging was done with a UPLanSApo 60x/1.20 Water UIS2 objective (Olympus, Japan).

Image processing and data analysis- Image processing and analysis was done using ImageJ. Rolling ball background subtraction was used to highlight features in Figures II.5, II.15, II.20, II.21 and II.33. Rolling ball radii were 100 pixel for actin and 20 pixel for myosin. For cases where single filament resolution was desirable to show structures, namely in Figures II.11 and II.12, a walking average was done using an ImageJ macro before an *a priori* correction for uneven illumination.

[2]For details, refer to PhD Thesis, Jonas Mücksch, LMU-Physik

Customized macros were made for most intensity and length scale analysed. Additional plugins used were Radial Profile Plot, Stack Moving Average and Kymo_wide_reslice, both available for free download online.

Statistical analysis and plotting of graphs was done on Origin. ANOVA analyses was used for significance testing of length scale measurements.

3 Supplementary figures

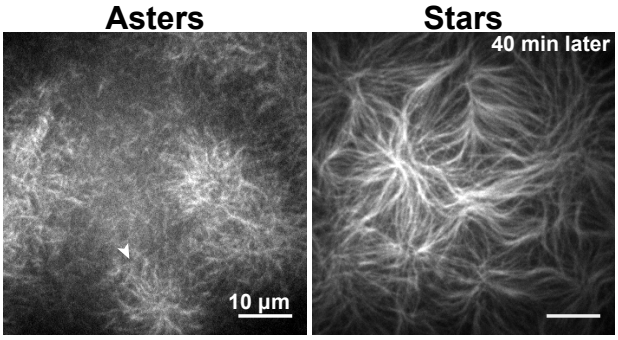

Figure A.1: Bundling leads to formation of large actin stars

The aster to star transition for a sample discussed in Figure II.11 is shown (white arrow denotes tha aster shown there). After 40 minutes from the last observation of aster, large stars were visible in the sample. Intensities are not comparable.

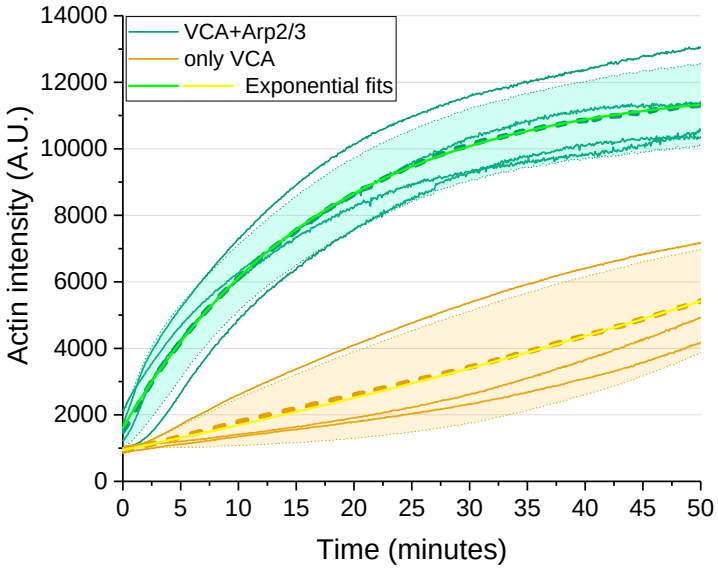

Figure A.2: Sample variability during actin assembly

Time profiles of actin intensity on the SLB in different conditions. Each line is an individual sample and the dotted lines denote an average curve these samples. Light green and yellow lines are an exponential fit. Initial 2 minutes were excluded in the VCA + Arp2/3 fit as the lag interferes with the fit. The fit curve in the graph is extrapolated.

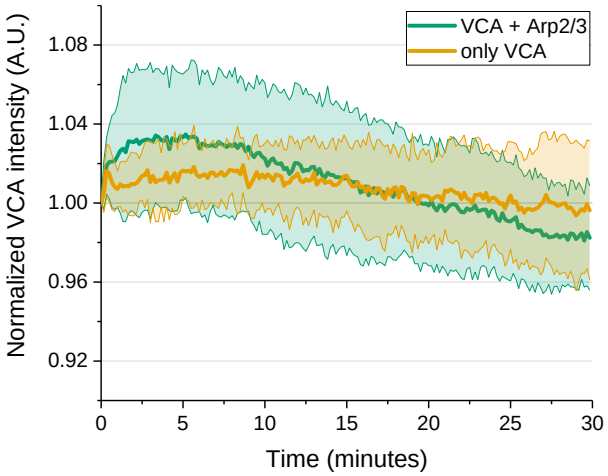

Figure A.3: VCA is stably attached to the membrane during actin assembly

Graph shows normalized VCA intensity on the membrane during actin assembly. The variation is limited to 6% within a 30 minute period of assembly.

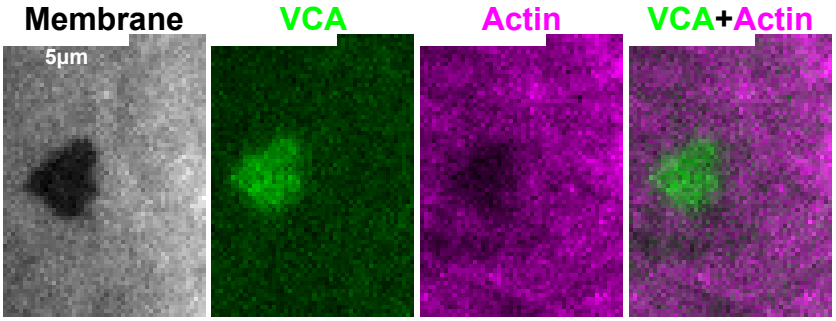

Figure A.4: Membrane is essential for actin assembly

VCA enriches on holes in the lipid bilayer, but actin assembly largely excludes these regions in our experimental conditions.

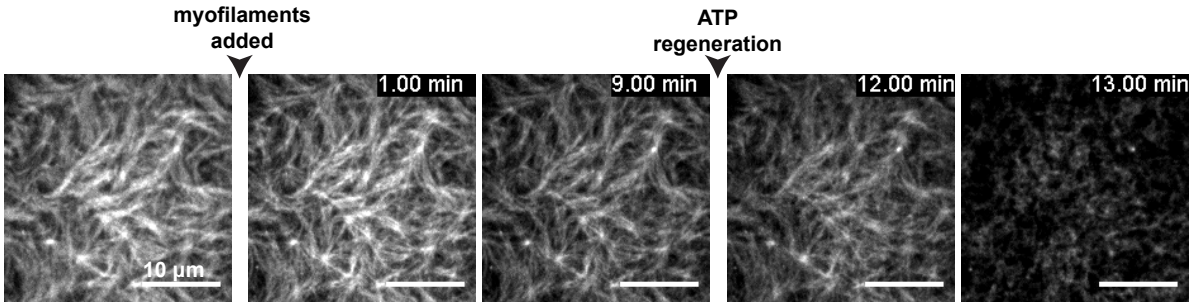

Figure A.5: Contraction proceeds with ATP consumption

If ATP runs out, the contraction process stalls at bundling. Only a drop of intensity is seen, possibly due to bleaching. ATP regeneration mix was added after 9 minutes and immediately results in breakdown of the actin network. Time is in reference to myosin addition. Scale bars are 10 µm.

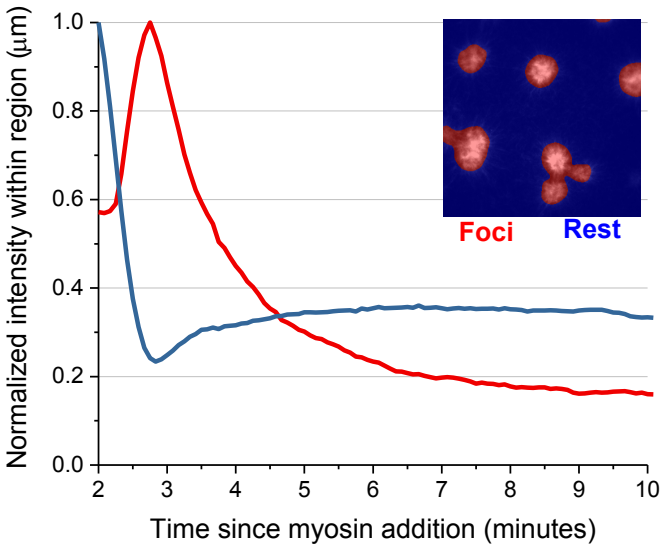

Figure A.6: Loss of actin from foci and increase in the vicinity occurs simultaneously
Image segmentation was used to separately measure intensity changes in the contraction foci formed during coarsening (red) and the region outside (blue).

B

SUPPORTING INFORMATION FOR CDC42 PROJECT

1 Materials and methods

Protein preparations- *S. cerevisiae* Cdc42 protein mostly used in this study was produced as a 6xHis-eGFP-tagged construct, co-expressed with untagged GDI (RDI1) in the insect cell line Sf9. A 48 hour long co-expression was carried out in the Purification Facility at Max Planck Institute of Biochemistry. The cells were resuspended in lysis buffer and lysed using the emulsiflex at 15,000 psi. The lysis buffer was composed of 20 mM HEPES, 300 mM NaCl, 5 mM $MgCl_2$, 0.1 mM EDTA, 1 mM DTT, 0.1 mM GDP, 1 mM PMSF and Roche complete ULTRA protease inhibitor mix. After a brief centrifugation at 2,000xg for 15 minutes to remove intact cells and nuclei, the supernatant was ultracentrifuged at 160,000xg for 40 minutes in a Type 60 Ti rotor. The supernatant was filtered and 10 mM Imidazole was added before loading into a HisTrap HP column (GE Healthcare) for Ni-affinity chromatography. A 40 column volume wash was conducted on column with lysis buffer, excluding the EDTA and GDP. A gradient elution to 300 mM Imidazole was used. Fractions pooled from affinity chromatography were concentrated in an Amicon device (15 kDa cut-off) and loaded onto a Superdex 200pg preparative scale size exclusion column. The peaks appeared to be unresolved so fractions with the right band size on SDS-PAGE were pooled for a rerun of size exclusion chromatography. A single peak with a blunt tip was obtained. Final storage buffer of the protein was 20 mM HEPES (pH 7.5), 300 mM NaCl, 5 mM $MgCl_2$, 10% Glycerol and 1 mM TCEP.

Another version of the yeast Cdc42 with a mCherry and a 10xHis tag was overexpressed in cell-free lysate according to protocol described in [Kai et al., 2012]. A standard purification with affinity and Size Exclusion Chromatography (SEC) was done. This was used in the prenylation experiments.

Yeast GDI, RDI1, was separately expressed in bacteria with a GST-tag. The purification was done by the MPI-B protein facility with a standard protocol of affinity chromatography followed by gel filtration. The only point to be considered for RDI1 expression is that over-expression should be limited to 3 hours to prevent aggregation of the protein.

The yeast CRIB-GEF fusion used in this study has been described in section 3.3. This protein also had a standard purification protocol of affinity chromatography, followed by SEC.

The prenylation enzyme GGTase-I was purified by Dr. Lei Kai. This protein has two subunits which were co-expressed in Rosetta T1 cells with 0.2-0.4 mM IPTG for 4 hours at 37 °C. The α-subunit had a GST tag on it for affinity, while the β- subunit was untagged. A standard GST affinity protocol was followed in phosphate buffer with 300 mM NaCl and 1 mM TCEP (pH 8.0). The peak fractions from affinity purification were combined and diluted 10-fold for loading to an anion exchange column. Elution was done over a gradient from 50 to 400 mM NaCl. Peak fractions were collected and dialyzed against buffer composed of 25 mM HEPES (pH7.2), 25 mM NaCl, 5 mM DTT. The protein was concentrated and equal volume of glycerol was added for storage in -80 °C.

Human Cdc42 protein was expressed using autoinduction protocols by Dr. Lei Kai and purified by affinity and SEC with 10XHis tag alone or the tag followed by sfGFP or mCherry. The important deviations from the yeast protocol was the use of optimized buffer conditions including 20 mM HEPES (pH 7.5), 500 mM NaCl, 2 mM $MgCl_2$, 0.1 mM GDP, 1mM TCEP. For storage, the buffer used salt concentration reduced to 150 mM NaCl and 10 % glycerol was added.

Buffer optimization- Basic quality control of proteins was done using LC-MS and DLS. Buffer optimization was carried done by testing thermal denaturation on the Prometheus NT.48 from NanoTemper Technologies.

Lipid preparation- SLBs were prepared as described in section 2 of previous Appendix chapter. The notable exception is that $CaCl_2$ was used for deposition of vesicles if PIP2 was missing from lipid composition. GUVs were prepared by electroformation in sucrose. Most experiments were done in coverglass-bottomed 96-well plates optimized for imaging.

***In vitro* prenylation on SLBs-** The buffer used for prenylation on SLBs was as follows: 50 mM HEPES (pH 7.4), 40 mM NaCl, 2 mM $MgCl_2$, 2 mM DTT, 20 µM $ZnCl_2$, 20 µM GDP, 0.4 mg/ml BSA. The reaction mix included 5 µM of protein substrate, 4 µM of GGTase-I enzyme and 110 µM of prenyl substrate GGPP. Where GTP regeration was needed in these experiments, the same mix as described for actin in previous chapter was used.

Image acquisition- Most experiments were done on a commercial Zeiss LSM 780 confocal microscope with a C-Apochromat 40xW, NA 1.2 DIC III objective (Zeiss AG, Oberkochen). The spinning disc confocal described previously was used for the CRIB-GEF construct screening.

Image analysis- Image analysis and processing was done on ImageJ with custom-made macros, where needed. Graphs were plotted in Origin.

2 Supplementary figures

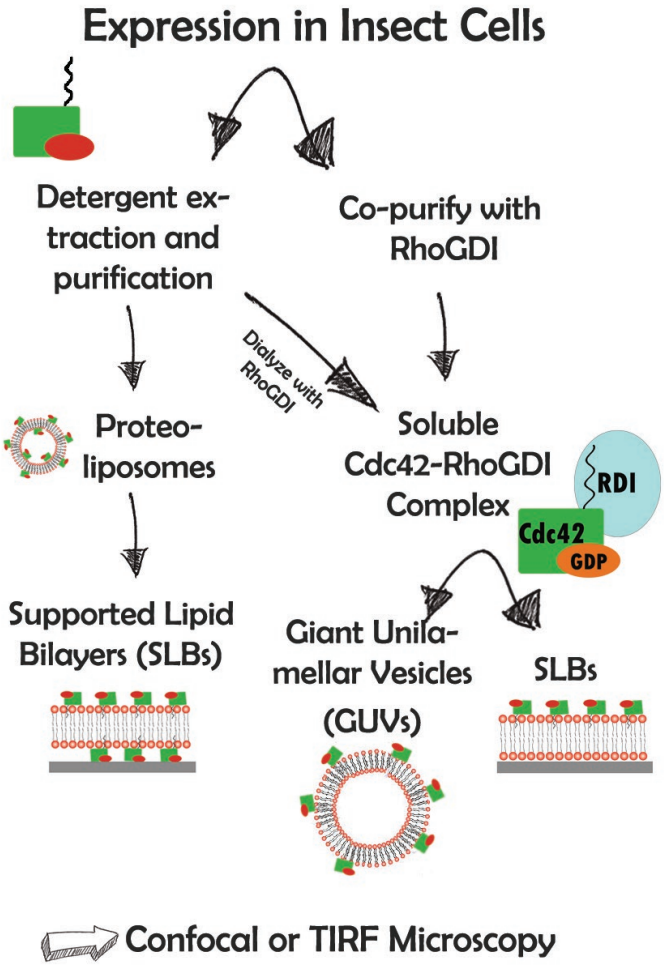

Figure B.1: Schematic depicting various routes to purification and reconstitution of functional Cdc42 on model membranes

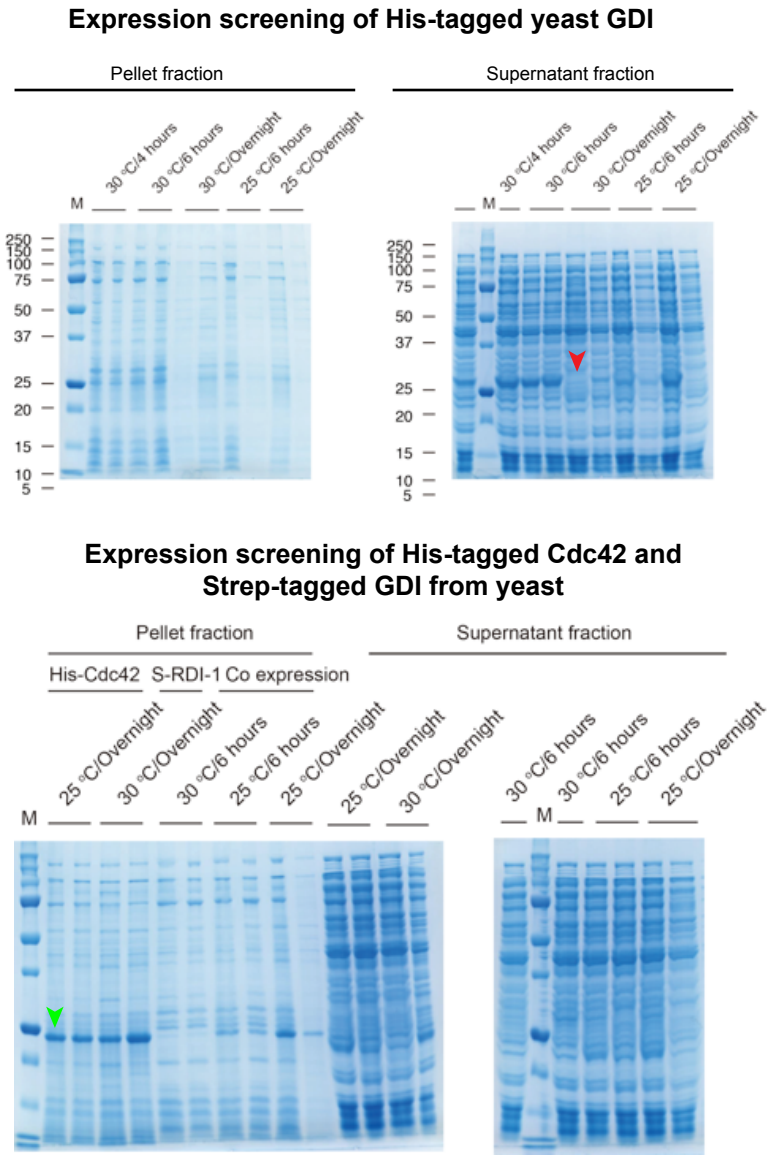

Figure B.2: Expression screening for yeast proteins of the polarization module
Two sets of expression screens are shown. The upper panel shows screening of conditions for His-tagged GDI. The two gels are for pellet and supernatant fraction. A band is observed at the right size of approximately 20 kDa in the supernatant fractions indicating soluble expression. However, red arrow indicates the absence of this band in overnight expression, indicating that the protein degrades over time. We thus know that expression time would be a critical critera. In the lower panel, expression of His-Cdc42 and Strep-GDI are attempted. His-Cdc42 bands are visible only in pellet fraction (green arrow) indicating that the protein is aggregated. No overexpression bands are visible for GDI at all. Data figure from Dr. Lei Kai

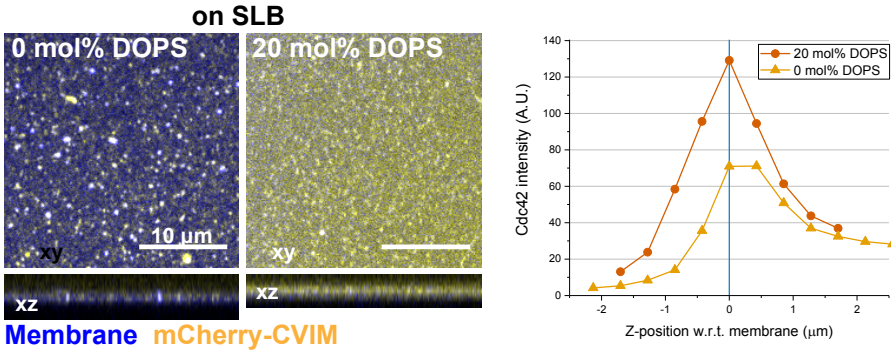

Figure B.3: Farnesylation of a chimeric protein with a CAAX motif on SLBs

A chimeric protein made up of an mCherry attached via a linker to the CAAX motif of human KRasB (CVIM) was prenylated using the enzyme FTase on top of an SLB. Higher binding was observed on negatively charged membrane. The bright puncta are vesicles sticking on the SLB due to inefficient washing

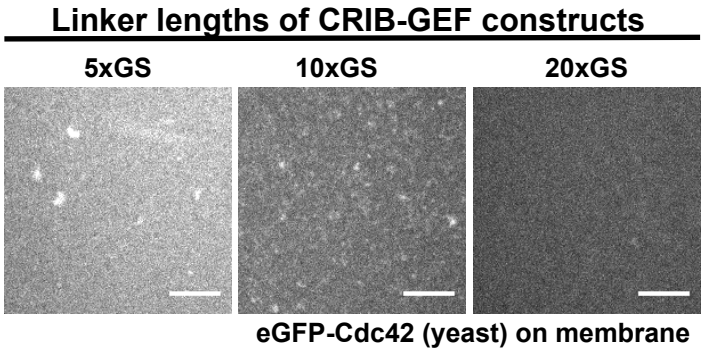

Figure B.4: Preliminary comparison of activities of different CRIB-GEF constructs using a lysate screening

Yeast CRIB-GEF constructs were designed with 3 different linker lengths- 5x, 10, or 15x of Gly-Ser repeats. SLBs were incubated with diluted lysates expressing these constructs. 100 nM of eGFP-Cdc42/GDI complex was then added with 10 µM of GTP. The differences in surface distribution after 15 minutes of incubation are shown. Date aquired on a spinning disk confocal.

ACKNOWLEDGMENTS

This thesis would not be possible without the invaluable input and unquestioning support of many people. I begin with thanking my supervisor Prof. Petra Schwille for bearing with me in this long and arduous journey, and giving me copious space and time (and resources) to follow my curiosity. These pursuits often lead to dead-ends and I'm grateful to have had a thesis committee to help keep me on track– Dr. Thomas Wollert, Prof. Erwin Frey and Dr. Roland Wedlich-Söldner. The latter two were also crucial to the conception of the Cdc42 project. Much of this work was fostered by frequent discussions with my collaborators– Dr. Lei Kai, Dr. Kristina Ganzinger, Dr. Sven Vogel, Jonas Mücksch, and Philipp Blumhardt. The frequent technical discussions with Stephan Uebel and Dr. Henri Franquelim also make them tacit collaborators.

On the technical side, the protein facility at MPI-CBG, Dresden and MPI-B, Munich were valuable for getting me started and keeping me going, respectively. An emphatic thanks to Michaela and Katharina for making tons of whimsical DNA constructs for me and Sigrid for running the membrane lab like clockwork. Prof. Klemens Rottner and the lab of Dr. Wedlich-Söldner provided useful plasmids for this research. The Gerisch lab and Gosia enabled parts of this project. The MaxSynBio consortium funded part of my journey, and the entire team of IMPRS-LS worked hard to make it likable. This thesis thanks Lei and Jonas for rushed technical notes and Bea and Kristina for their language skills.

I can think of something to thank every single colleague in the Schwille lab for, but this document is long enough already. Suffice to say, I might agree to write a thesis again for the privilege of such company! A special thanks to the ones who have tolerated me the longest– Alena, Henri, Jonas and Gosia; and to the ones who share/d the not-silent office (Phil, Diego, Cate, Hiro). The absorbers of my culture shock in Dresden deserve a special note of mention– Hetvi, Franzi, Janine, Senthil, Grzesiek and Ilaria.

A long-distance hat tip to my family for keeping home alive in their lively phone calls. A holler out to my brother, for no particular reason. A high five to Deepti and Jatin for being closer by (in situation, as in geography). And finally, I can say without exaggeration that either this thesis, or I, would not have survived without the unwavering support of Norbert Borgmann.

A big thank you to all of you for making this possible!